EGG-CAAP-5190

June 1980

TRAC-P1A CALCULATIONS FOR A 200%, 0.25 m-DIAMETER, AND 0.10 m-DIAMETER COLD LEG BREAK IN A PRESSURIZED WATER REACTOR

P. D. Wheatley
M. A. Bolander

U.S. Department of Energy
Idaho Operations Office • Idaho National Engineering Laboratory

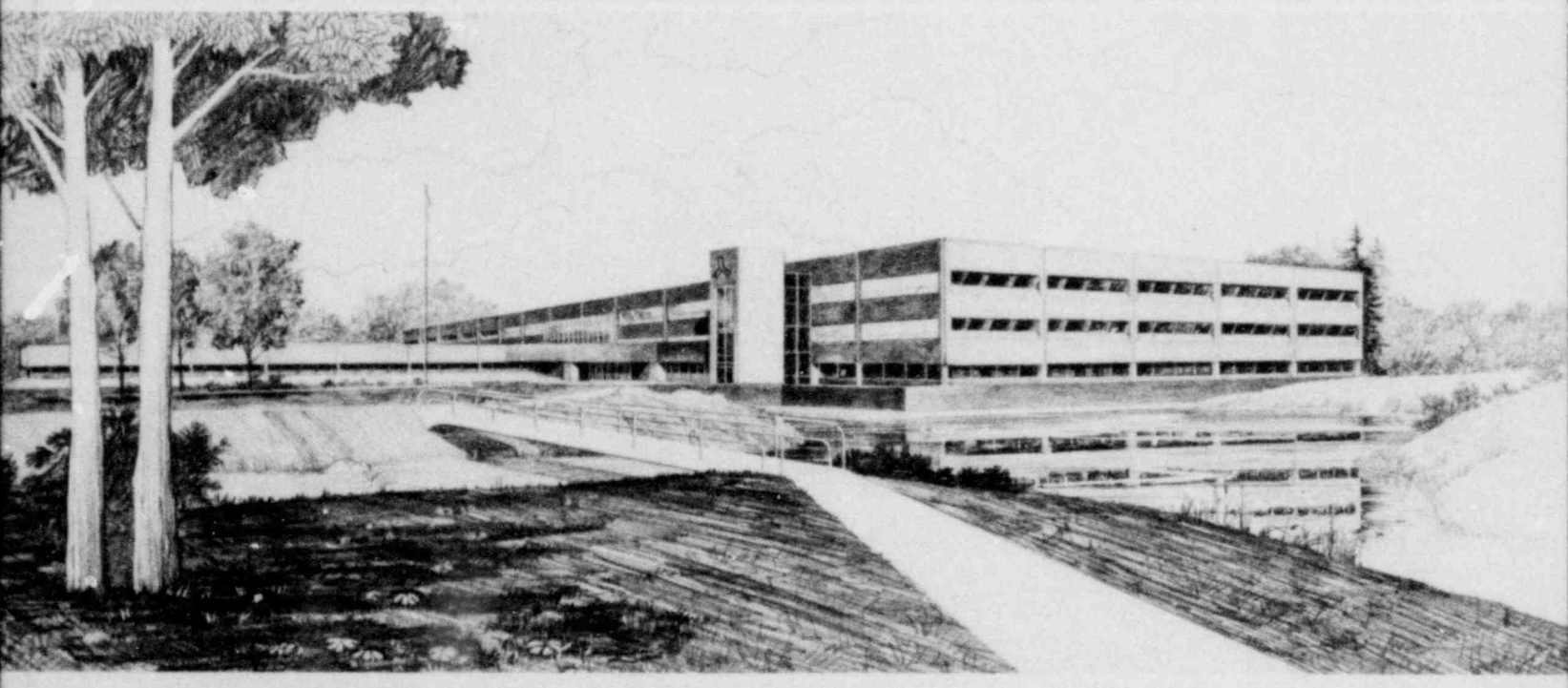

Prepared for the
U.S. Nuclear Regulatory Commission
Under DOE Contract No. DE-AC07-76ID01570
NRC FIN No. A6047

EG&G Idaho

EG&G Idaho, Inc.

FORM EG&G-398
(Rev. 11-79)

INTERIM REPORT

Accession No. _____

Report No. EGG-CAAP-5190

Contract Program or Project Title: Code Assessment and Applications Program

Subject of this Document: TRAC-P1A Calculations for a 200%, 0.25 m-Diameter, and 0.10 m-Diameter Cold Leg Break in a Pressurized Water Reactor

Type of Document: Preliminary Assessment Report

Author(s): P. D. Wheatley
M. A. Bolander

Date of Document: June 1980

Responsible NRC Individual and NRC Office or Division: F. Odar, NRC-RSR

EG&G Idaho, Inc.
Idaho Falls, Idaho **83415**

Prepared for the
U.S. Nuclear Regulatory Commission
Washington, D.C.
Under DOE Contract No. **DE-AC07-76ID01570**
NRC FIN No. A6047

INTERIM REPORT

ABSTRACT

TRAC-P1A is currently being assessed at the Idaho National Engineering Laboratory. Part of the assessment effort includes analysis of seven loss-of-coolant accidents (LOCAs) for a large pressurized water reactor. This report documents the results of three LOCAs which are initiated in the cold leg. Calculations were performed for a large (200%) break, an intermediate (0.25 m-diameter) break, and a small (0.10 m-diameter) break. The 200% break was run 207 s into the transient, the intermediate break was concluded at 212 s and the small break was stopped after 1224 s. Sensitivity studies were undertaken for both the 200% break and intermediate break exploring modeling techniques. The strong points, as well as the deficiencies of the code, are indicated within this report.

ACKNOWLEDGEMENTS

The authors of this report wish to thank J. R. Larson for his help and contributions to this report. A. C. Peterson provided important advice in the preparation of this report.

We would like to express our appreciation to Dawnie Terry and Colleen Polk, Engineering Assistants, for their effort and timely contributions.

We would also like to thank Joan Mosher for her efficiency and patience in the preparation of this report.

CONTENTS

FIGURES

TABLES

SUMMARY

Seven calculations for large pressurized water reactor LOCAs have been conducted at INEL using TRAC-P1A. This report documents the results of three calculations for different sized cold leg breaks. The break sizes were: (1) a 200% break, (2) an intermediate (0.25 m-diameter) break, and (3) a small (0.10 m-diameter) break.

The 200% cold leg break was terminated at 207 s with lower portions of the core quenching. Rod cladding temperatures throughout the core remained below about 1365 K.

The intermediate break calculation was concluded after 212 s of transient. Accumulator water had been injected recovering the core and all rod cladding temperatures were less than 450 K.

The small break calculation was terminated at 1224 s. Accumulator injection had not been initiated; however, rod cladding temperatures throughout the core were less than 540 K. It appeared that no core heatup would occur before the initiation of accumulator injection which would start in about 250 s. The system depressurization appeared to be calculated reasonably well however, the void distribution in the core did not appear reasonable at the termination of the calculation.

1. INTRODUCTION

TRAC-P1 [a] has been used at the INEL to perform seven LOCA (Loss-of-Coolant Accident) calculations for a LPWR (Large Pressurized Water Reactor). The Westinghouse Zion I facility was used as the model plant for all calculations. These calculations are part of the overall assessment program for TRAC-P1A being conducted at INEL. Three of the seven calculations are reported herein.[b] The three reported calculations were cold leg breaks representing; a large (200%) break, an intermediate (0.25 m-diameter) break, and a small (0.10 m-diameter) break.

Section 2 discusses the modeling and noding for the TRAC model and identifies the initial and boundary conditions used for the calculations. The results of each calculation are discussed in Section 3. Additional sensitivity studies are presented in Section 4 along with their results. Section 5 contains conclusions and recommendations which were obtained from these calculations.

---

a. Identified internally as TRACN1 and stored at INEL under Configuration Control Number H0038858.

b. Results of the other calculations may be found in References 1 and 2.

2. MODEL DESCRIPTION

The calculational model was developed using the Zion I pressurized water reactor as a basis for providing input to the TRAC computer code. The input data came from three sources: the BE/EM study,[3] a PWR model developed by LASL[4] and the Safety Analysis Report for the Zion I pressurized water reactor.[5] The BE/EM study[3] was the primary source of information unless more complete information was available elsewhere. The following sections briefly describe the code version used, model nodalization, code options, and the initial and boundary conditions for the calculations. Details concerning the nodalization and boundary conditions of the components may be found in Appendices A and B, respectively.

2.1 Code Description

The code version used was TRAC-P1A[4] with the updates described in the TRAC Newsletter No. 1.[6] The configuration control number for the steady state model and changes for the transient calculation is H007785B.

2.2 Nodalization

The 200% cold leg break model consisted of four separate loops (one broken and three intact) and a vessel. The steady state model consisted of 55 components and 548 cells. The steady state model was transformed into a transient model by the addition of BREAKS 47 and 48 in loop 1 as shown in Figure 1. For comparison the USPWR1 model developed by LASL consisted of 42 components and 634 cells. The Zion I model used in this analysis contains 13 more components due to a more detailed modeling of the steam generators, vessel, and the inclusion of broken loop ECC components. The steam generator had outlet valves and the vessel contained internal pipes to model the upper head bypass passages. Additional cells were required in the USPWR1 model because the vessel consisted of 5 radial rings.

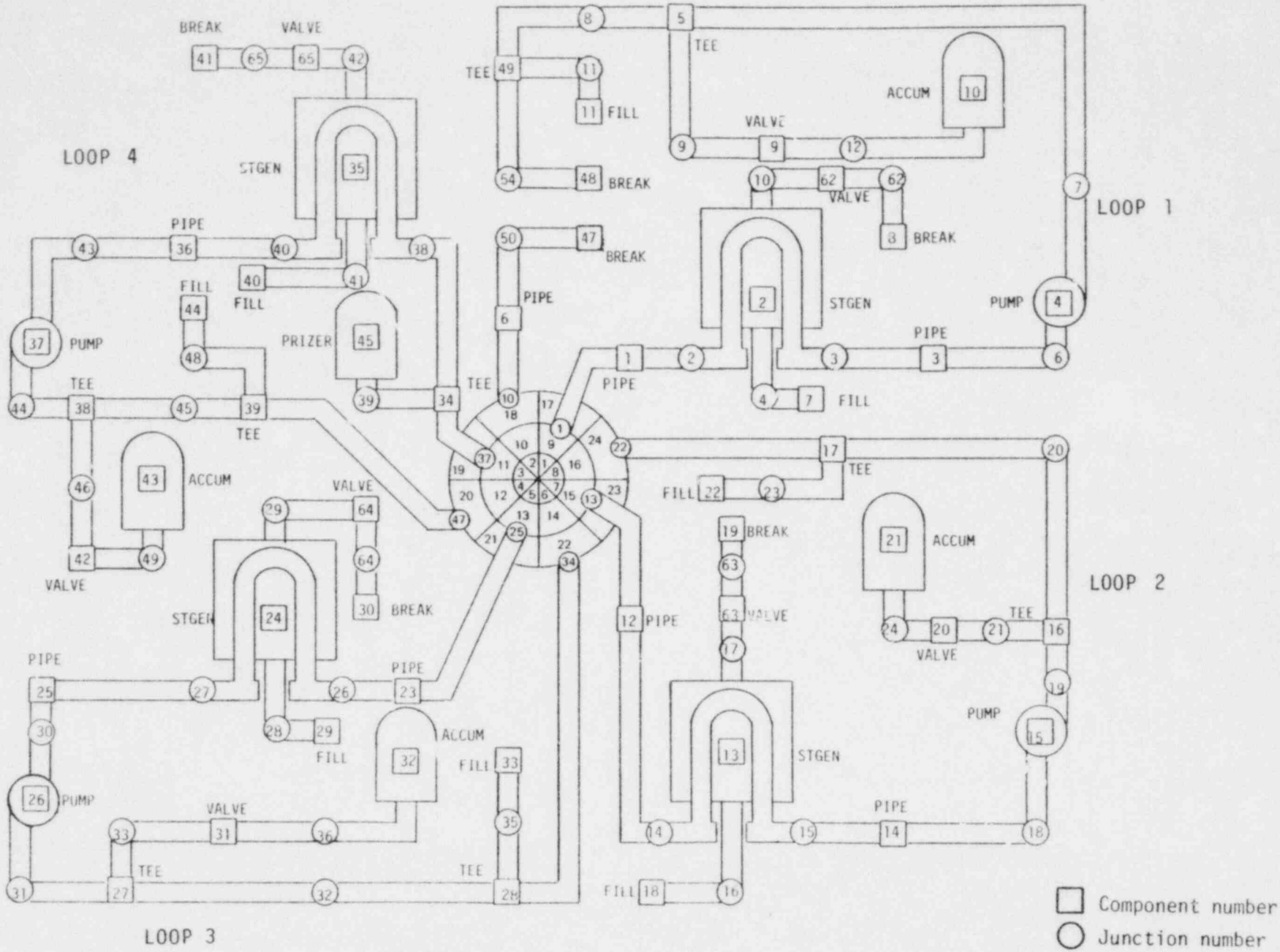

Figure 1. TRAC nodalization of Zion I for large break.

Figure 1 shows the nodalization of the loops and vessel level 10 where the loops connect to the vessel for the transient model. Steady state calculations were made by elimination of the components BREAK 47 and 48 and joining TEE 49 and PIPE 6. Each loop consisted of a pump, steam generator, accumulator, ECC injection and the associated piping. Loop 1 contained the breaks and loop 4 the pressurizer.

The vessel nodalization consisted of 12 axial levels with each level subdivided into 3 radial and 8 azimuthal zones for a total of 288 mesh cells.

Detailed descriptions of the vessel, pressurizer, accumulator, breaks, ECC injection and steam generator are discussed in Appendix A. A detailed listing of the code input and steady state conditions at the beginning of the transient are provided in Appendix C.

2.3 Code Options

Few code options exist in TRAC-P1A. A major choice concerns the friction factor correlation to be used in components other than the vessel. Based on the TRAC Developmental Assessment Report,[7] the annular flow correlation (NFF=4) was selected for all components.

The option permitting the code to calculate the fuel rod gap conductance was also selected (NFCI=1). This resulted in a lower than reasonable gap conductance and a peak centerline temperature at steady state that was excessively high. The effect of this parameter on cladding surface temperature is discussed in Section 4.

The option for determining core power versus time (IRPOP=7) was selected. The power-time table was taken from the BE/EM study.[3]

The partially implicit numerical hydrodynamics option (IHYDRO=0) was used throughout the loop piping except for piping adjacent to the breaks, accumulator, and pressurizer where the fully implicit option (IHYDRO=1) was used.

2.4 Initial and Boundary Conditions for a 200% Break

The system operating conditions at the start of the transient are compared to the BE/EM study[3] and shown in Table 1. The initial conditions calculated by TRAC were nearly identical to those of the BE/EM study.[3] Slight differences in the pump head and core differential pressure were due to the complex system geometry and resulting difficulties in determining the additive frictions to be used in the code input. The inlet and outlet temperatures compared well and the core differential temperature varied by only 0.1 K.

2.5 Intermediate and Small Break Nodalization

The intermediate and small break calculations used a simpler model than the 200% break due to the anticipated lengths of the transients and the computer running time. The three intact loops were volumetrically combined to form one intact loop. All component lengths remained the same with volumes and flow area being larger by a factor of three. The broken loop represented a single loop similar to the broken loop of the 200% break. A tee component was used as the connection to the break to model a communicative break. Figure 2 shows the nodalization of the loops and vessel level 10 where the loops connect to the vessel. The vessel was simplified by reducing the number of azimuthal segments from eight to two. The axial and radial zones remained the same as the 200% eight segment vessel. The coarsely noded vessel contained 72 cells whereas the eight segment vessel had 288 cells, reducing the running time by approximately a factor of four. The transient model consisted of a total of 32 components with 208 cells. The break nodalization is discussed in Appendix A.

2.6 Initial and Boundary Conditions for Intermediate and Small Breaks

This section describes the initial and boundary conditions applied to the intermediate and small break calculations. All initial conditions from

TABLE 1. SYSTEM OPERATING CONDITIONS FOR ZION I PWR COMPARED TO BE/EM STUDY[1]

	ZION I	BE/EM
Core power (MWt)	3223	3228
Loop Mass Flow Rate (kg/s)		
Loop 1	4621	4604
Loop 2	4621	
Loop 3	4620	
Loop 4	4563	
Hot Leg Entrance Temperature (K)		
Loop 1	583.4	582.9
Loop 2	583.4	
Loop 3	583.5	
Loop 4	583.5	
Cold Leg Exit Temperature (K)		
Loop 1	550.5	550.0
Loop 2	550.5	
Loop 3	550.6	
Loop 4	550.5	
Pump Head (MPa)		
Loop 1	0.606	0.514
Loop 2	0.644	
Loop 3	0.644	
Loop 4	0.621	
Upper Head Temprature	580.0	569.8
Core ΔT (K)	33.0	32.9
Core ΔP (MPa)	0.081	0.170
Average Rod Peak Power Rating (kw/m)	31.73	32.74

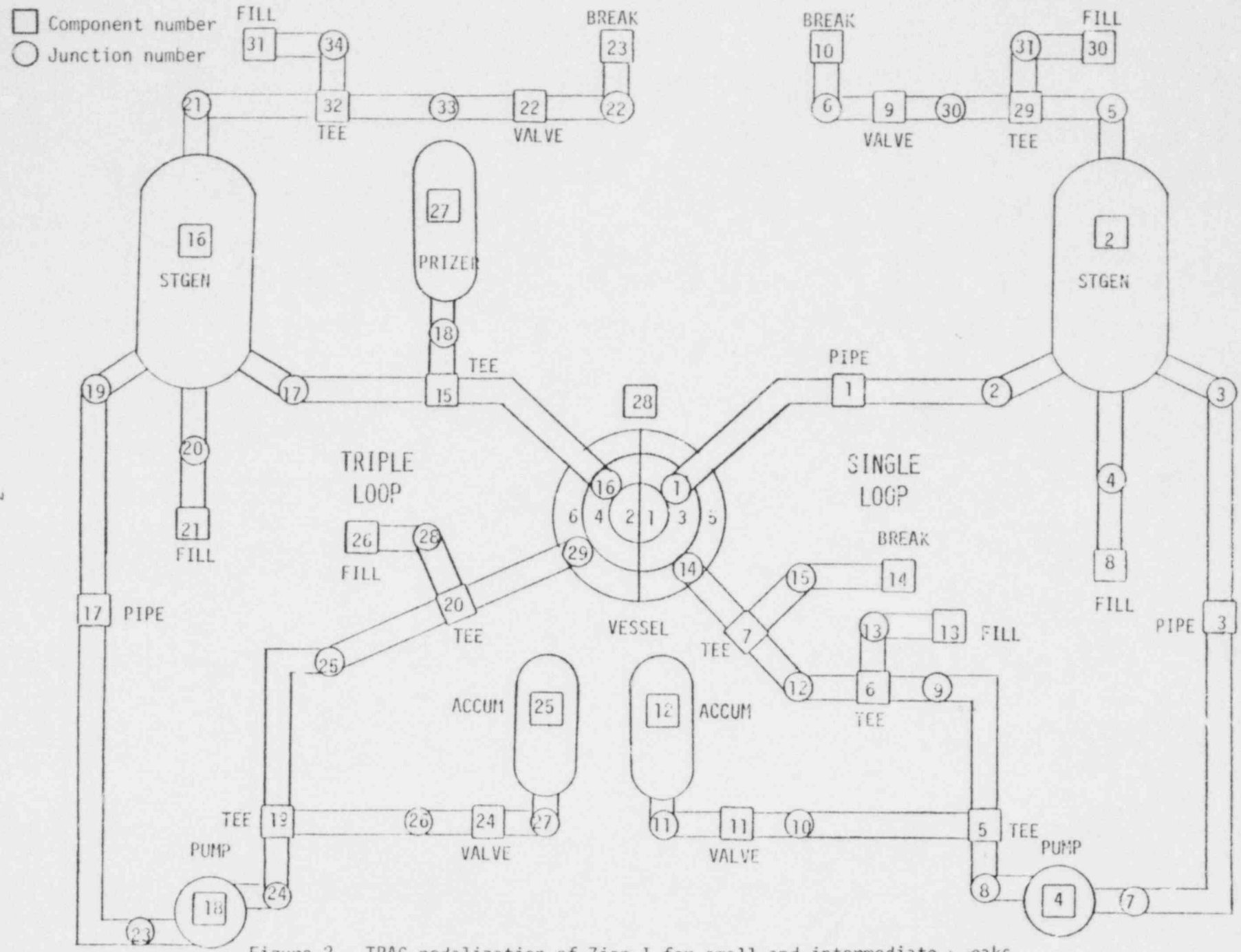

Figure 2. TRAC nodalization of Zion I for small and intermediate breaks.

a steady state calculation were within 1% of the large (200%) cold leg break which were discussed in the preceding section. Selected boundary conditions were changed to simulate smaller breaks and are discussed in Appendix B.

3. RESULTS

The results of three TRAC-P1A calculations for cold leg breaks using Zion I as a model are presented herein. These calculations simulated a large (200%) break, an intermediate (0.25 m-diameter) break, and a small (0.10 m-diameter) break. The large cold leg break calculation was concluded at 207 s into the transient; it required 18.0 h of CPU time. The lower portions of the core had quenched by 207 s. The calculation was terminated because the code was running slowly and it was judged that no additional information on code capability would be obtained by continuing the calculation. The intermediate break was run to 212 s at which time the core had been quenched. The small break calculation was terminated at 1224 s. The system was depressurizing and accumulator injection would occur before core uncovery. The intermediate break calculation required 8.25 CPU h and the small break calculation used 19.5 CPU h. The time of occurrence of significant events for the three calculations is shown in Table 2.

3.1 Large (200%) Cold Leg Break

The upper plenum pressure response for a 200% cold leg break, shown in Figure 3, was typical of a large cold leg break experiment. The system pressure fell sharply to approximately 9.5 MPa which corresponded with the hot leg liquid saturation pressure. The pressure continued to decrease until 27 s at which time a large volume of water entered the core as shown in Figure 4 and the increased steam generation caused a slight increase in pressure. The increased pressure caused a flow reversal in the core and downcomer increasing the cold leg break flow which is shown in Figure 5. The rapid increase in core inlet flow at 27 s was a result of liquid depletion in the loop accumulators and the following sharp rise in volumetric flow out of the accumulator due to gas injection, Figure 6. The accumulator flow was higher than expected and the accumulator emptied somewhat early due to the modeling technique employed. Figure 7 shows that

TABLE 2. MAJOR EVENT SEQUENCE

Event	Time (s)		
	200% Cold Leg	Intermediate	Small
Time of Rupture	0.0	0.0	0.0
Reactor Scram	0.53	6.04	13.3
Initiation of Broken Loop Accumulator	2.81	147.58	--
HPIS/LPIS Flow Initiation	3.05	3.35	37.02
Initiation of Intact Loop Accumulators	13.00	147.58	--
Pressurizer Emptied	16.3	150.00	350.0
Termination of Broken Loop Accumulators	20.0	184.0	--
Termination of Intact Loop Accumulators	26.30	184.0	--
Start of Refill	24.25	160.0	--
Lower Plenum Refilled	28.0	172.0	--
Start of Reflood	28.1	172.0	--
Core Recovered	--	184.00	--

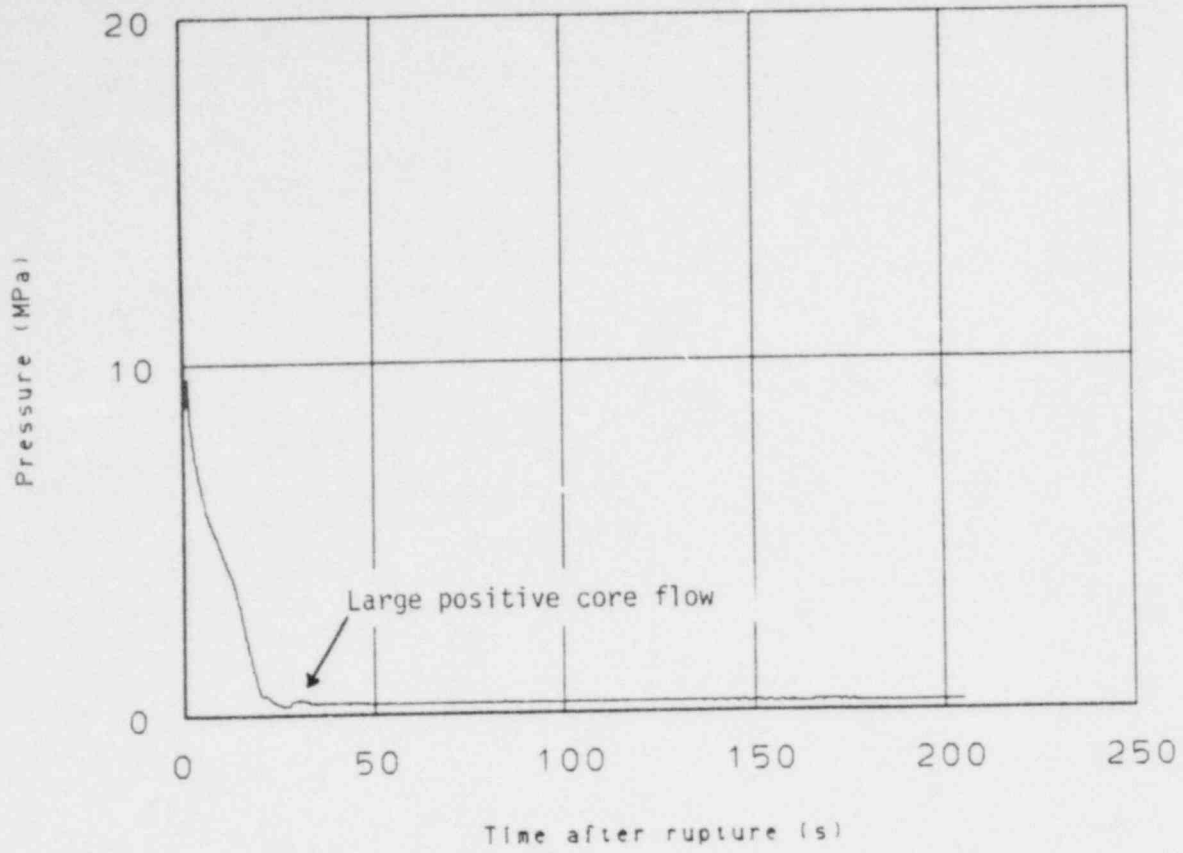

Figure 3. Upper plenum pressure, large break.

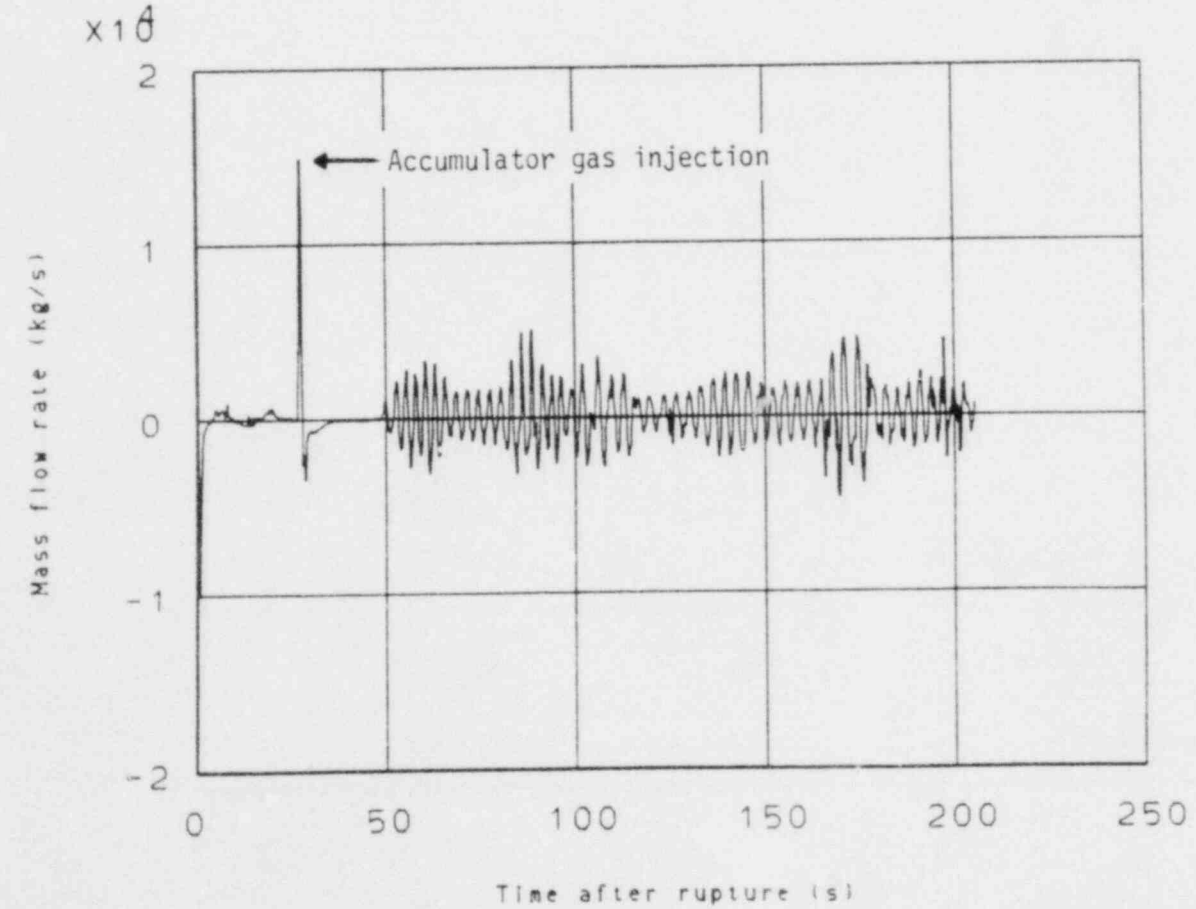

Figure 4. Core inlet mass flow rate, large break.

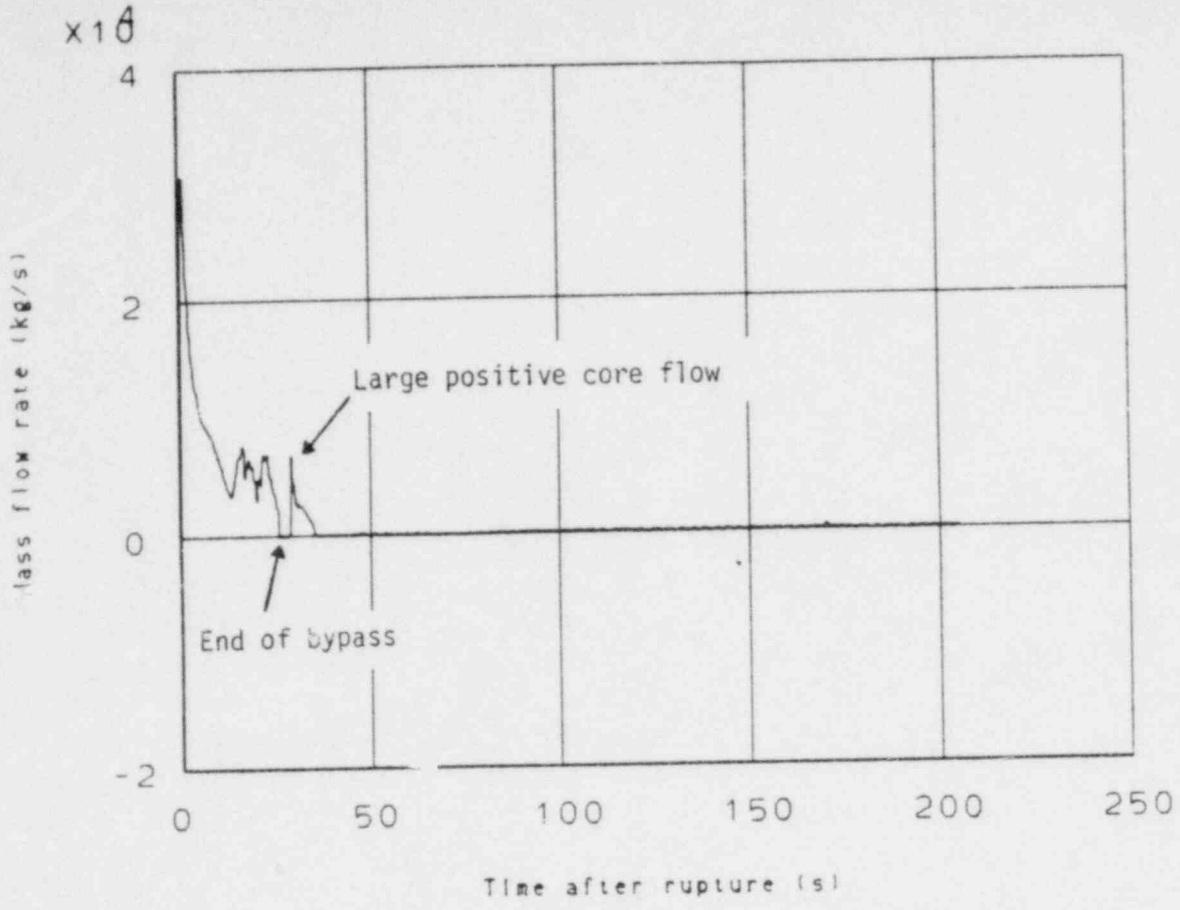

Figure 5. Cold leg break mass flow rate, large break.

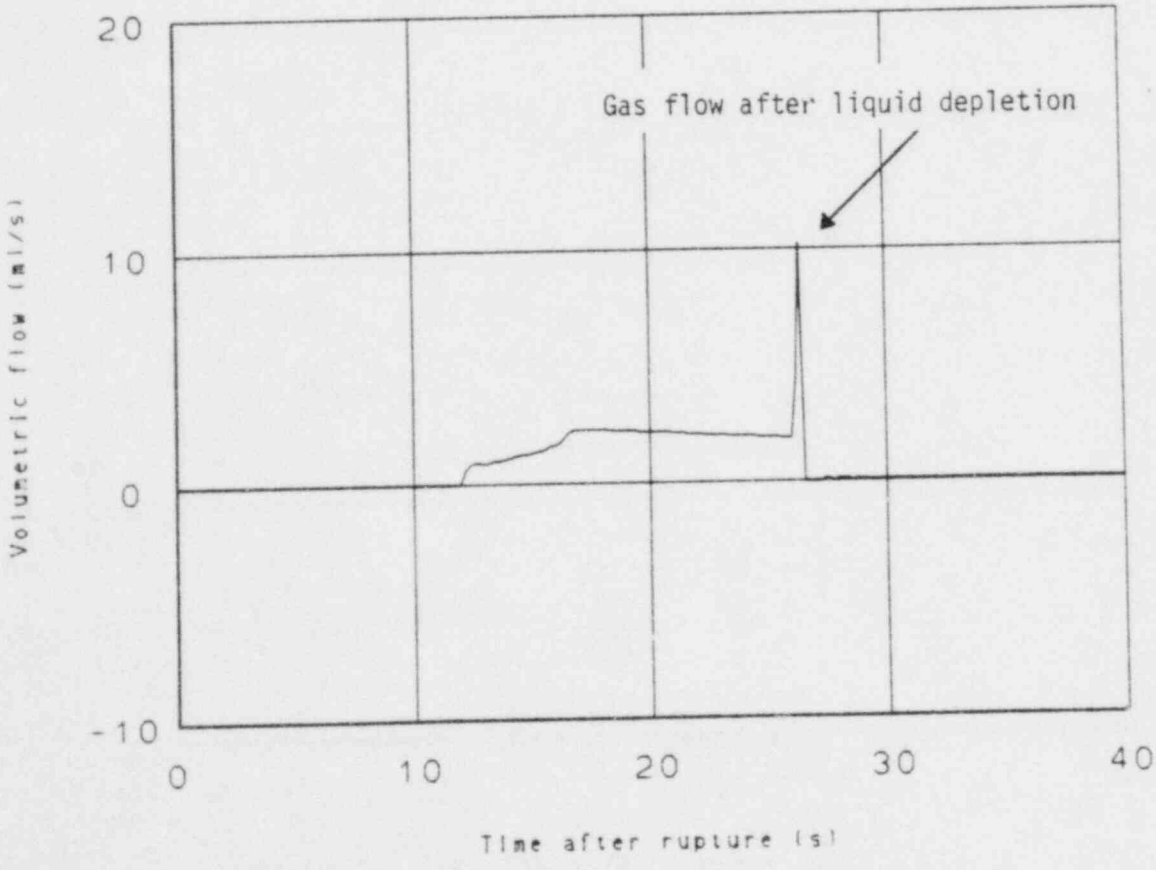

Figure 6. Accumulator volumetric flow rate, large break.

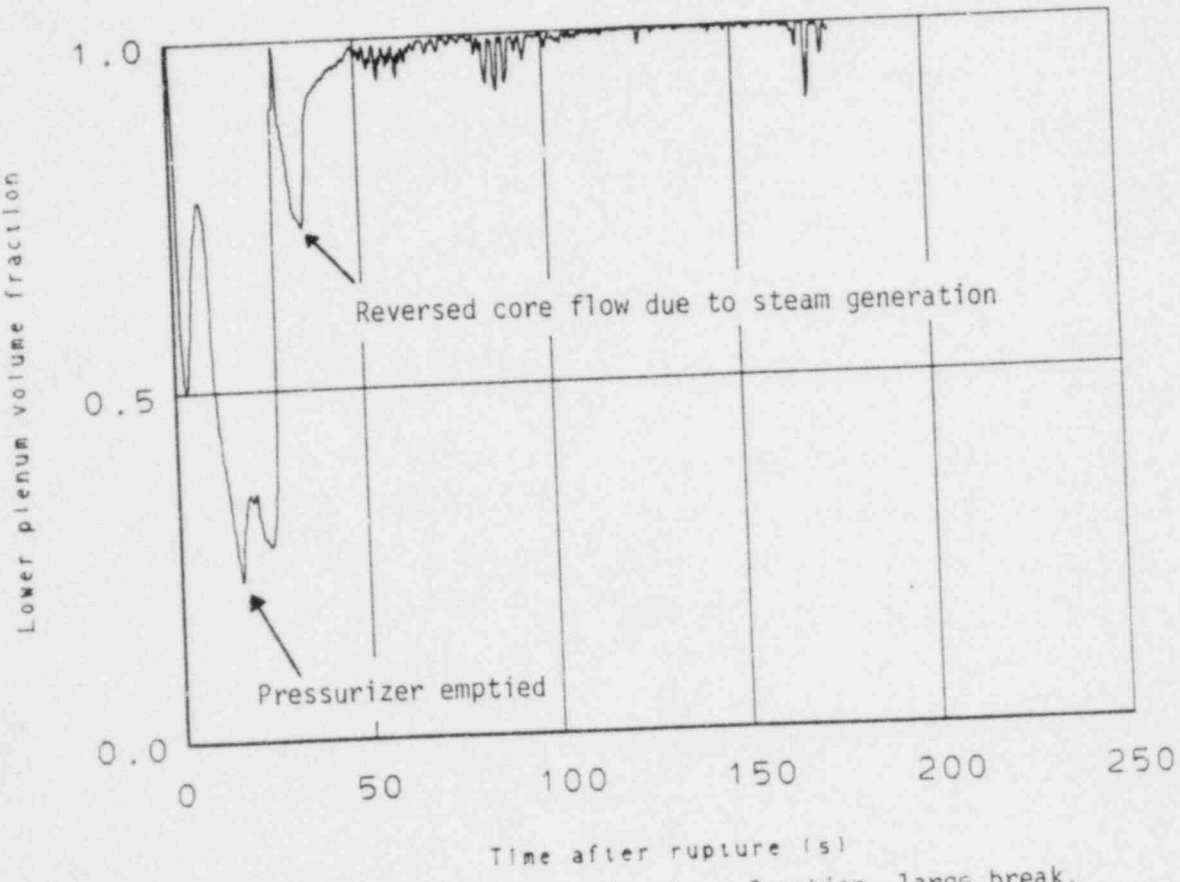

Figure 7. Lower plenum liquid volume fraction, large break.

the mass remaining in the vessel after the flow reversal was adequate to nearly fill the lower plenum. HPIS and LPIS flow was then the only source of liquid which required considerable time to reflood the core.

Short term cladding temperatures for rod 5 (inner ring) are shown in Figure 8. The onset of critical heat flux ranged from 0.9 s to 1.4 s and was dependent on the axial position. Rod 13 (outer ring) short term cladding temperatures are shown in Figure 9. The variation of critical heat flux times ranged from 1.0 s for core midplane to 3.8 s for the upper most axial position. The onset of critical heat flux was followed by a rapid rise in cladding temperature as heat transfer degraded and the stored energy of the fuel was redistributed. Rod cladding temperature behavior early in the transient was typical of that observed in LOFT Test L2-3.[8] The axial rod cladding temperature profiles for rod 5 and rod 13 are shown in Figure 10. A peak cladding temperature of 1365 K occurred late in the transient at about 150 s in core level 4. This peak temperature was somewhat higher than expected and upon investigation it was determined that the internally calculated gap conductance was considerably lower than expected. A sensitivity calculation was conducted with a higher value input for the gap conductance which resulted in approximately 200 K lower cladding temperature. A discussion of these results is contained in the following section. Quenching occurred in core level 1 from 74 s for the rods in the outer radial ring to 113 s for the inner rods. At 207 s when the calculation was stopped, the cladding temperatures in level 2 were decreasing and approaching a quench temperature. During reflood the quench front was propagated from the bottom only whereas results from scaled experiments[9] showed a top quench front also. Little entrainment of core fluid was calculated during the reflood contributing to the quench from the bottom only. From the rod clad temperature trends it was judged that continuation of the calculation beyond 207 s would have resulted in all rods quenching. Also, none of the cladding temperatures were expected to exceed the earlier peak clad temperature of 1365 K.

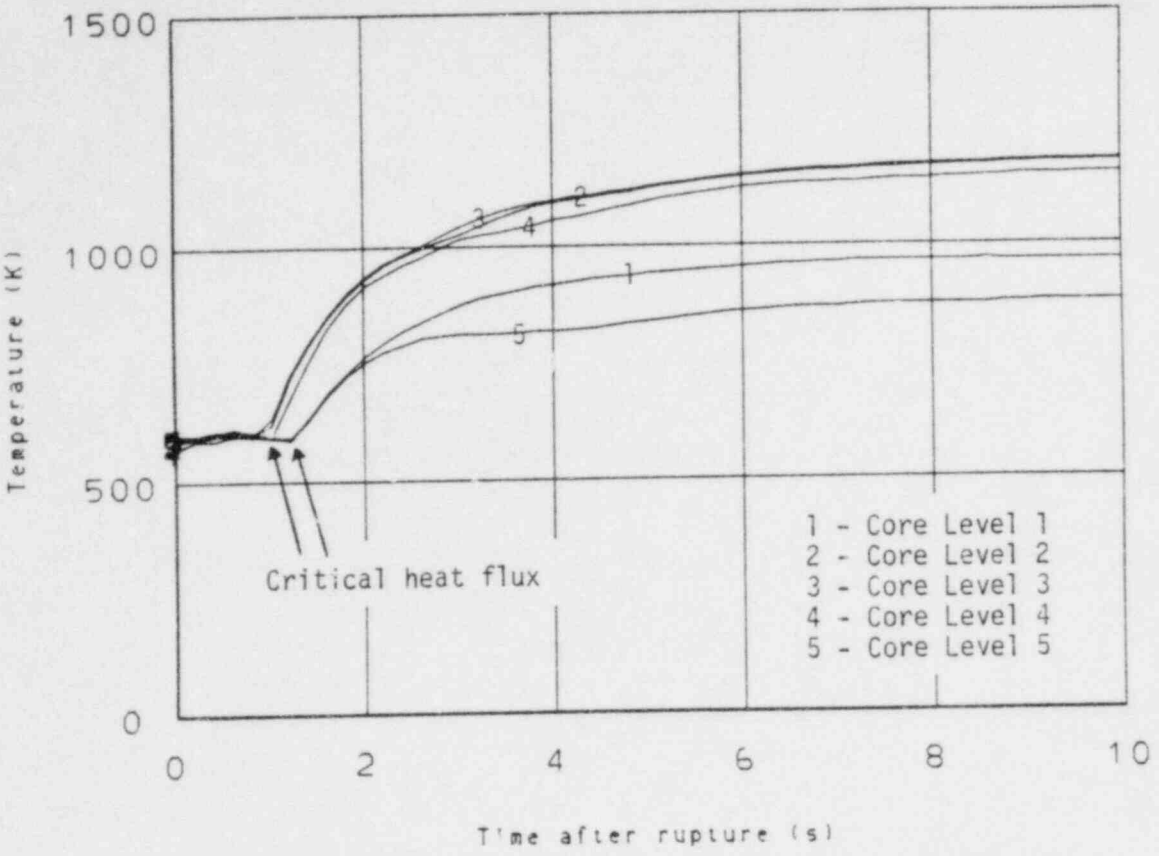

Figure 8. Rod 5 cladding temperatures short-term, large break.

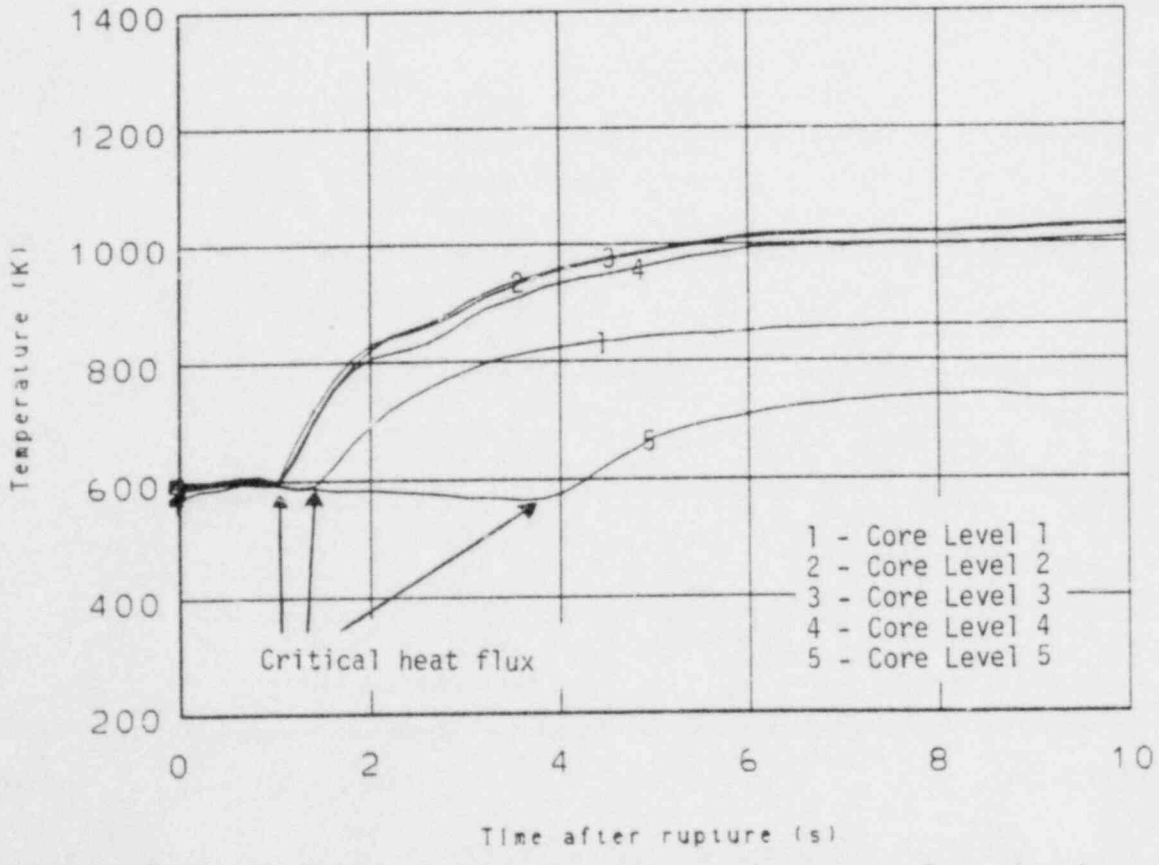

Figure 9. Rod 13 cladding temperatures short-term, large break.

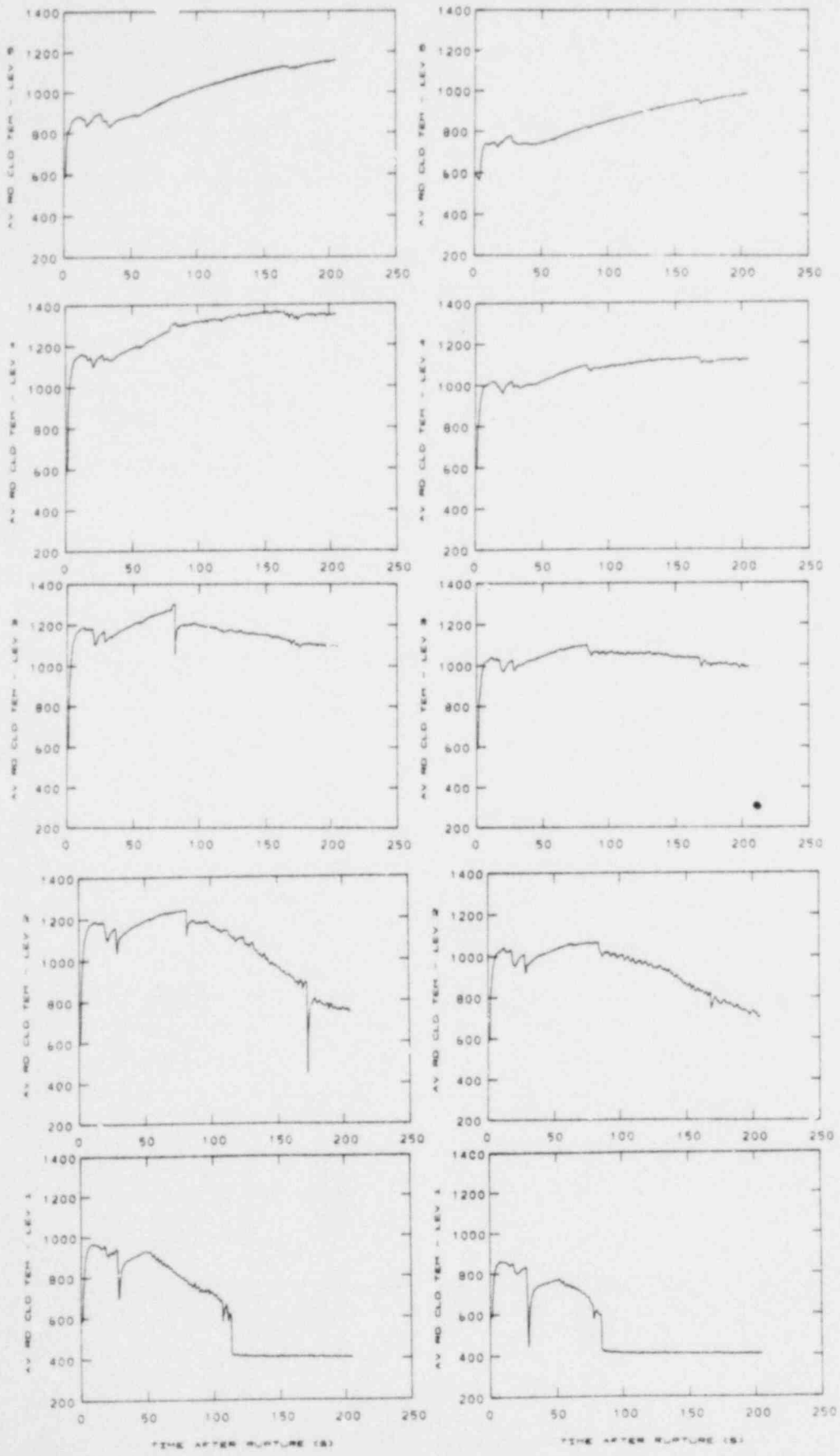

Figure 10. Rod 5 and Rod 13 long-term cladding temperatures, large break.

The effects of the pressurizer are shown in Figure 11 which shows the mass flow rate in loop 2 and 4 hot legs. The flow was predominately into the upper plenum from loop 4 which contained the pressurizer until about 16 s whereas flow in the other loops hot legs was out of the upper plenum until about 9 s. The flow into the vessel from the pressurizer tended to delay the depressurization of the upper plenum. At 16.5 s when the pressurizer was empty, less than 0.1 m liquid level as shown in Figure 12, the loop 4 hot leg flow reversed helping vent the upper plenum. This upper plenum venting permitted the lower plenum to begin its refill (Figure 7). The loop 2 hot leg flow also reversed direction at 9 s as a result of steam generation in the primary system from the steam generator.

Behavior in the cold leg is illustrated by Figure 13 which is typical of the mass flow in each intact loop cold leg. A mass flow rate of just over 5000 kg/s was maintained until 4.5 s when the void fraction in the cold leg began increasing as shown in Figure 14. The mass flow at 13 s had dropped to 650 kg/s when the accumulator flow was initiated.

Accumulator flow reduced the void fraction and increased the mass flow in the cold leg at this time. The void fraction dropped with initiation of the accumulator and reached 0.75 at 15.2 s after 2.2 s of accumulator injection. The void fraction then increased for 1.3 s before being reduced sharply to less than 0.20. The increase in void fraction during a time of accumulator flow was a result of condensation reducing the local pressure shown in Figure 15. The mixture velocity shown in Figure 16 illustrates the rapid increase in velocity caused by the local pressure decrease. This increased velocity tended to sweep out the liquid forcing the void fraction up to 0.92 at 16.4 s. Condensation sharply reduced the local pressure at the same time the void fraction reached 0.75. The interfacial heat transfer model is flow regime dependent with void fraction being the indicator for the flow regime. A transition occurred at a void fraction of 0.75 to an interpolated model between annular mist and slug flow, at a void fraction of 0.50. In the annular mist region the vapor side heat transfer coefficient was too small by a factor of 10 as indicated by U.S.

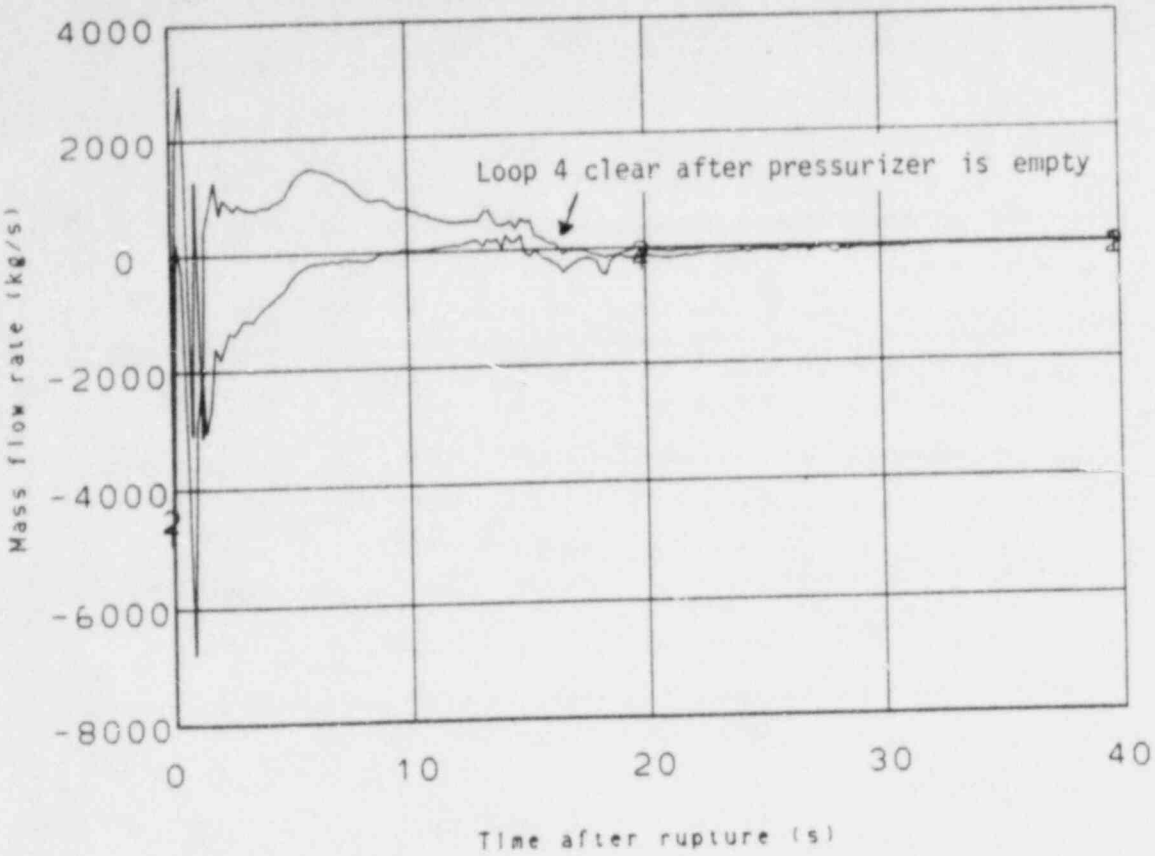

Figure 11. Hot leg mass flow rate, Loops 2 and 4, large break.

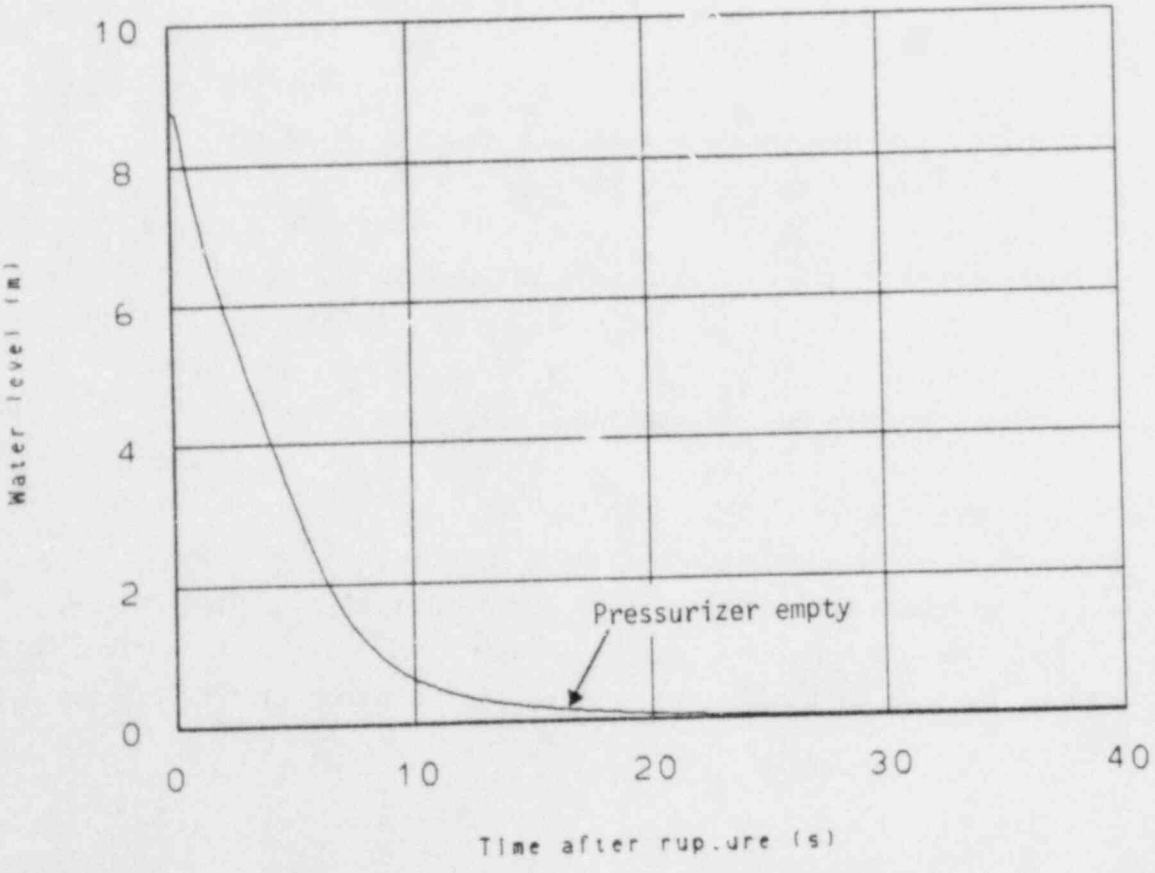

Figure 12. Pressurizer water level, large break.

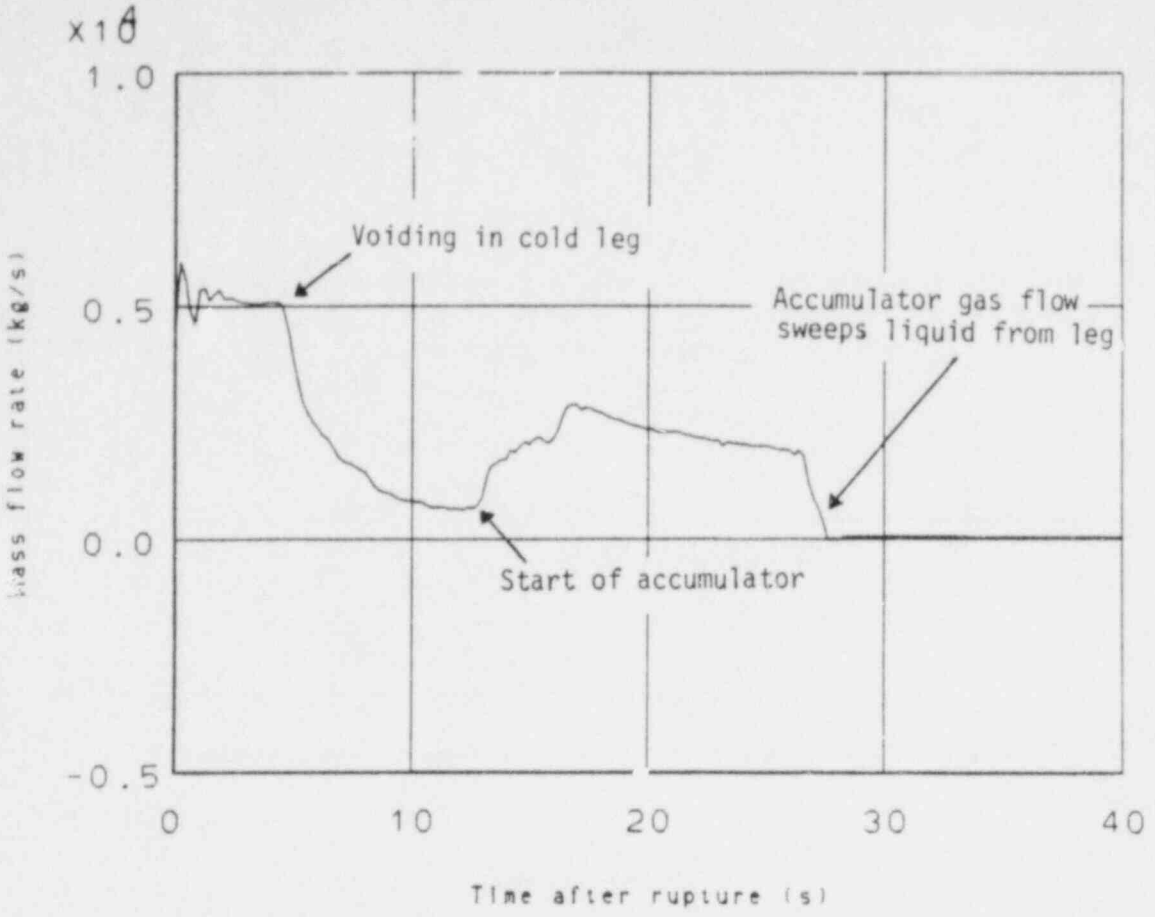

Figure 13. Loop 2 cold leg mass flow rate, large break.

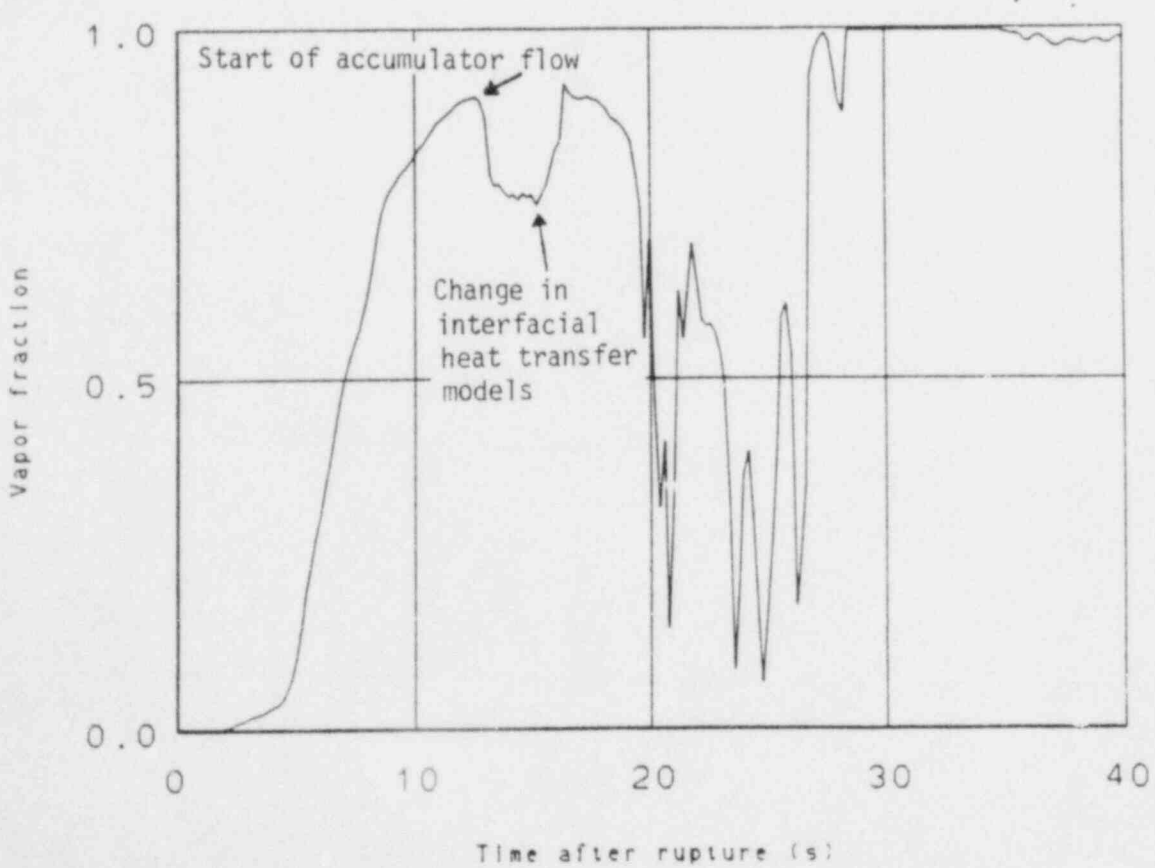

Figure 14. Loop 2 cold leg void fraction, large break.

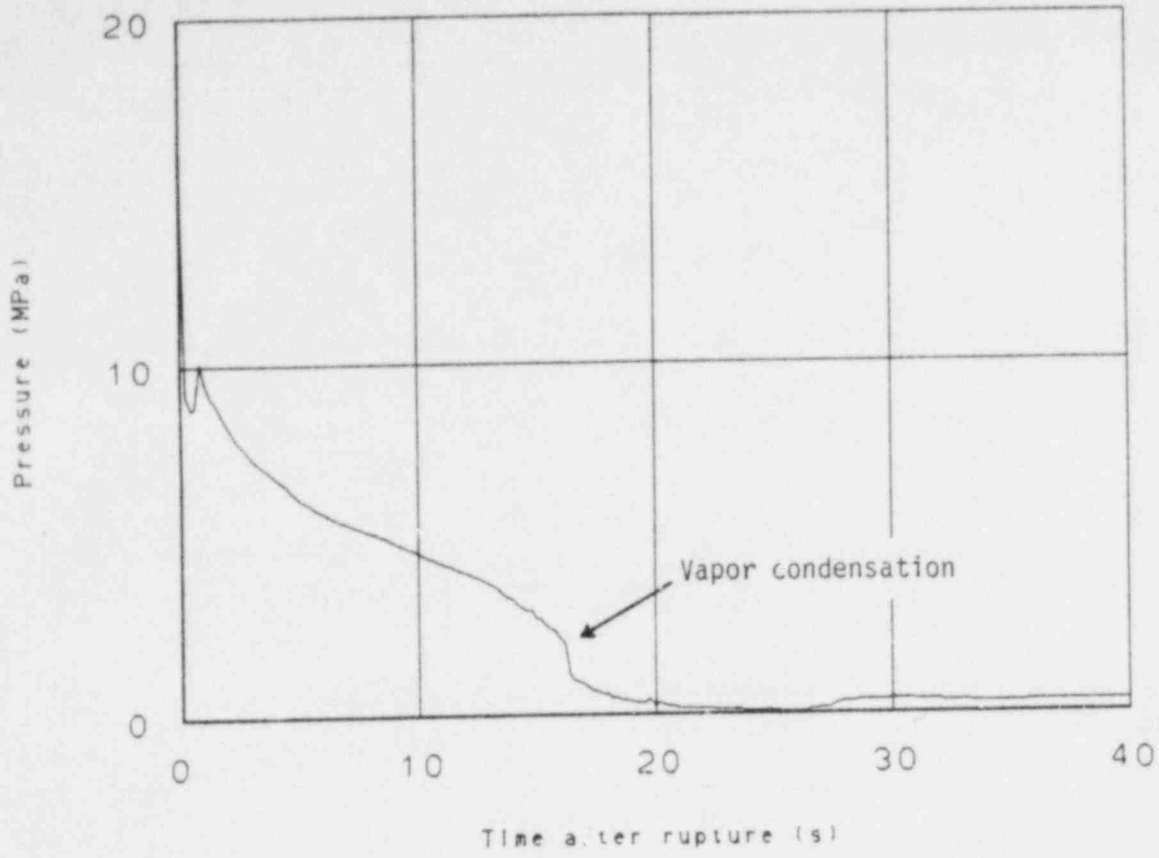

Figure 15. Loop 2 cold leg pressure, large break.

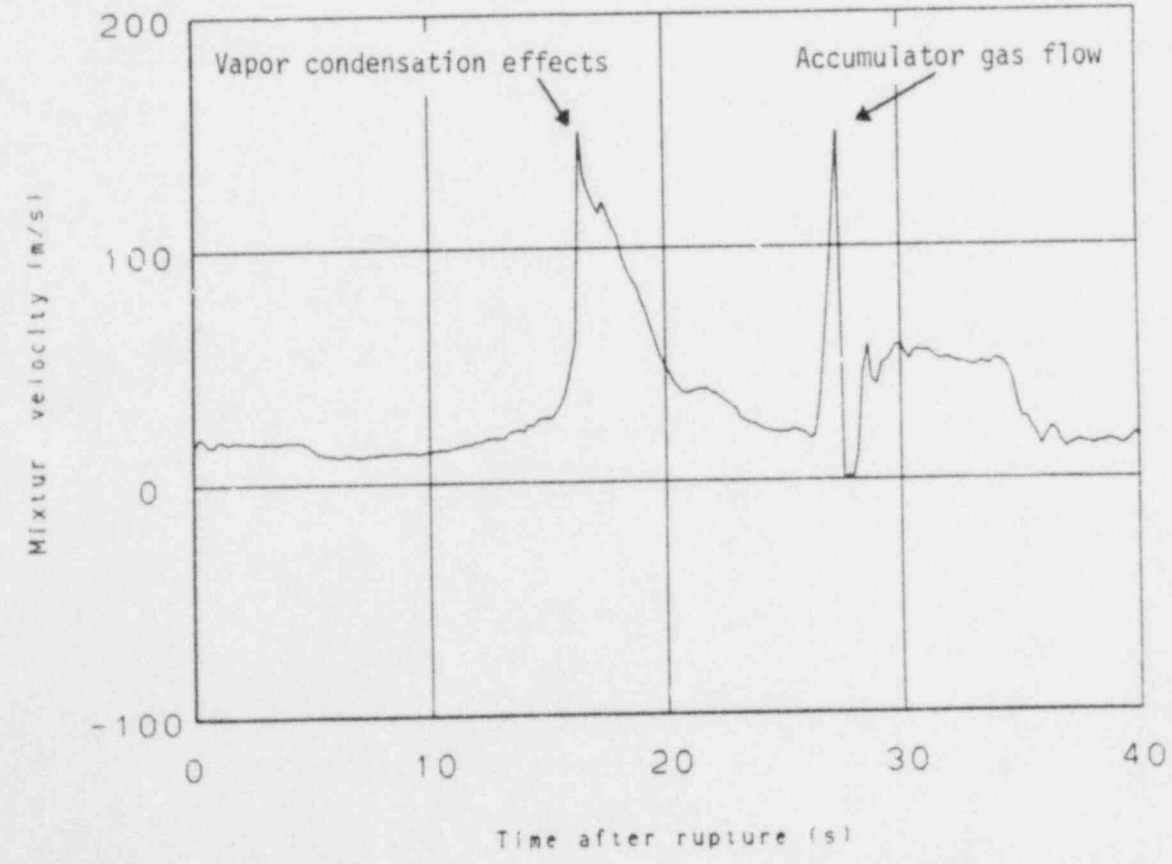

Figure 16. Loop 2 cold leg mixture velocity, large break.

Rohatgi.[10] Local condensation should be a continuous process from the time of accumulator injection of subcooled water but the calculation appeared discontinuous as calculational models were changed at a void fraction of 0.75 causing the effects displayed.

Cold leg liquid temperature, shown in Figure 17, dropped with accumulator initiation at 13 s but the vapor temperature, shown in Figure 17, showed no decrease until 16.0 s. A transition in calculational models at 16.0 s and the smaller heat transfer coefficient during annular flow resulted in the delay in vapor temperature decline and the condensation effect exhibited.

As the velocity in the cold leg decreased the accumulator flow resulted in a decreased vapor fraction in the cold leg. Loop mass flow rate and vapor fraction both show the effects of the increased accumulator volumetric flow shown in Figure 6 at 26 s. The mass flow dropped to zero as the void fraction approached 1.0 due to the liquid being swept out of the pipe by the gas flow. At 28 s mass flow increased as the HPIS and LPIS flow replaced the fluid removed by the gas flow.

Figure 18 shows the void fractions of the unwrapped downcomer. The downcomer was voided during vessel blowdown. At about 26 s the downcomer was refilled from accumulator fluid and the gas injection of the accumulator. Shortly after refill the core flow reversed and voided the downcomer. After 30 s the only source of water was the HPIS and LPIS flow which required considerable time to refill the downcomer and core. After 50 s the downcomer cells having intact cold leg connections showed void fractions which were less than 1.0 in the upper elevations. As the fluid progressed downward the flow was distributed around the downcomer.

A peculiarity was noted in the transient calculation at the vessel connection with the broken pipe. During refill for a short period the break pressure, or containment pressure, exceeded the broken cold leg and downcomer pressure. This could reasonably be expected due to condensation

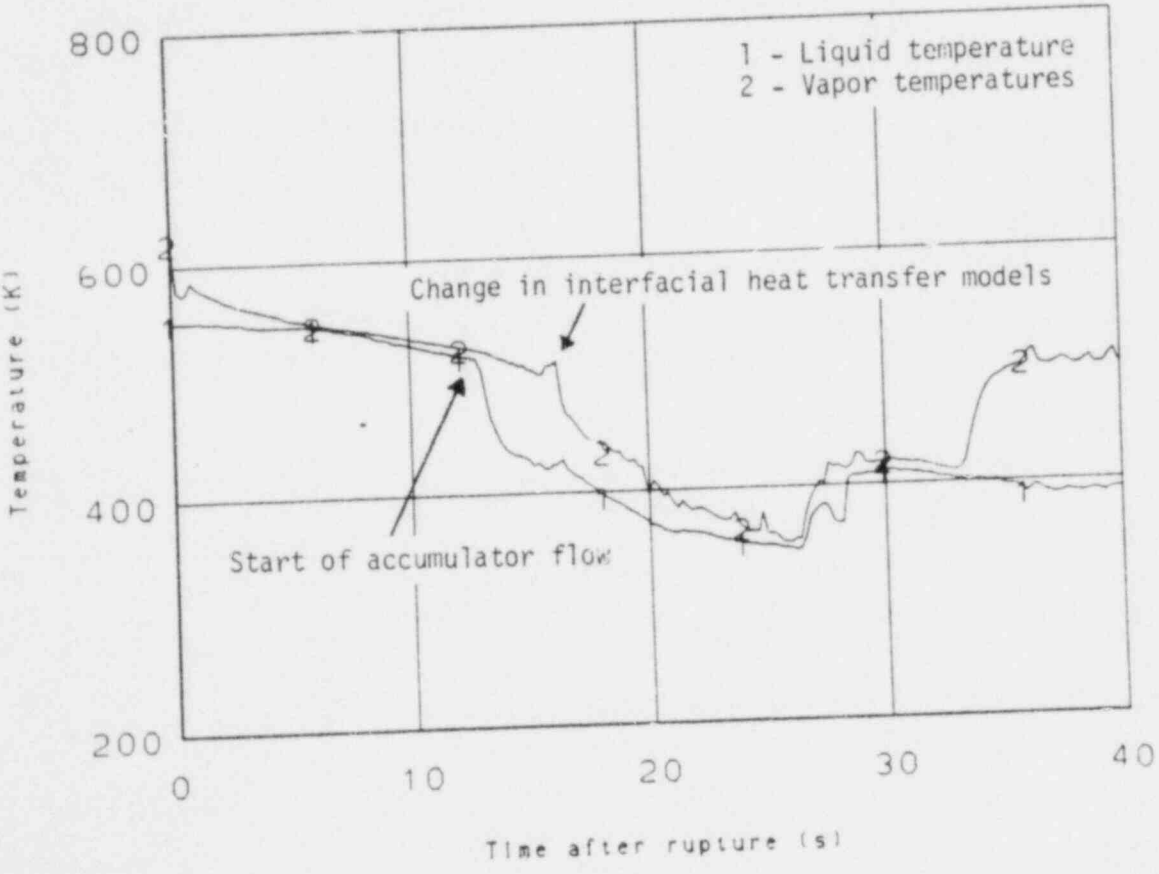

Figure 17. Loop 2 liquid and vapor temperatures, large break.

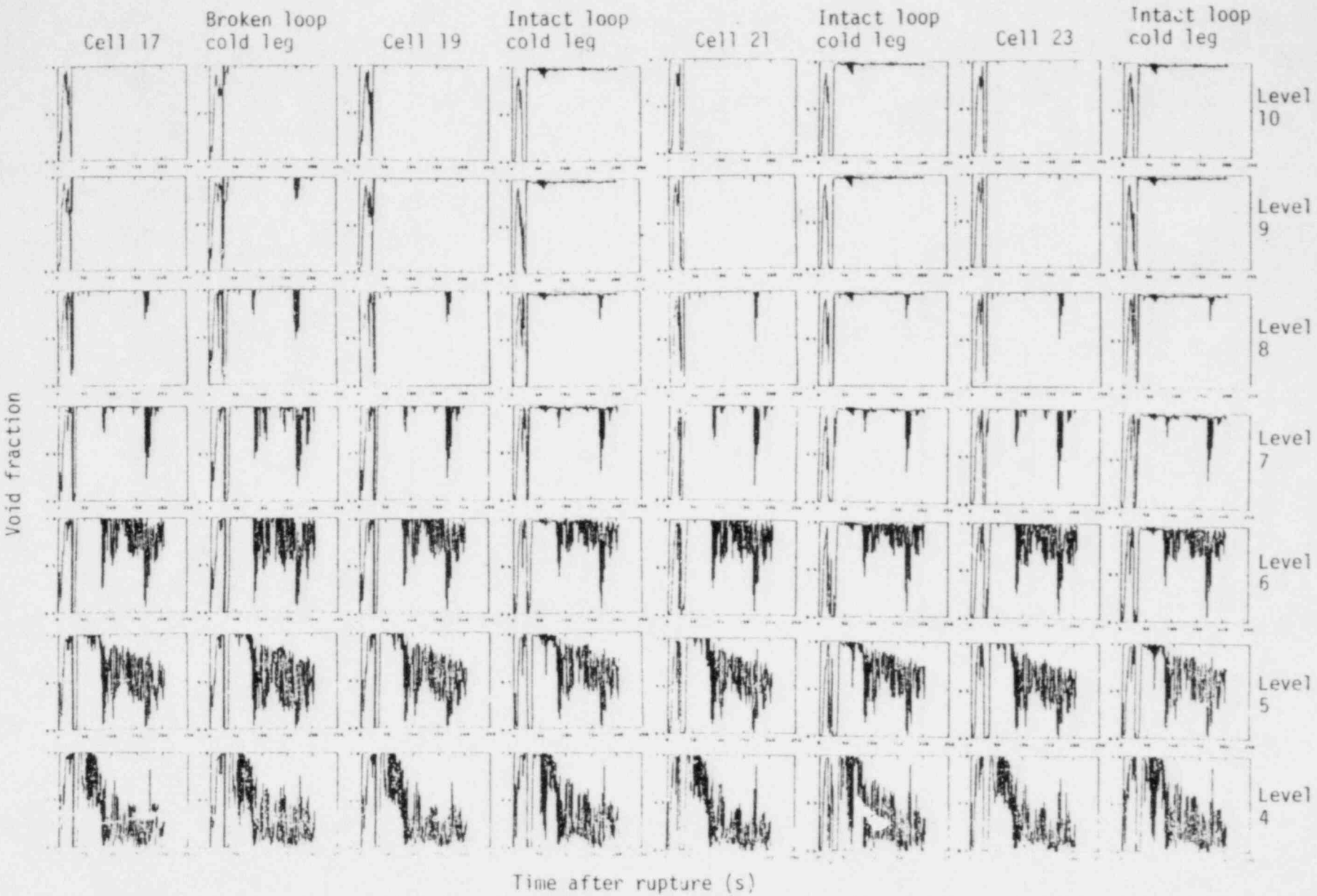

Figure 18. Unwrapped downcomer void fraction, large break.

in the inlet annulus and downcomer. However, TRAC-P1A calculated a flow toward the break against the pressure gradient. The momentum of the fluid was reviewed and was determined insufficient to support counter flow against the pressure gradient. The phenomena seemed to occur at the vessel-broken pipe junction, where a transition occurred from the three dimensional vessel to the one dimensional pipe.

A few key parameters were selected from the BE/EM study[3] best estimate calculation for comparison with the TRAC-P1A calculation. Figure 19 shows the cold leg break flow. Both calculations are reasonably similar in the early stages of the transient with the TRAC calculation exhibiting a higher mass flow during subcooled blowdown and after initiation of accumulator flow at 13.0 s. Both calculations show the break flow going to zero and then experiencing flow spikes due to the core repressurization. The broken loop hot leg mass flow shown in Figure 20 also compares well to about 20 s where the TRAC calculated flow decreased about 8 s sooner than the BE/EM calculation. This early decrease was a result of the accumulator emptying sooner in the TRAC calculation.

The accumulator flows shown in Figure 21 indicate the TRAC accumulator empties faster than the BE/EM accumulator. The difference in flow rates and emptying times was due to the modeling techniques used for the accumulator. Both accumulators agree well on the time of initiation at about 13 s.

Figure 22 compares the rod cladding temperatures at the midplane for the TRAC-P1A calculation and the BE/EM study.[3] The large disagreement between the two calculations was due to the gap conductance calculated by TRAC and a sensitivity study is reported in the following section.

The overall response of the large (200%) cold leg calculation was somewhat similar to the LOFT L2 series of nuclear tests. The calculated depressurization was faster due to different initial system conditions. Figure 23 compares the system pressure for LOFT L2-3[8] with the TRAC-P1A

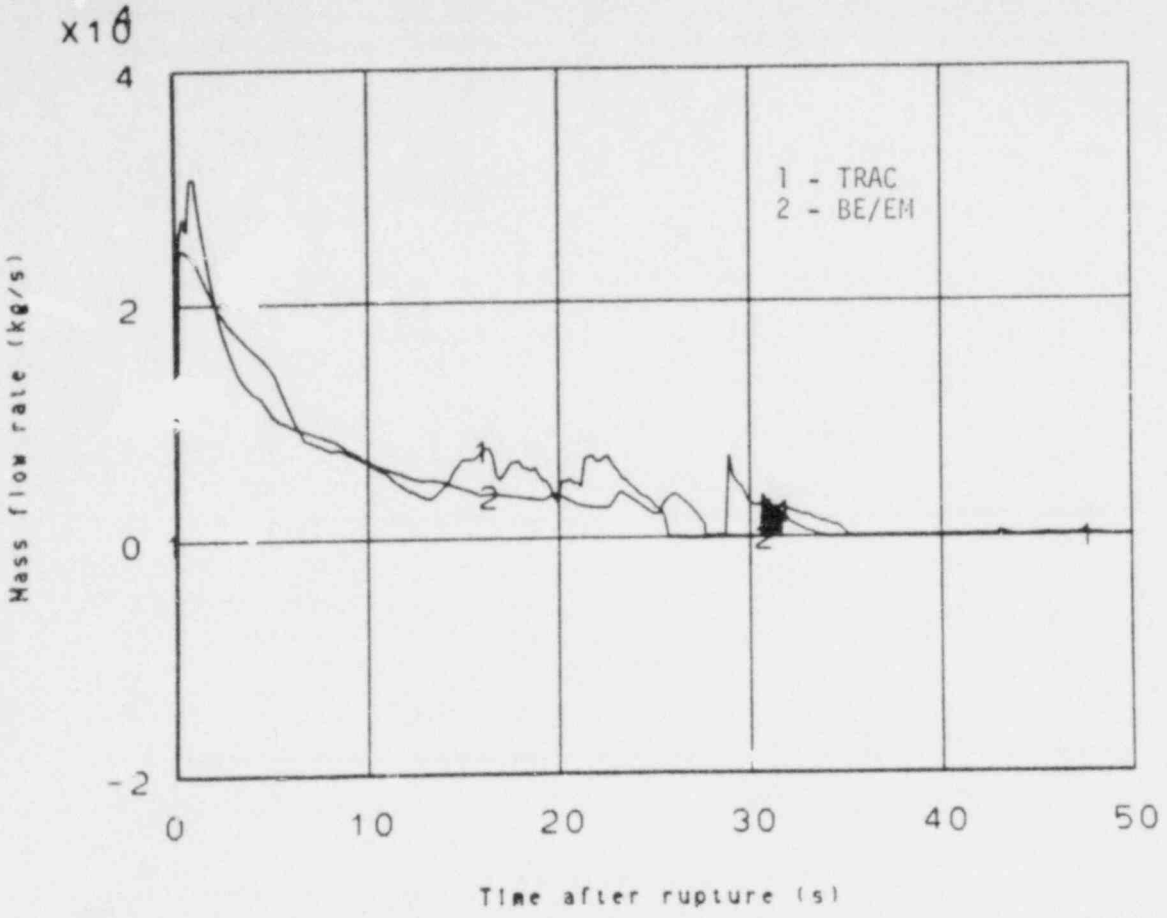

Figure 19. Cold leg break mass flow comparison, large break.

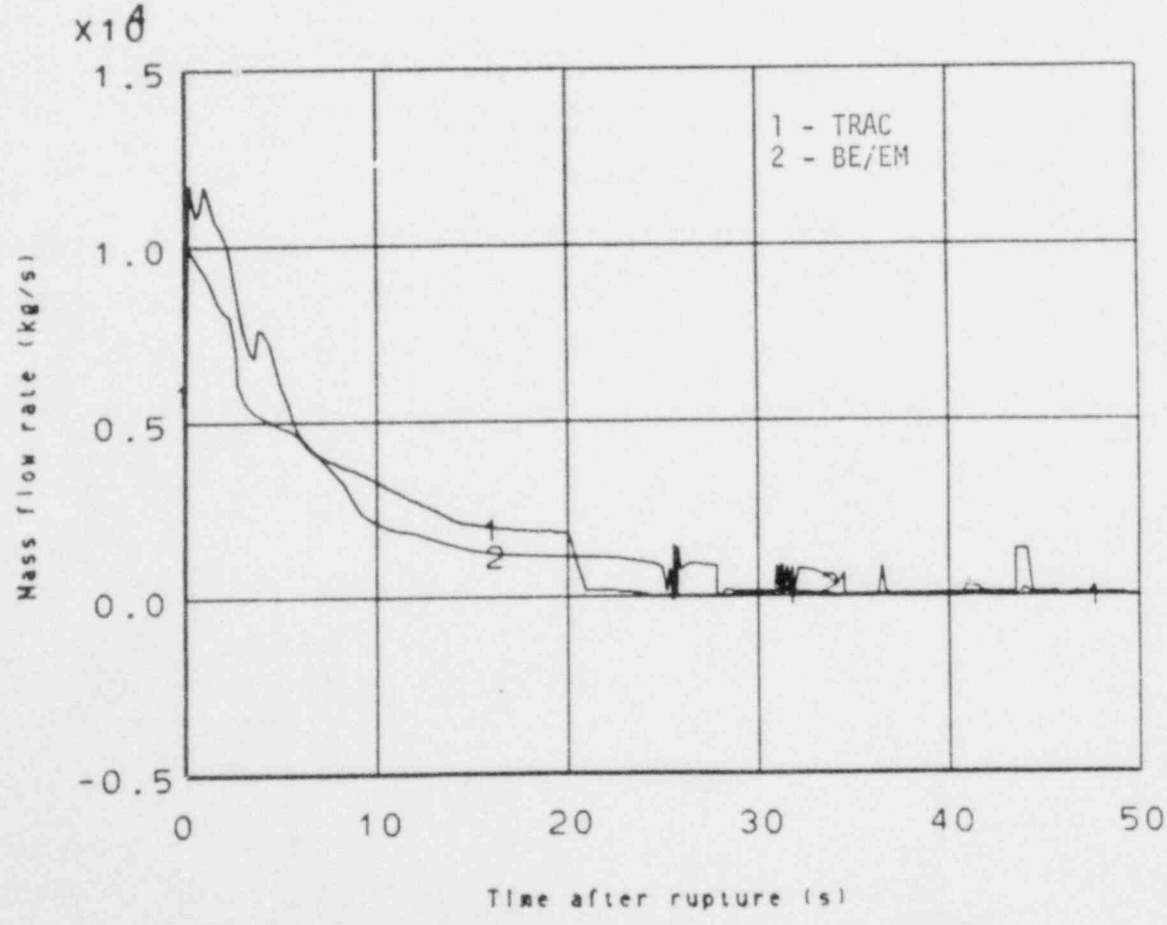

Figure 20. Hot leg break mass flow comparison, large break.

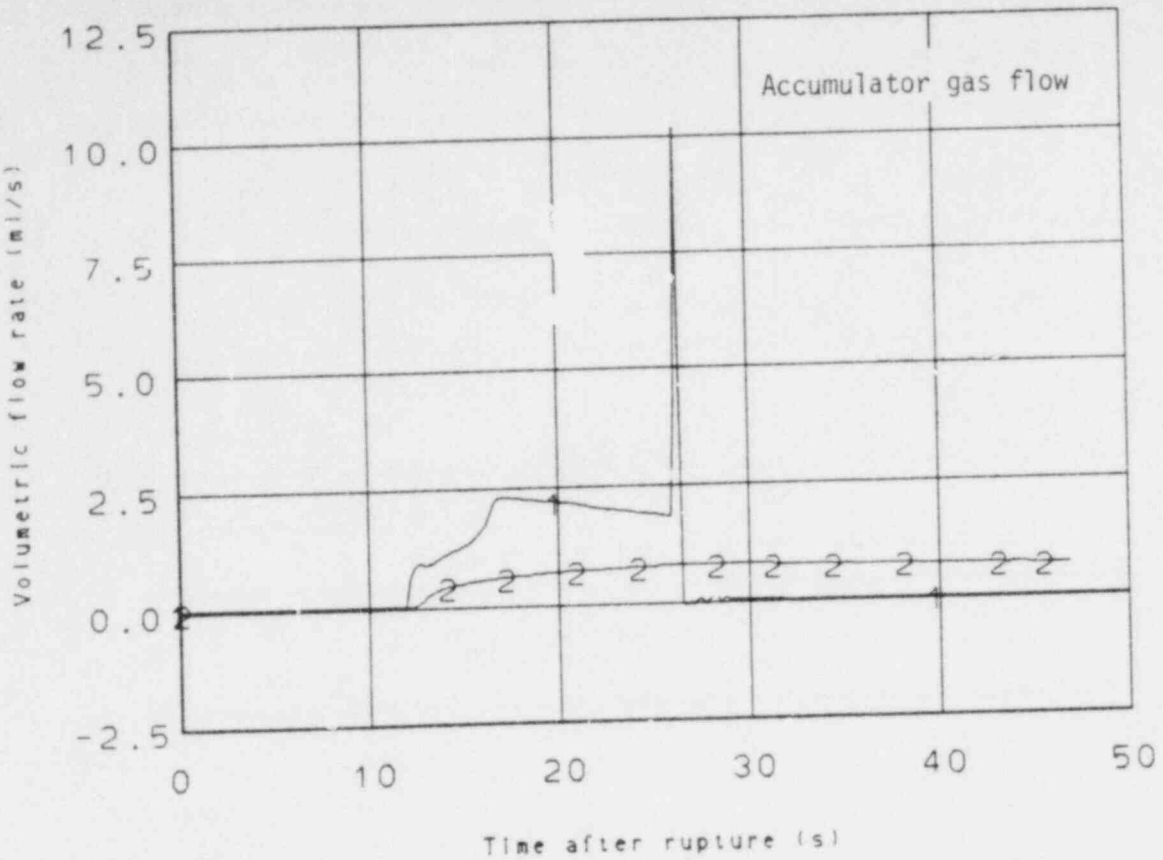

Figure 21. Accumulator volumetric flow comparison, large break.

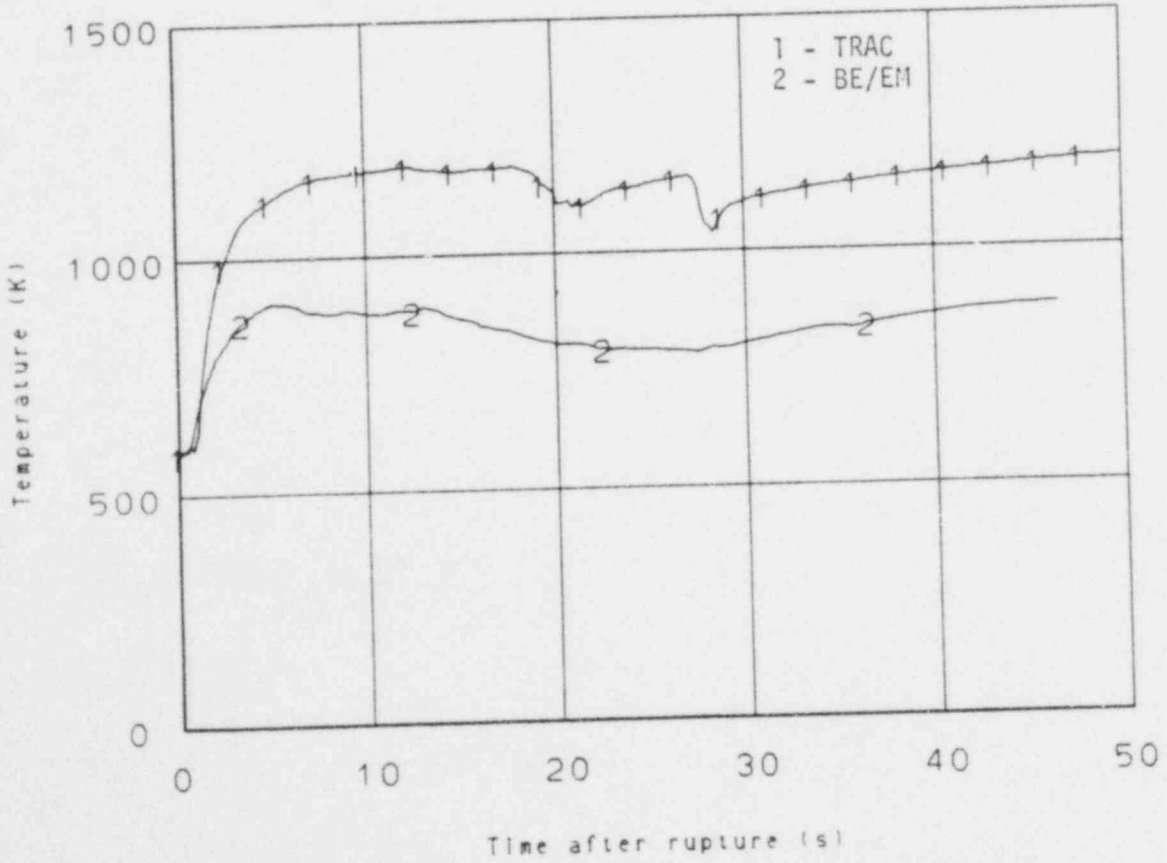

Figure 22. Rod cladding temperature comparison, large break.

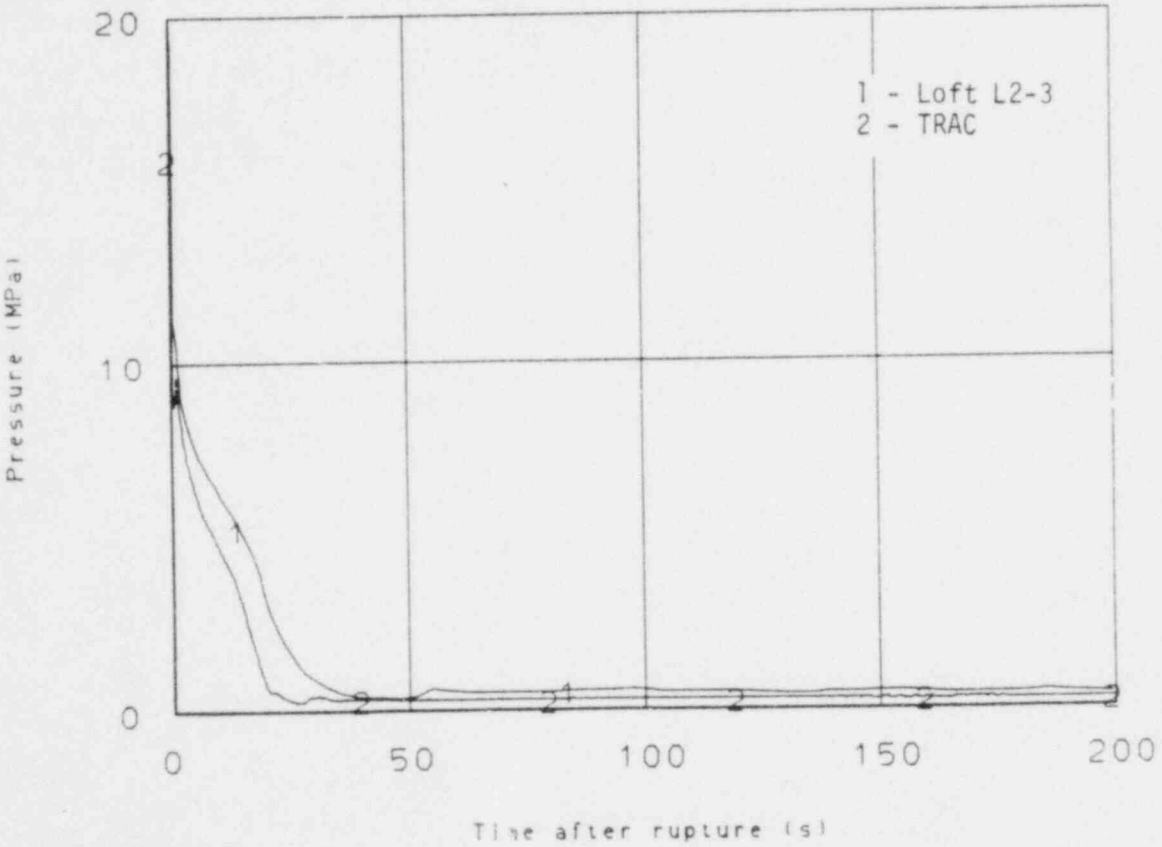

Figure 23. Large break pressure comparison with LOFT test L2-3.

calculation. The hot leg temperature for LOFT Test L2-3 was higher which resulted in a smaller initial depressurization to saturation temperature. Both pressures decreased at similar rates until 13 s when the TRAC calculation showed a increased depressurization due to accumulator injection about 4 s earlier than the experiment. The rod cladding temperatures looked similar early in the calculation before LOFT experienced a rewet.

3.2 Intermediate (0.25 m-diameter) Break

The initial system depressurization for the intermediate break was similar to a large (200%) break where system pressure dropped to saturation pressure corresponding to the hot leg fluid temperature. Upper plenum pressure shown in Figure 24 decreased rapidly to 10.9 MPa and remained nearly constant until 6.0 s. Reactor scram occurred at 6.0 s reducing the energy input from the core and the core liquid temperatures decreased. As the liquid temperature dropped in the upper plenum the system pressure followed the saturation temperature. At about 9 s the vapor fraction at the break increased rapidly resulting in an increase in the system depressurization rate. From 18 s to 164 s the pressure followed the saturation temperature of the fluid, similar to a large break. At 164 s subcooled liquid injected by the accumulator caused rapid condensation of steam and the lowering of saturation temperature.

Figure 25 shows the mass flow rate at the break. The mass flow rate was constant from just after the break until 6.0 s when the reactor scram occurred. From 6 s to 15 s the void fraction at the break, shown in Figure 26, was rapidly increasing which caused a reduction in the break mass flow rate. From 15 s to 160 s the break mass flow decreased due to the reduction in the system pressure and increased void fraction. The small discontinuity at 57 s was investigated but no phenomenological explanation could be given and it was believed to result from a numerical error. The break flow increased at 160 s as subcooled fluid from the accumulator reached the break, as shown in Figure 26. At 185 s the break

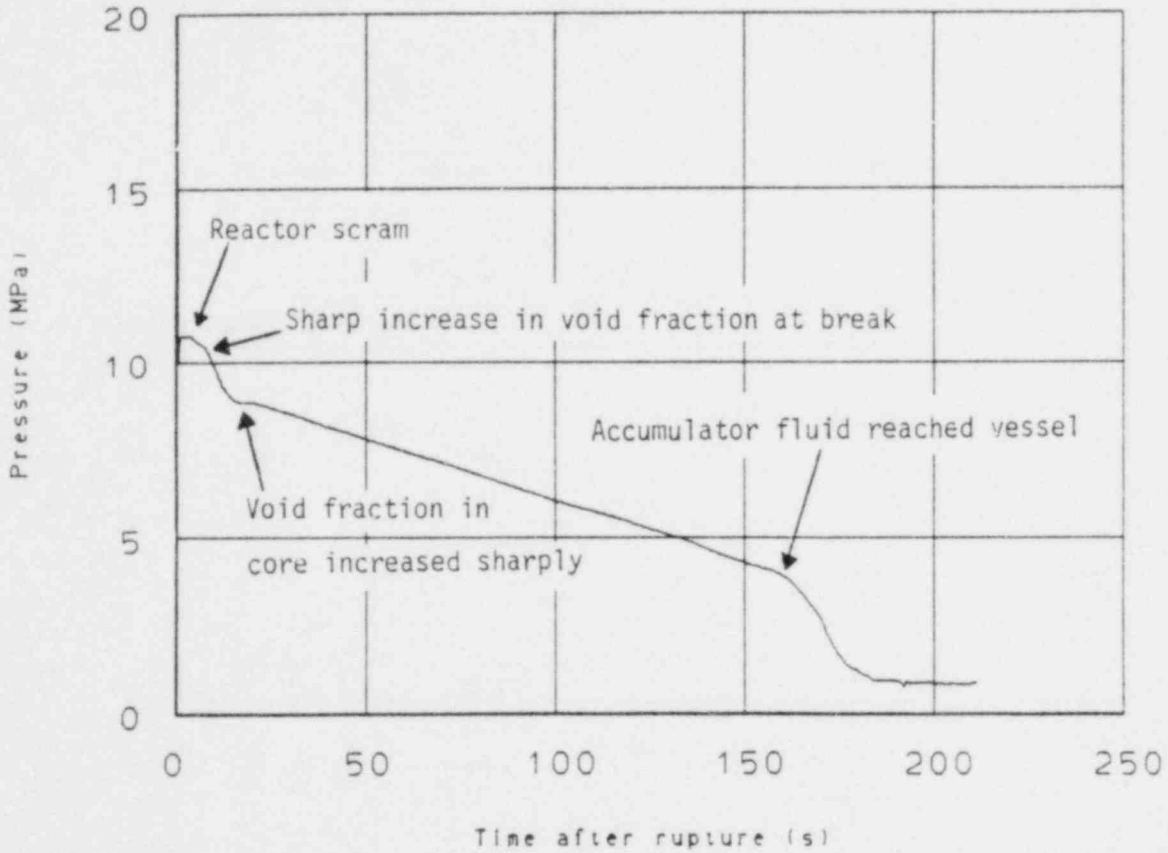

Figure 24. Upper plenum pressure, intermediate break.

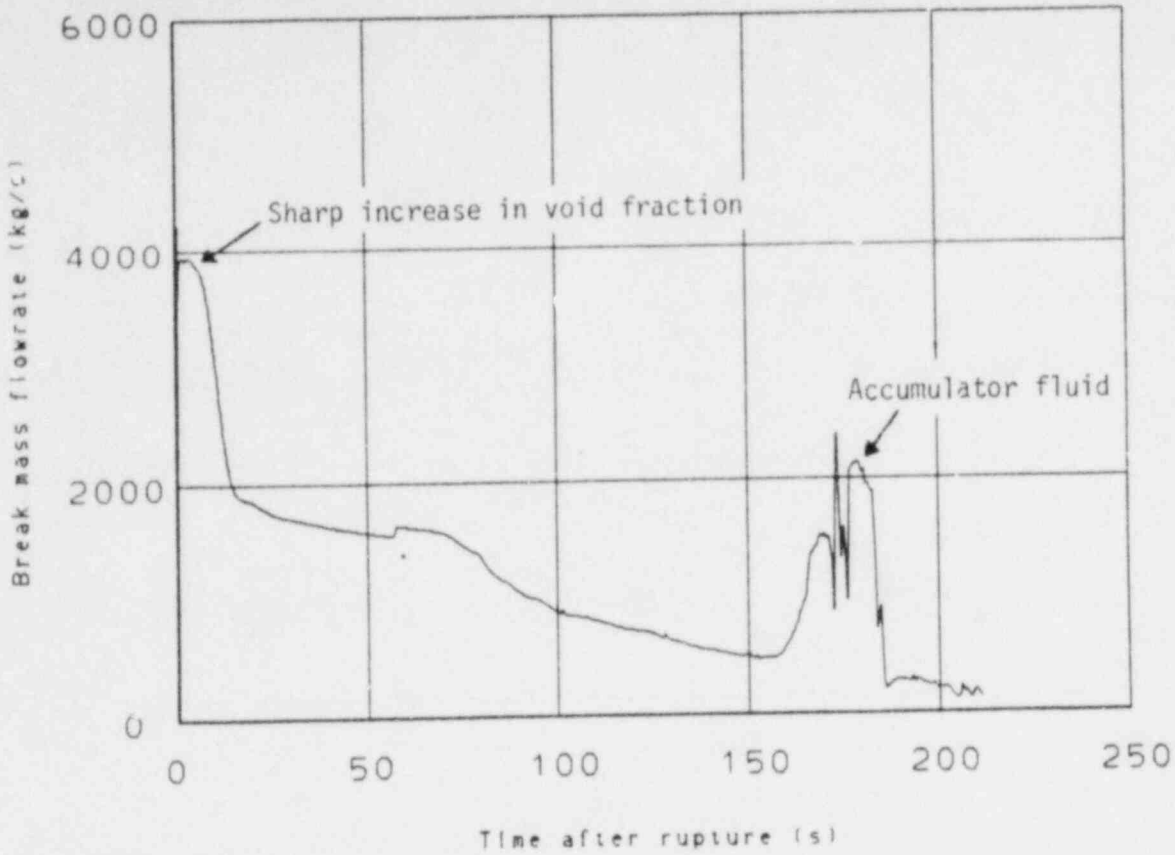

Figure 25. Break mass flow rate, intermediate break.

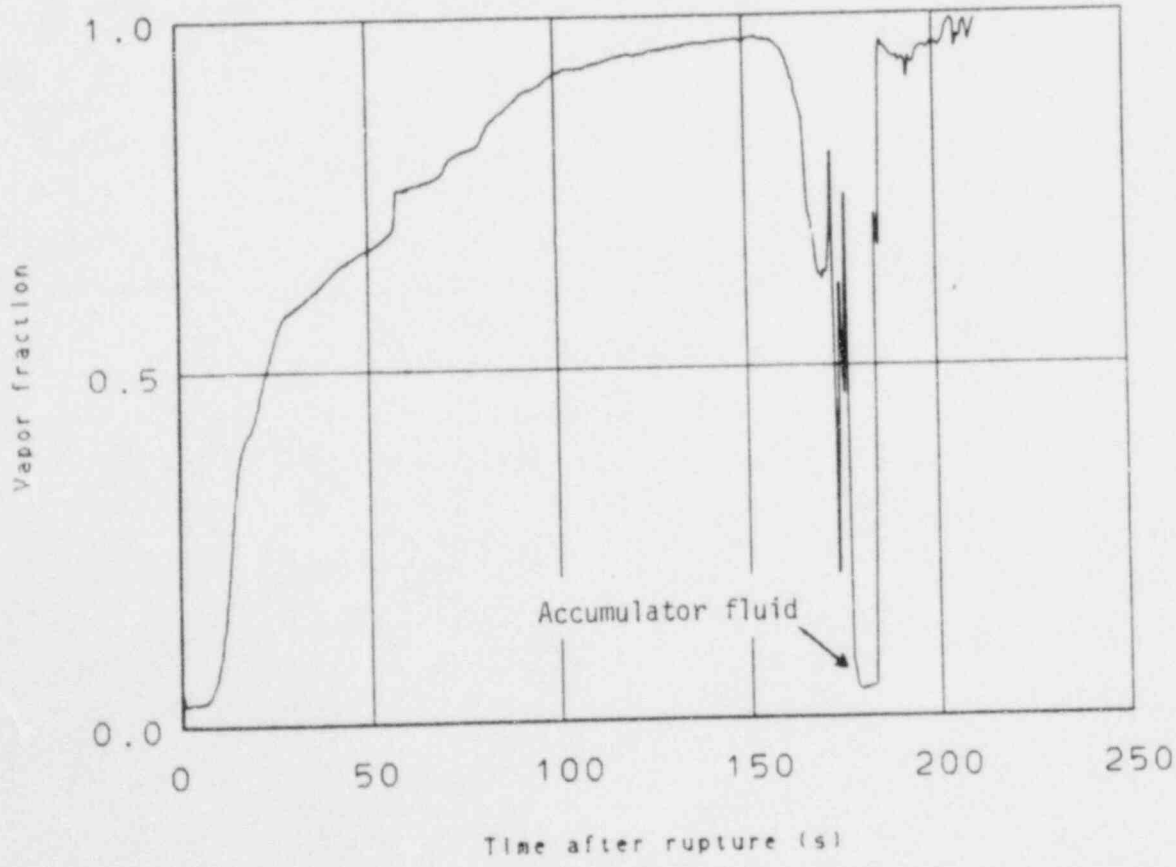

Figure 26. Vapor fraction at the break, intermediate break.

flow dropped as accumulator fluid was depleted and the increased volumetric flow from the accumulator swept the fluid into the vessel leaving only high quality fluid at the break.

Steam generator feedwater was terminated at 2.6 s and the steam outlet valves were closed on the low pressurizer pressure scram signal. The secondary side pressure, shown in Figure 27, began to rise and opened the secondary side safety valves at 14 s when the pressure reached 7.62 MPa. The safety valves closed at about 30 s as the secondary pressure dropped below the setpoint. The secondary pressure continued to decrease until 130 s and then remained constant. The depressurization of the primary side shown in Figure 27 was not delayed by the secondary side response. The volumetric flow rate at the break and low primary side heat transfer due to a high void mixture in the steam generator primary resulted in continued system depressurization. The primary system pressure was less than the secondary from 77 s to the end of the calculation. The steam generator response appeared typical of the larger breaks and reasonable for the intermediate break.

Core inlet mass flow shown in Figure 28 was reduced from 18,000 kg/s initially to 15,000 kg/s as fluid was diverted to the break. The reduced core mass flow resulted in a rod cladding temperature rise of about 10 K as shown in Figure 29. The core inlet flow was nearly constant from this time until 15 s when voiding began in the inlet legs and the lower plenum. Core mass flow was sharply reduced at 160 s as subcooled water from the accumulator entered the cold leg and downcomer collapsing the voids and reducing the pressure. The core flow was reversed due to the resulting differential pressure across the core. Core inlet flow became positive as the lower plenum was filled and water was forced into the core. When the accumulator emptied at 184 s a volume of vapor was forced into the lower plenum decreasing the liquid mass in the lower plenum as shown in Figure 30. The water in the core fell back into the lower plenum causing a momentary negative core inlet flow.

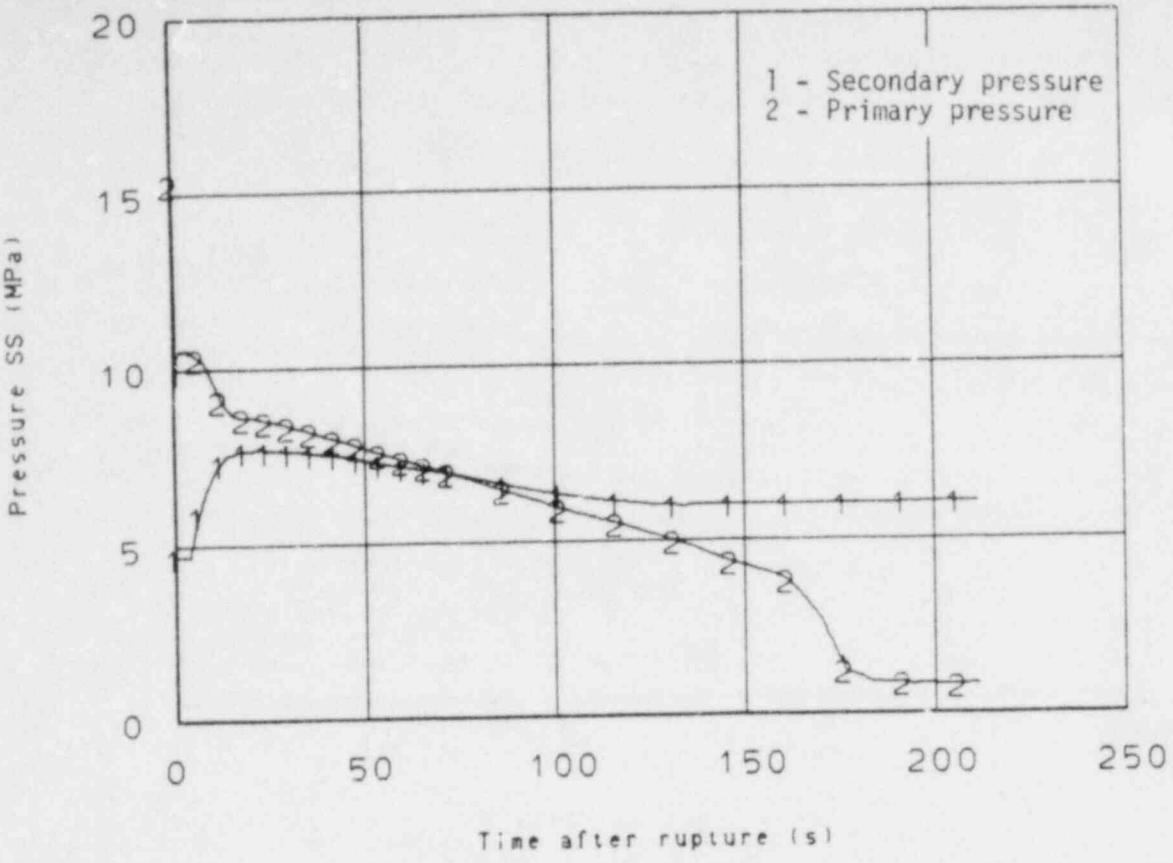

Figure 27. Steam generator pressure, primary and secondary, intermediate break.

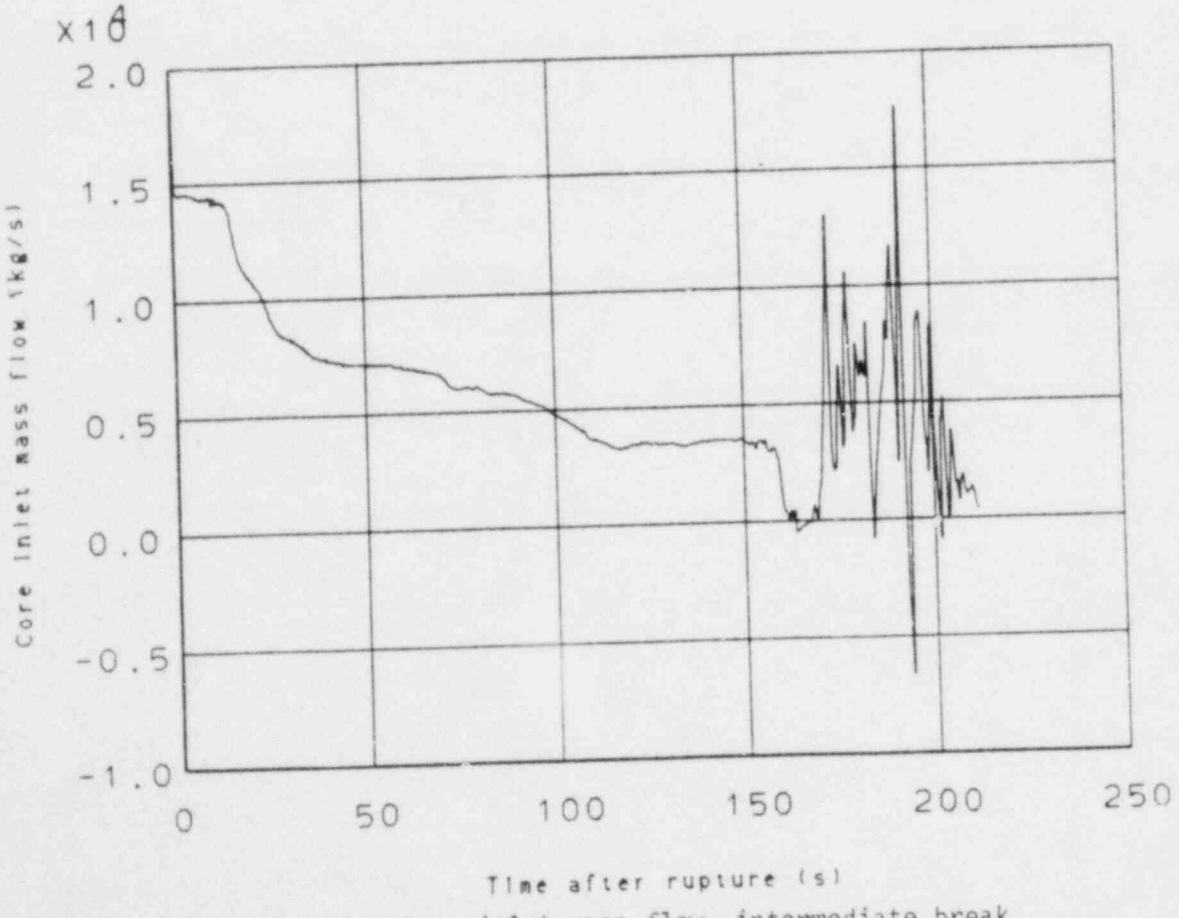

Figure 28. Core inlet mass flow, intermediate break.

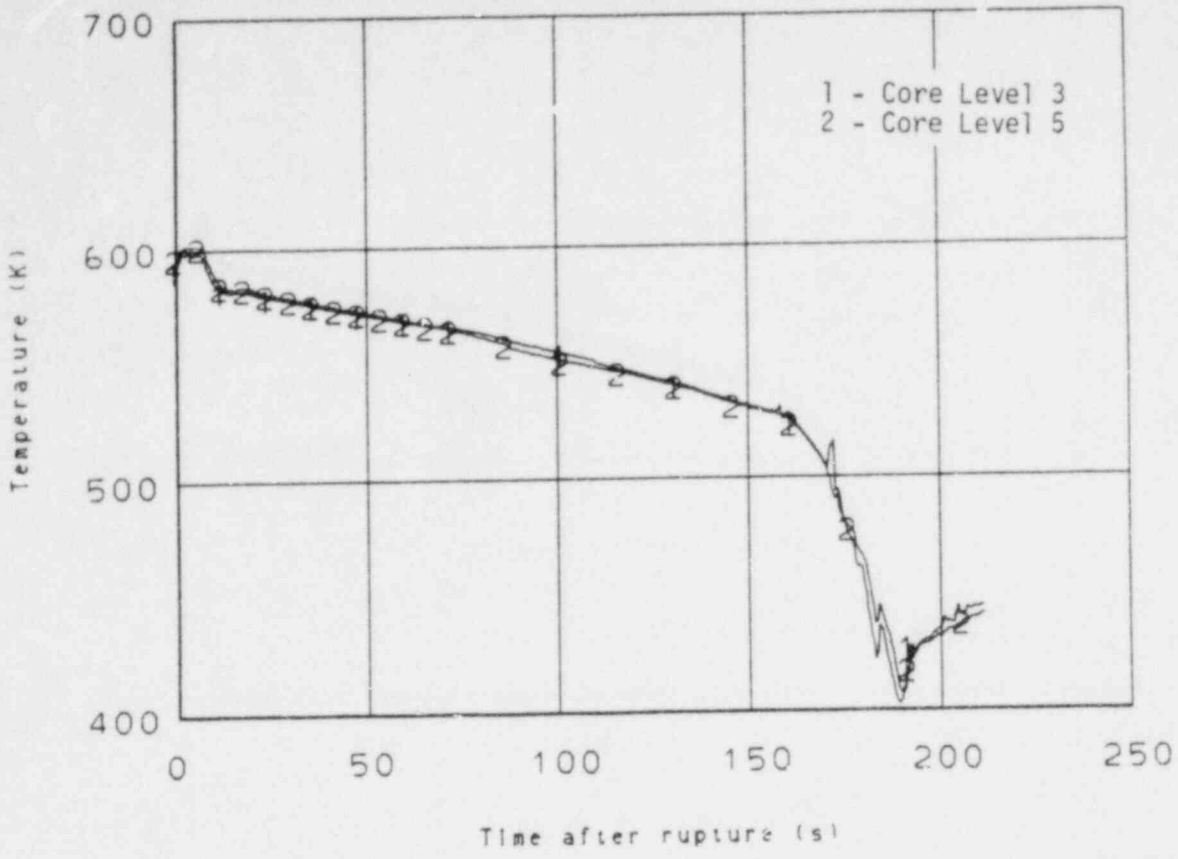

Figure 29. Rod cladding temperature core Level 5, intermediate break.

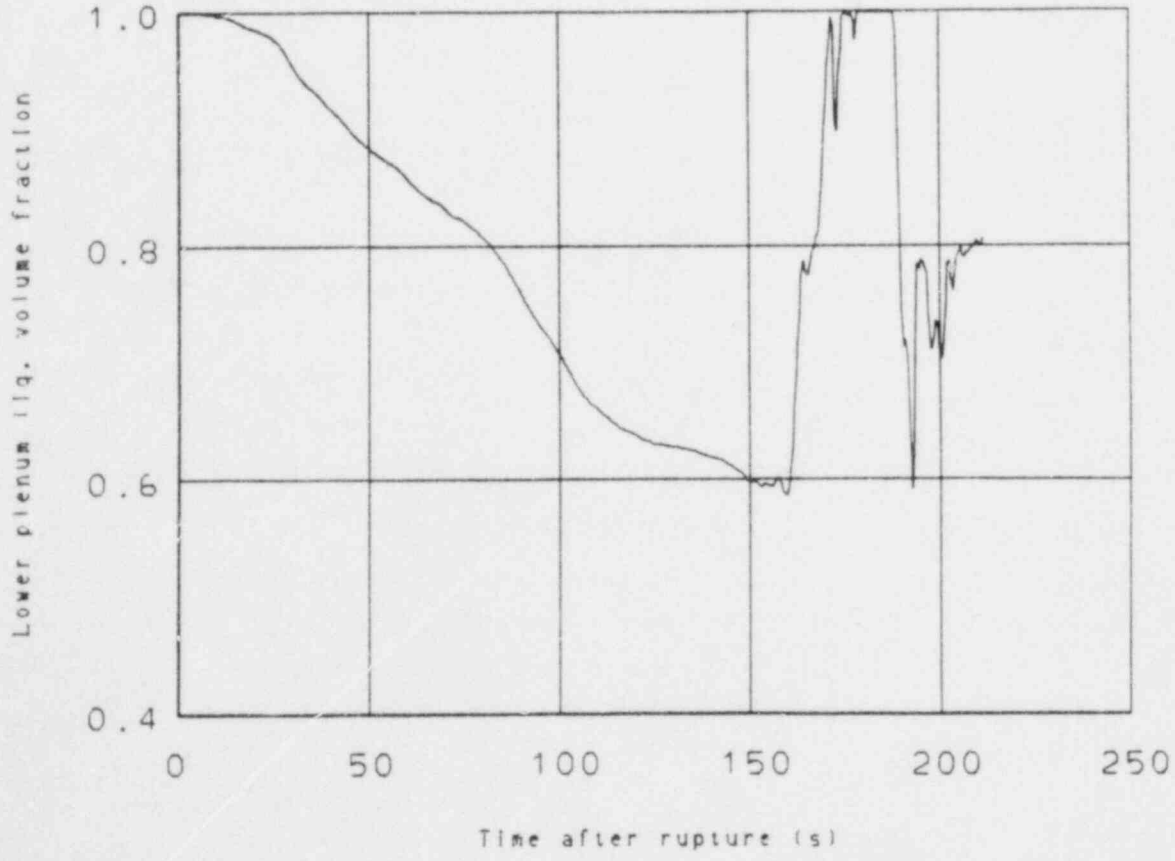

Figure 30. Lower plenum liquid volume fraction, intermediate break.

The core remained cool throughout the transient due to the positive core inlet flow. None of the rods experienced a critical heat flux. Rod cladding temperatures were the highest in core level 5 and only exceeded 600 K by a few degrees early in the transient as shown in Figure 29. The flow through the core was two phase for much of the calculation but still provided adequate cooling. The radial void distribution in the core showed significantly more water in the center of the core than the outer ring. Figure 31 shows the void fraction in the core center of level 5 and indicates a dryout of the core at 160 s during the period of reverse core flow. The void fraction was then reduced and no significant increase in rod cladding temperatures was noted in Figure 29. Gas flow from the accumulators forced some of the liquid out of the core but the rod temperatures remained less than 450 K. The upper portions of the core were nearly covered again at 212 s when the calculation was stopped.

Accumulator flow, shown in Figure 32, was initiated at 147.5 s in both loops at a pressure of 4.06 MPa. Accumulator flow was initially small due to system pressure remaining near the setpoint. As the subcooled accumulator water entered the loops the local pressure shown in Figure 32 was decreased resulting in an increase in accumulator flow at 160 s. The accumulator liquid was exhausted at 184 s after 36.5 s of flow. The large spike in Figure 32 was a result of accumulator steam flow after the depletion of the liquid.

The results of the TRAC-P1A calculation of the intermediate break were compared with the experimental results of Semiscale Test S-07-10,[11] a 10% break. System responses were similar in both the calculation and experiment. Figure 33 shows the Semiscale system pressure for Test S-07-10[9] compared to the TRAC-P1A calculated system pressure. Semiscale system temperature was somewhat higher which resulted in a higher system pressure early in the transient. The intermediate break calculation had a larger break area than the Semiscale test allowing a higher depressurization rate after 20 s. Test S-07-10 pressure did not show the drop at 160 s because the accumulator flow was delayed until after 300 s to allow core heatup.

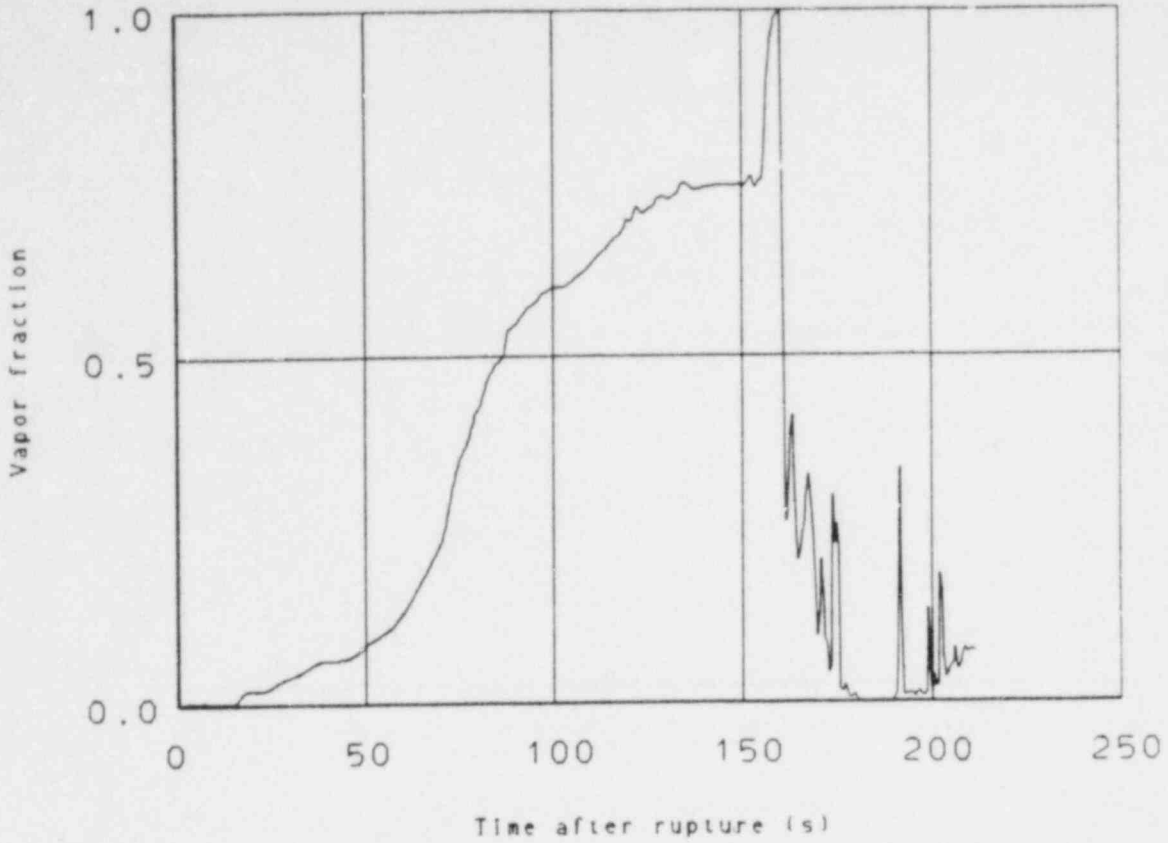

Figure 31. Void fraction core Level 5, intermediate break.

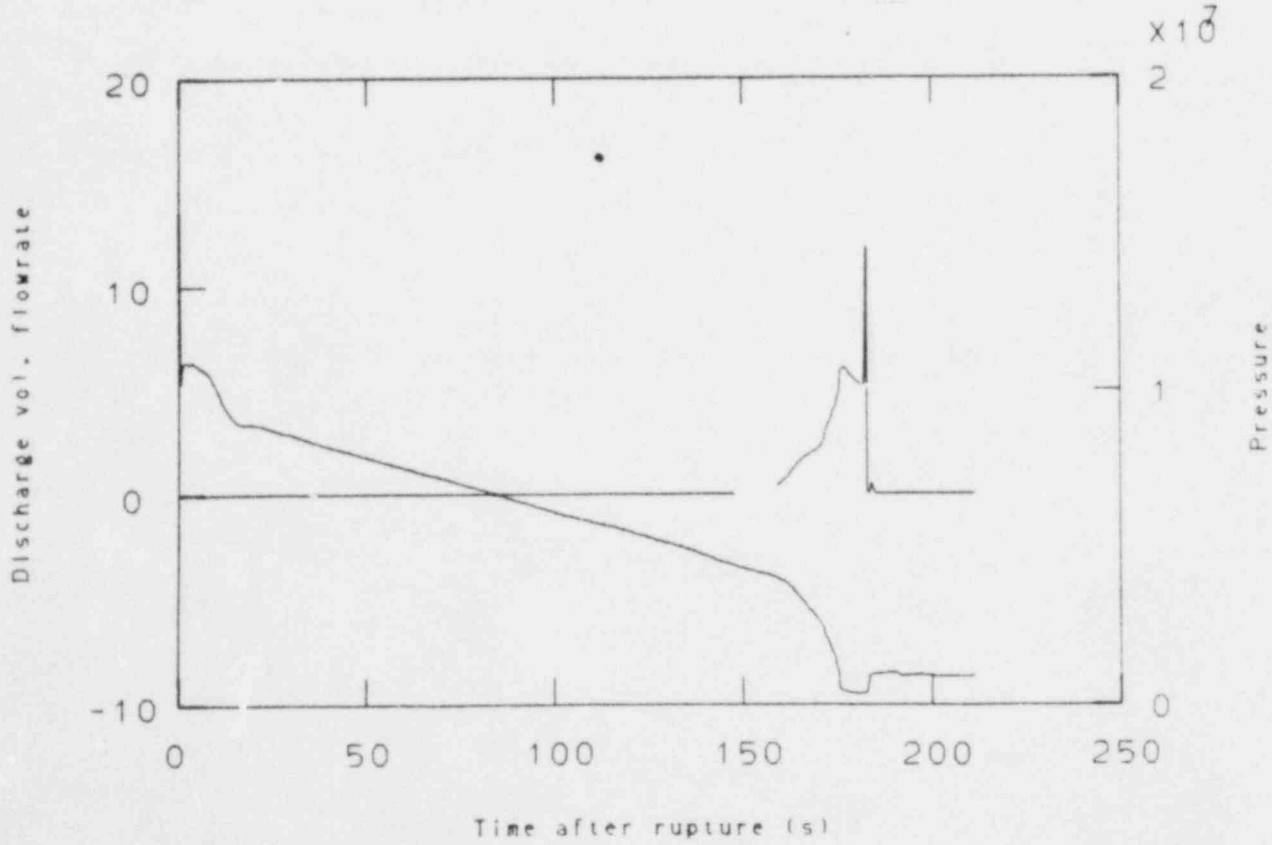

Figure 32. Accumulator volumetric flow rate and local pressure, intermediate break.

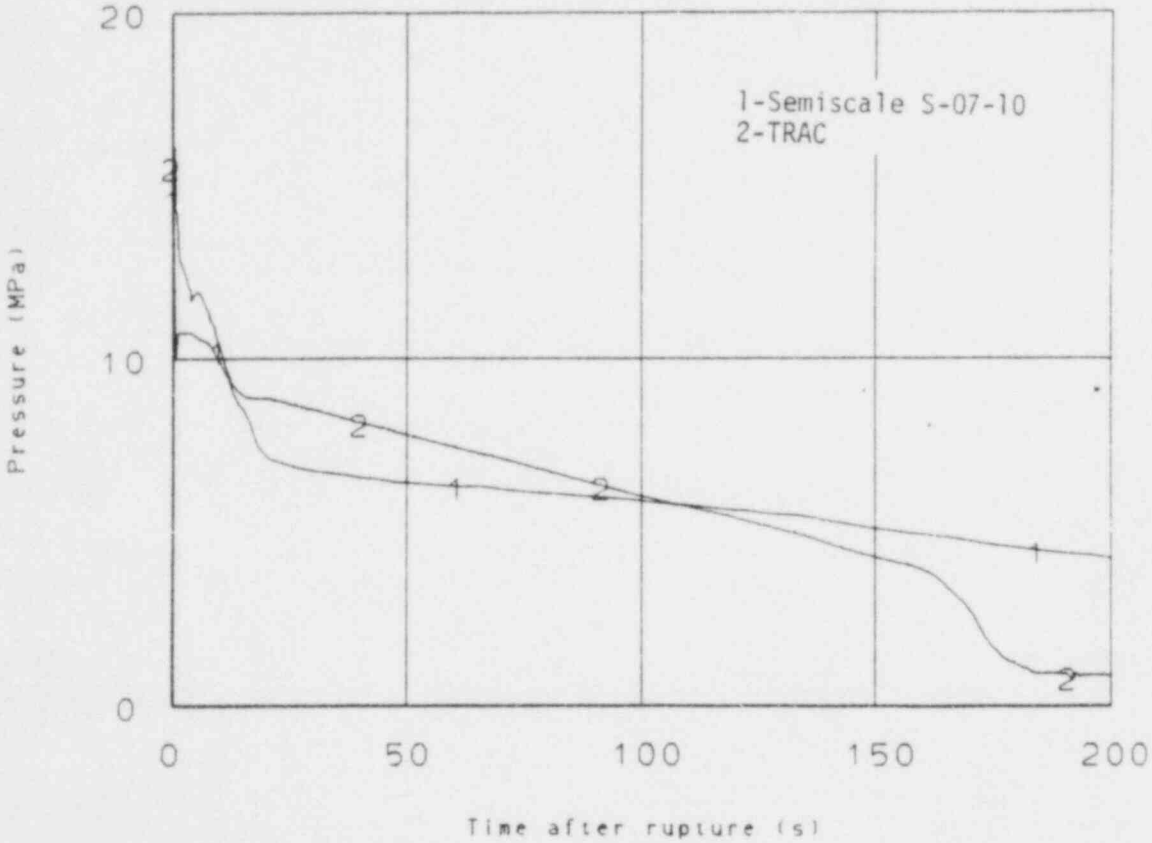

Figure 33. Intermediate break pressure comparison with Semiscale test S-07-10.

3.3 Small (0.10 m-diameter) Break

This section describes the results of the 0.10 meter cold leg break. Table 3 describes the major events of the calculation.

At the initiation of the break (0.0 s) a subcooled blowdown commenced as shown in Figure 34. By 9.93 s the system pressure had dropped below the scram signal setpoint of 12.7 MPa. The scram signal was received and the steam outlet valves began to close. At 11.43 s the steam outlet valves were fully closed. The control rods were completely inserted by 13.33 s. At 14.93 s the steam generator main feedwater flow began to decrease and by 20 s the flow was completely off, isolating the steam generator secondary from any inflow or outflow. Between 20 and 30 s the secondary pressure rapidly increased from 4.7 MPa to the safety valve setpoint of 7.6 MPa. The safety valves opened, and began to relieve the secondary pressure. At 70 s the auxiliary feedwater flow was established injecting subcooled liquid into the steam generator secondary, lowering the pressure below the safety valve setpoint. The primary depressurization decreased at 40 s when voiding in the upper plenum was initiated. The flow out of the break was saturated at about 40 s as shown in Figure 35. At about 170 s the secondary side pressure began to rise as indicated in Figure 34.

At 215 s the primary and secondary pressures equalized. The secondary pressure increased to the safety valve setpoint at 356 s. The safety valves opened and began to relieve secondary pressure and remained open throughout the duration of the calculation as indicated in Figure 36. The reasons for the increase in the secondary side pressure and the secondary pressure remaining at the relief valve setpoint are not completely understood. A preliminary check of a mass balance on the secondary side indicated a numerical mass loss rate about equal to the auxiliary feedwater flow rate and this could contribute to the steam generator pressure remaining high.

System depressurization continued until 680 s. From 680 s to 870 s the heat transfer across the steam generators decreased such that the net

TABLE 3. MAJOR EVENTS IN 0.10 METER DIAMETER BREAK CALCULATION

Time (s)	Event
0.0	Break opened, subcooled blowdown commenced
9.93	Scram signal received, steam outlet valves began to close
11.43	Steam outlet valves fully closed
13.33	Reactor scram
14.93	Main feedwater started to ramp off
19.93	Main feedwater completely off
37.02	Safety injection initiated
69.93	Auxiliary feedwater initiated
1224.0	Calculation terminated

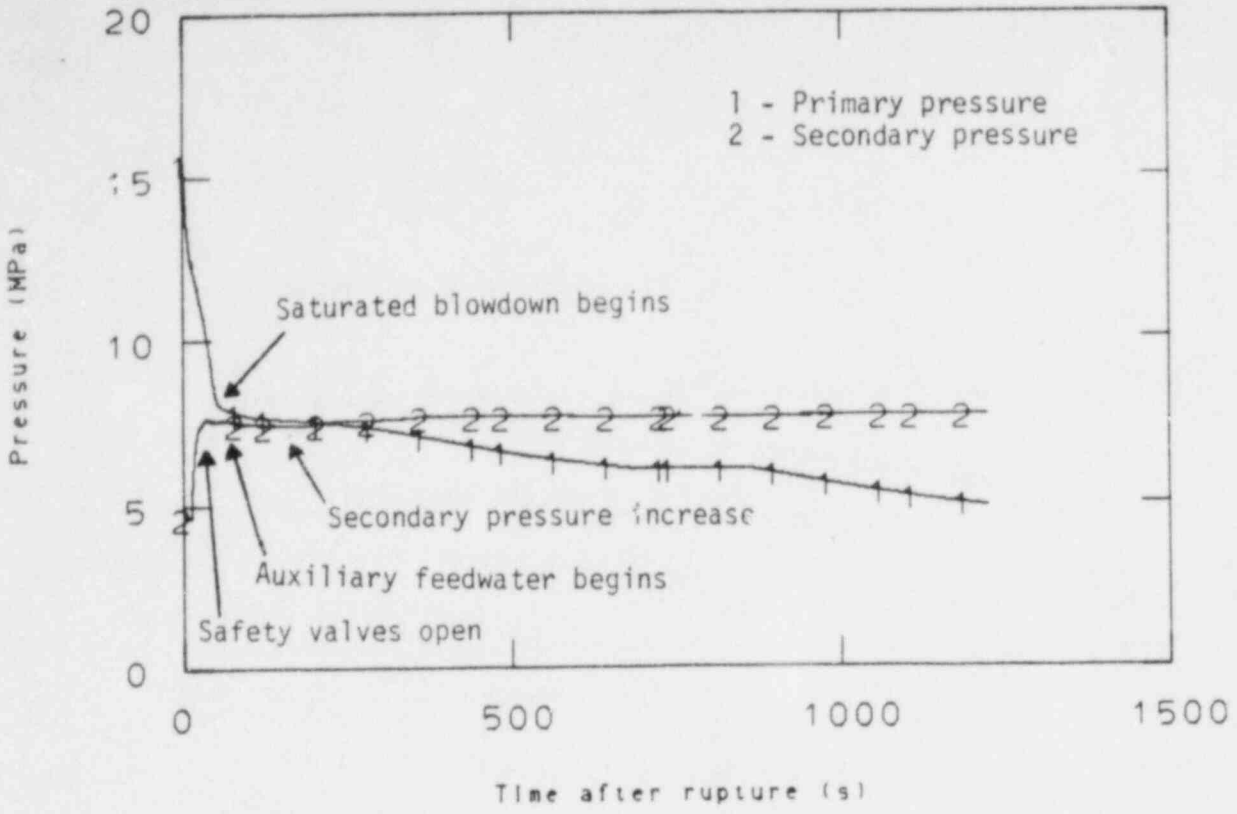

Figure 34. Steam generator pressure, primary and secondary, small break.

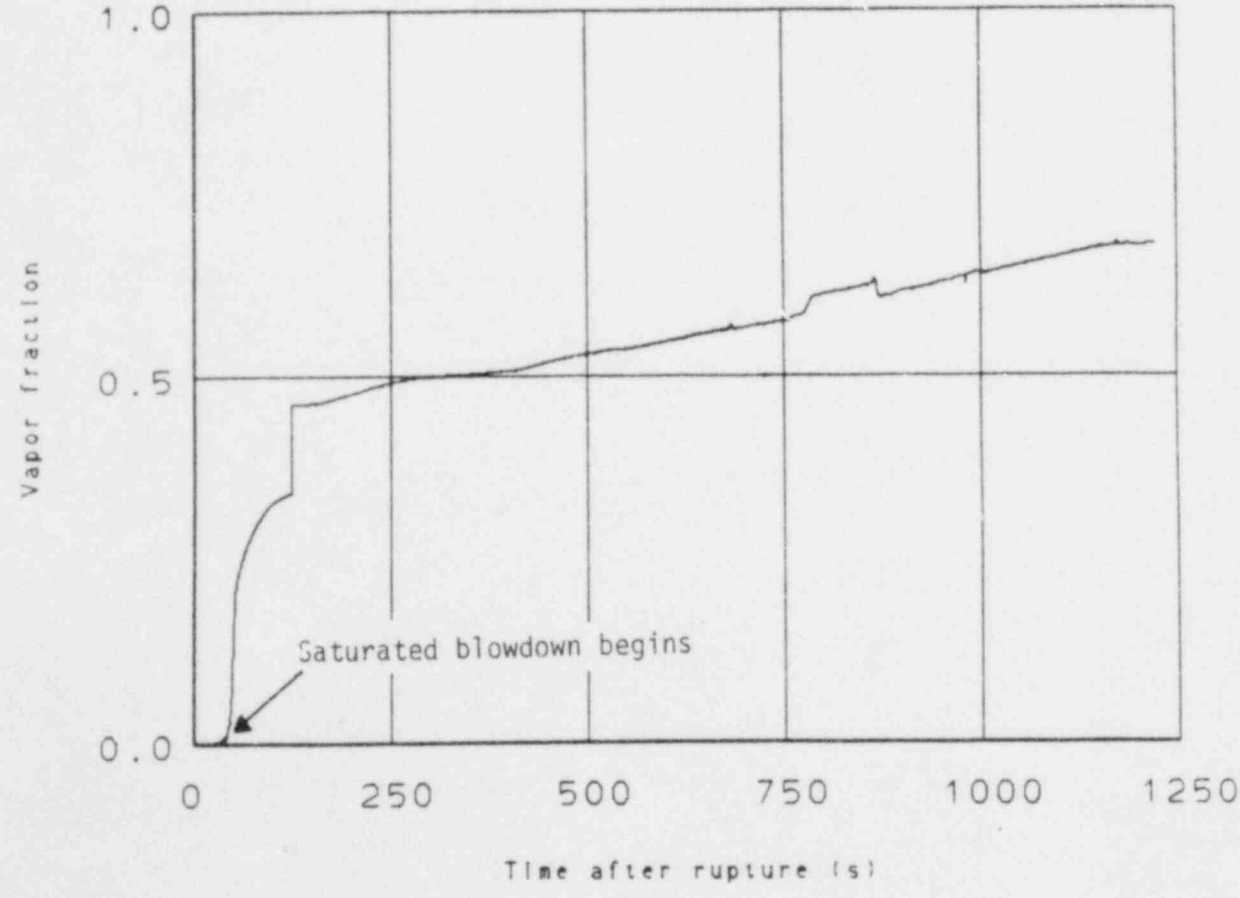

Figure 35. Vapor fraction at break, small break.

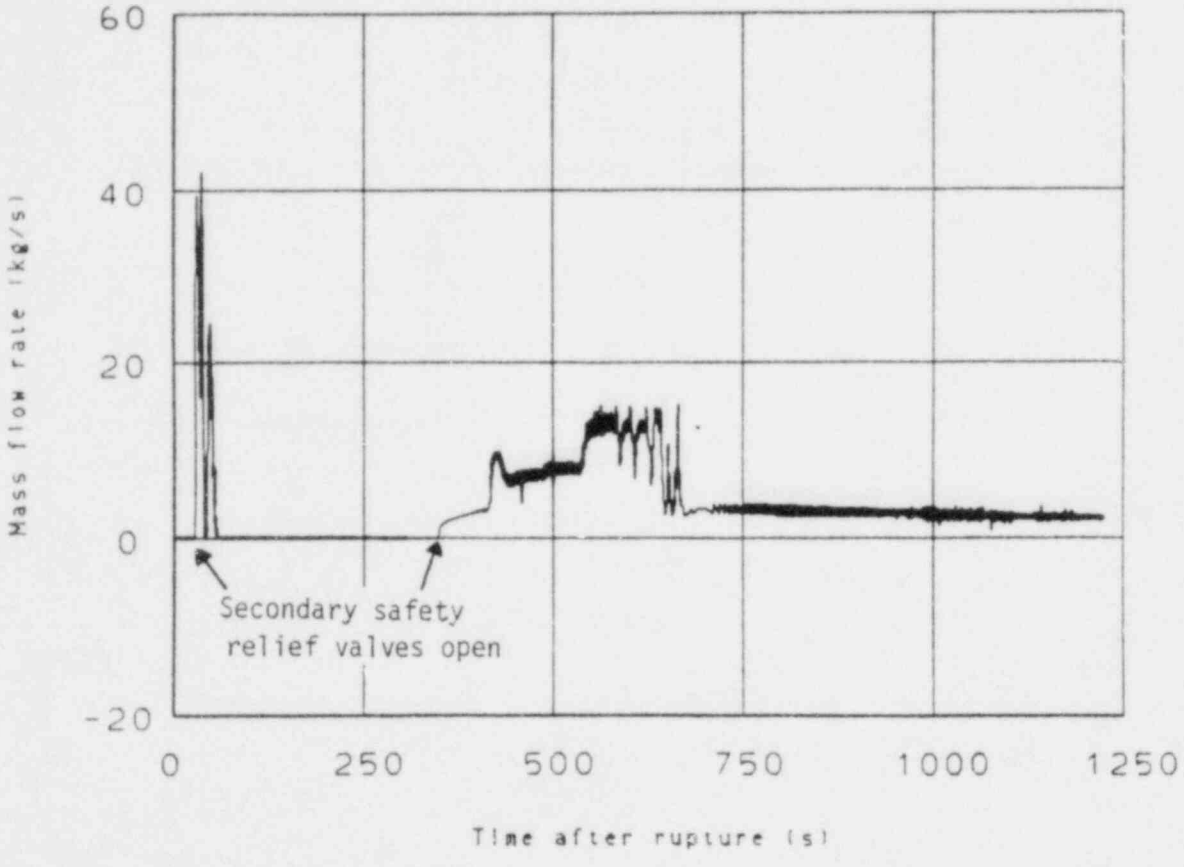

Figure 36. Secondary safety relief valve mass flow rate, small break.

energy lost from the system equaled the net energy gained by the primary system, resulting in the primary system pressure remaining constant as shown in Figure 34. The system continued to lose mass during this period increasing the voids throughout the system. After 870 s primary system depressurization was reestablished due to an increase in the primary to secondary heat transfer in the steam generator.

The vessel voided from the upper head through the upper plenum and into the core. The upper head was voided by 700 s and the upper plenum level began to drop. At the termination of the calculation level 11 of the vessel component was completely voided and the void fraction in levels 10 and 9 was 50-60%. Core flow remained positive throughout the duration of the calculation as indicated in Figure 37. The void distribution in the core was asymmetric during the later period of the calculation. The void fraction in the outer ring of the core was significantly higher than in the inner ring as shown in Figure 38. This void distribution is unrealistic in the core of a PWR. However, the void fraction in ring 2 was low enough that a rod heat up did not occur. The rod clad temperature response followed the system saturation temperature response as seen in Figure 39. A study of the effect of vessel nodalization for small breaks should be performed.

The calculation was terminated at 1224 s because of the response of the steam generator secondary pressure. The steam generator in the broken loop remained a heat sink from 690 s to the termination of the calculation. The lower cell of the steam generator was a heat sink whereas the upper two cells were a heat source. This difference in heat transfer was primarily a result of about a 20 K stratification in the secondary side of the steam generator. The steam generator in the intact loop was a net heat source, but the energy transferred from the secondary to primary system was relatively small and the secondary pressure remained at the setpoint through the duration of the calculation. The unexpected results of the secondary side response are attributed to the general steam generator model used and are probably not reasonable. Other modeling

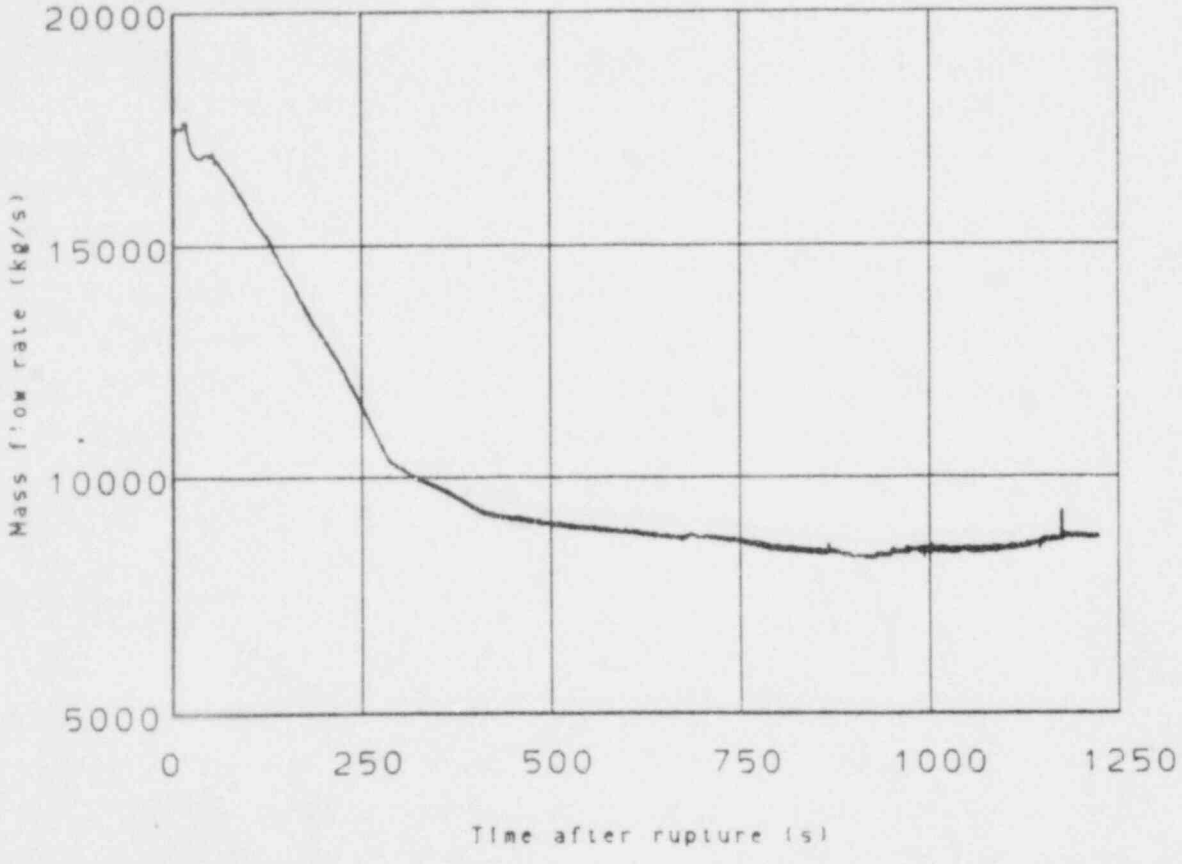

Figure 37. Core inlet mass flow, small break.

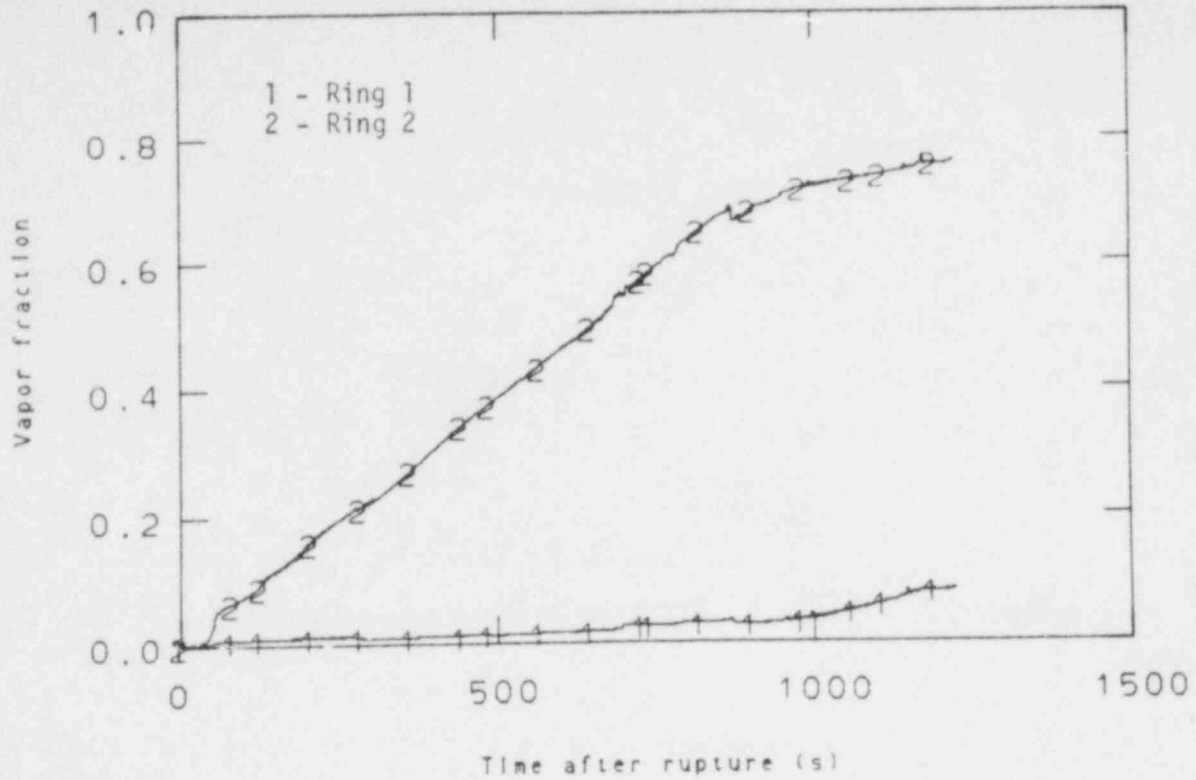

Figure 38. Core midplane vapor fraction, small break.

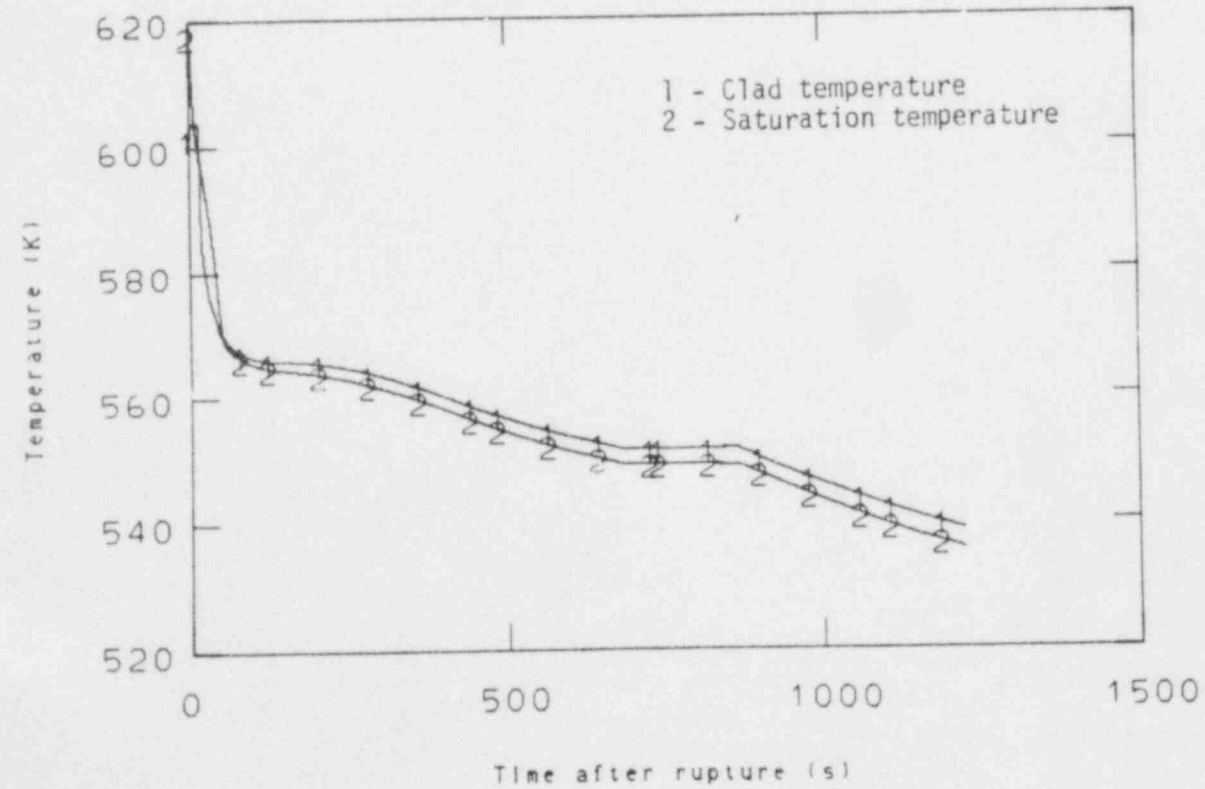

Figure 39. Rod cladding temperature comparison with saturation temperature, small break.

methods that include a recirculation path between the steam generator outlet and the inlet may decrease the temperature stratification and result in a response similar to that observed in experiments. An additional investigation of the modeling of steam generators should be performed. At 1224 s when the calculation was terminated the core temperatures were at the system saturation temperature and it was anticipated that the core temperatures would remain low until accumulator injection occurred in about 250 s.

The results of the calculation were compared to a Semiscale 2.5% communicative cold leg break Test S-SB-P7.[12] The trend in system behavior was the same for both the calculation and the test. Figure 40 compares the system pressure response of the calculation and the experiment. Early in the transient the calculation agreed quite well with the experiment, but after 50 s the pressure calculated by the code remained high. The major events in the calculation occurred at earlier times because the pressure setpoint for steam was higher (12.7 MPa for the calculation and 12.48 MPa for the test). In the experiment the temperature stratification in the secondary side liquid was relatively small.

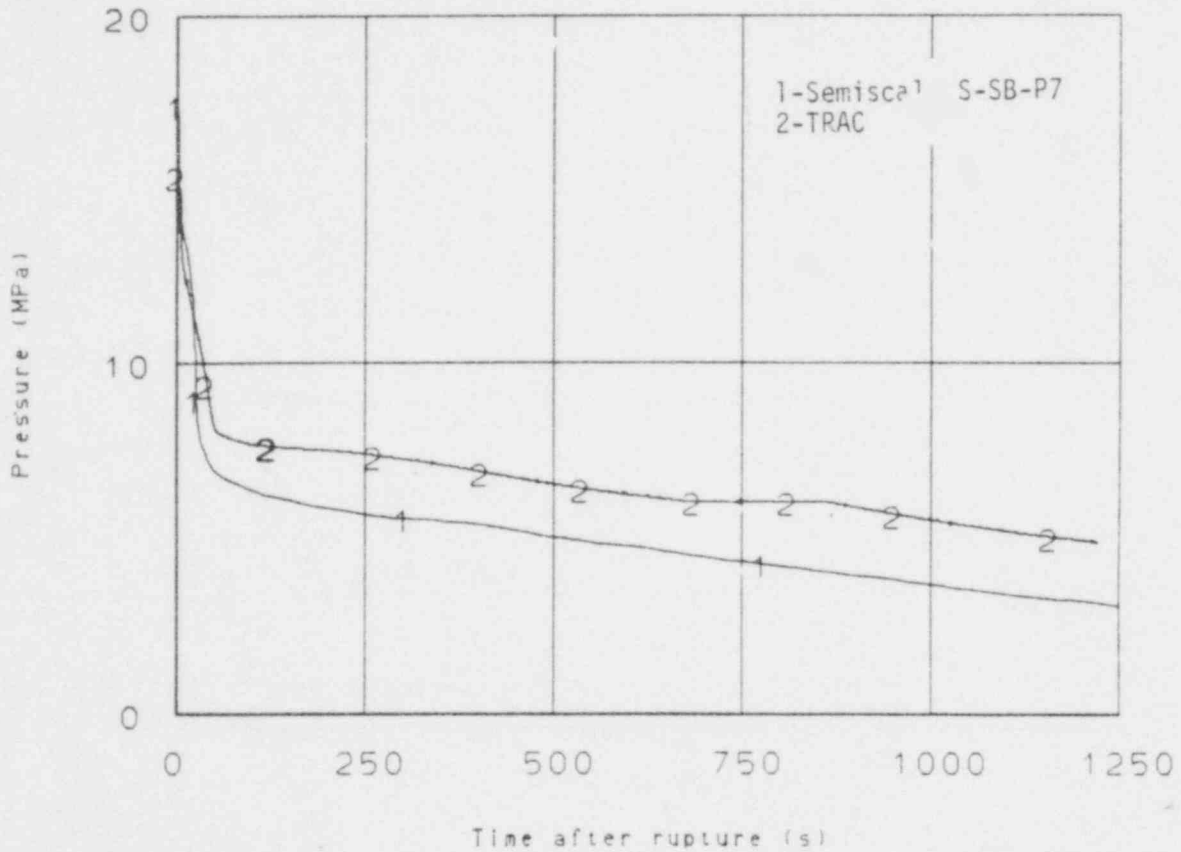

Figure 40. Small break system pressure comparison with Semiscale test S-SB-P7.

4. SENSITIVITY STUDIES

Three sensitivity studies were conducted to investigate the effect of different modeling techniques and code options on the calculational results. The three studies were structured to provide insight into the following areas.

1. Effects of rod gap conductance on cladding temperatures.

2. Vessel modeling for intermediate breaks.

3. The effect of tee component secondary side modeling on break flow and system response in intermediate and small breaks.

All of the sensitivity calculations were started at the time of break initiation and run for a short period of the transient.

4.1 Modeling of Rod Gap Conductance

The first study was undertaken after reviewing the rod cladding temperatures for the 200% cold leg break. Cladding temperatures throughout the core were higher than both experimental data and calculational results for similar transients. After reviewing the calculation it was determined that the internally calculated rod gap conductance using the dynamic gap option was low by at least a factor of two. The gap conductance was 2387 W/m^2K at the core midplane of rod 5. The TRAC calculated gap conductance resulted in a peak fuel centerline temperature of 2075 K. Available data indicated that 1600 K was a more accurate fuel centerline temperature for operating PWRs. The BE/EM study[1] used 6660 w/m^2K for the rod gap conductance. Using this value and the constant gap conductance option in TRAC, the fuel centerline temperature was lowered to 1600 K. A short calculation was made for the first 40 s of the large (200%) cold leg break with the user input constant value of the gap conductance. Figures 41, 42 and 43 show a comparison of the rod cladding temperatures of

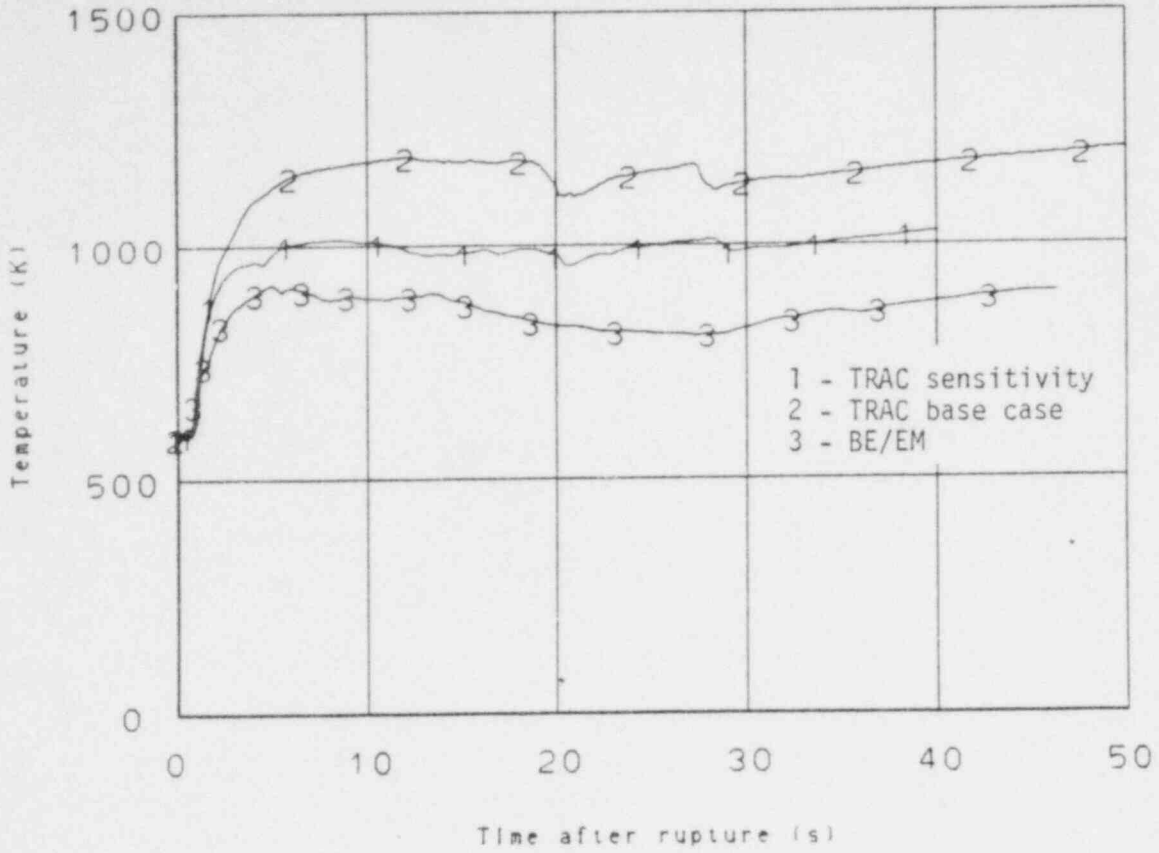

Figure 41. Midplane inner rod cladding temperature comparison with BE/EM.

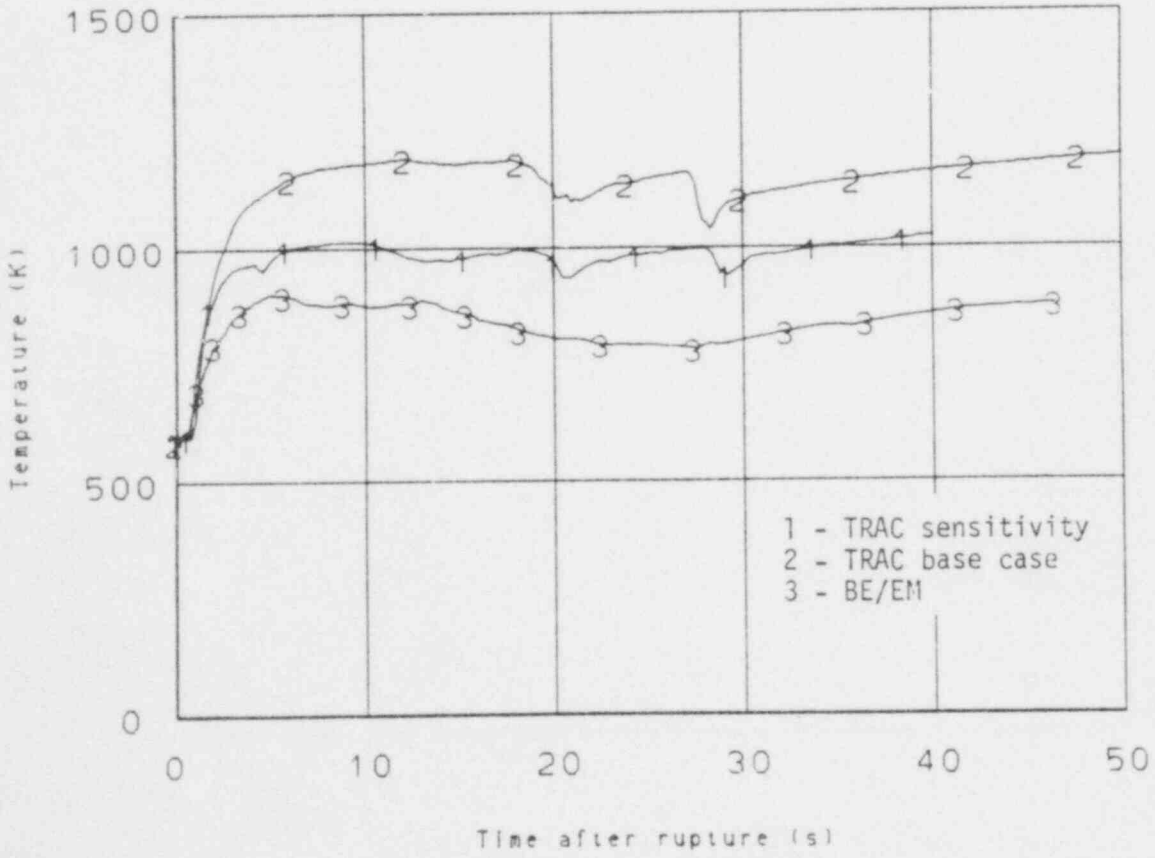

Figure 42. Level 2 inner rod cladding temperature comparison with BE/EM.

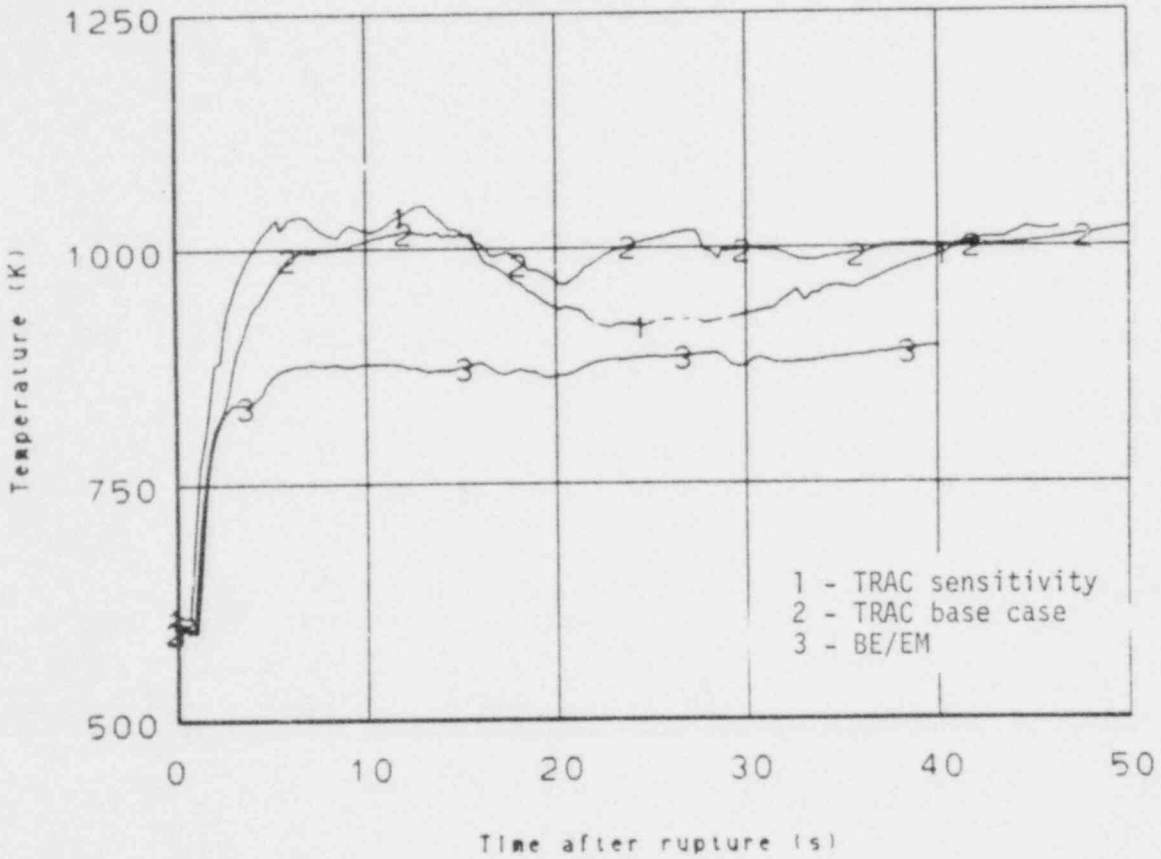

Figure 43. Level 4 outer rod cladding temperature comparison with BE/EM.

the base case, the run with user input gap conductance, and results from the BE/EM study.[3] The rod selection from the BE/EM study[3] was performed by matching the linear heat generation rate of the fuel as closely as possible.

It was evident that the code calculated rod gap conductance was low and the user input value more closely represents experimental rod conditions. The calculated rod clad temperatures from the run with a gap conductance of 6660 w/m^2K are somewhat closer to the BE/EM results. A difference of only 160 K in the rod clad temperature is calculated at 40 s between TRAC and BE/EM. This was a decrease of about 200 K when compared with the base case calculation. Figure 43 shows the cladding temperature of an outer rod at level 4. Calculated cladding temperatures of the two TRAC rods are not significantly different indicating the gap conductance model may not be as important for cooler outer rods. The hydraulics of the calculation were not changed significantly by the user input rod gap conductance. However, the flow reversal at about 28 s in the core and downcomer that was discussed in Section 5.1 was not as large and the lower plenum filled about 15 s earlier. With lower rod cladding temperatures in the sensitivity study it appears that the rods would quench about 15 s earlier for the calculation with the lower peak centerline temperature. At this time it is suggested that the rod gap conductance be input by the user based on the fuel history of the system being modeled.

4.2 Selection of Vessel Models for Intermediate Break Calculations

The intermediate calculation utilized a coarse model (2 azimuthal segments) vessel. Review of the calculation showed several similarities to a large break; system pressure was not delayed by the steam generator, and portions of the core and lower plenum were filled with a two phase mixture early in the transient. Considering the similarities, a sensitivity calculation was run for the first 50 s of the transient using the eight azimuthal segment vessel from the 200% break. The break mass flows shown

in Figure 44 and the lower plenum volume fractions shown in Figure 45 appear the same for both calculations. Rod temperatures shown in Figure 46 were also reviewed and no differences were noted. The eight segment vessel calculations required about four times more CPU time. It appears that a simply noded vessel will produce similar results to a more detailed noded vessel when used for intermediate break transients.

4.3 Modeling of Tee Component Secondary Side at the Break

A method of noding a small or intermediate break in TRAC is by the use of a tee component. The primary side of the tee acts as part of the primary coolant piping system with the secondary side connected to a break component. When modeling the secondary side of the tee, two code limitations need to be considered. The noding at the break must be fine enough to adequately calculate the break mass flow and the first cell in the secondary side of the tee must be long enough that Courant limiting of the time step was not excessive. The original secondary side length was kept as short as possible. After review of the intermediate calculation an alternate noding for the secondary was developed to raise the Courant imposed time step which was limiting the speed and increasing the cost of the calculation. The new noding utilized a 0.8 m long cell as the first secondary cell and reduced the cell length by half to an end cell of 0.01 m. This noding results in a total secondary length of 1.07 m. The original secondary side has a 0.10 m cell as the first in the secondary side and reduced to 0.0032 m at the break. The total length of the original secondary side was only 0.20 m. The sensitivity calculation was run for 50 s of the transient. The increased tee secondary length resulted in a 40% reduction in CPU time used.

The break mass flow rate shown in Figure 47 revealed a large difference in early break mass flow rates. The added length of the secondary side resulted in an increased pressure drop from the primary side to the break reducing the mass flow out the break. The decreased break

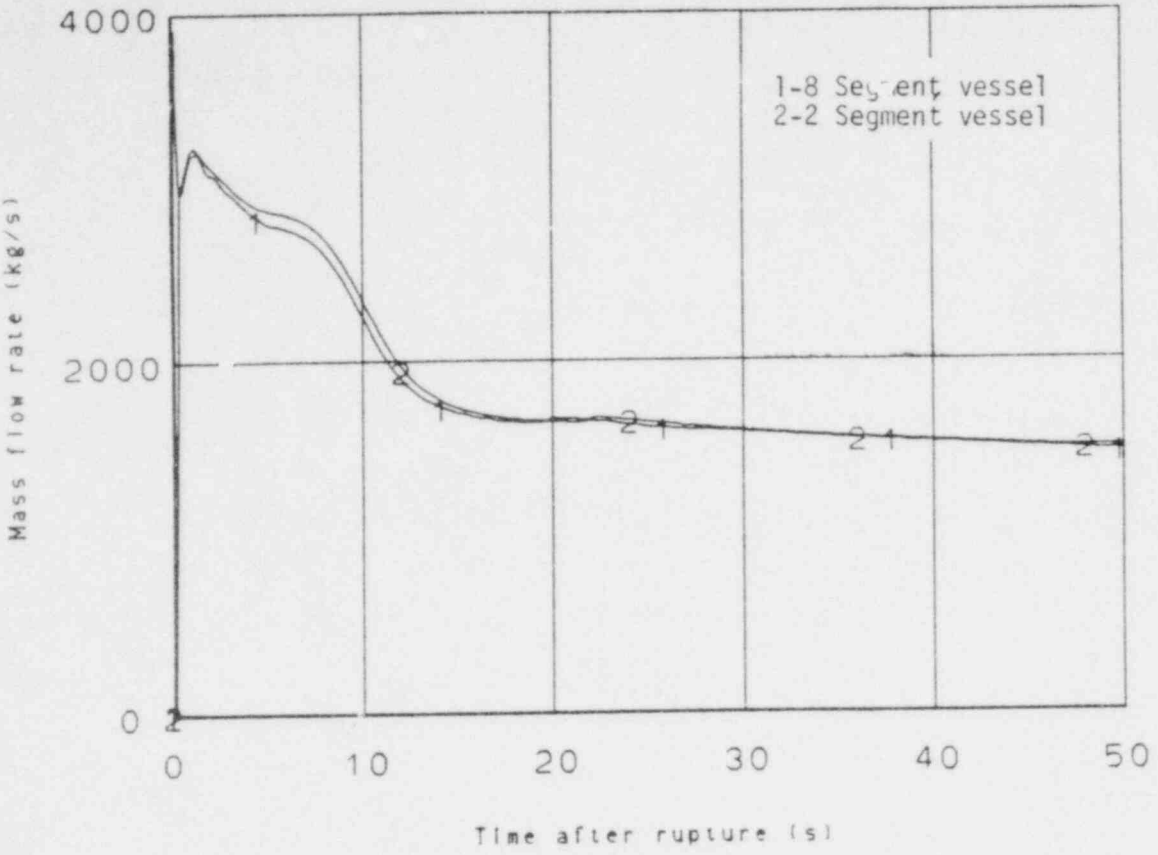

Figure 44. Break mass flow comparison for 2 and 8 segment vessel models.

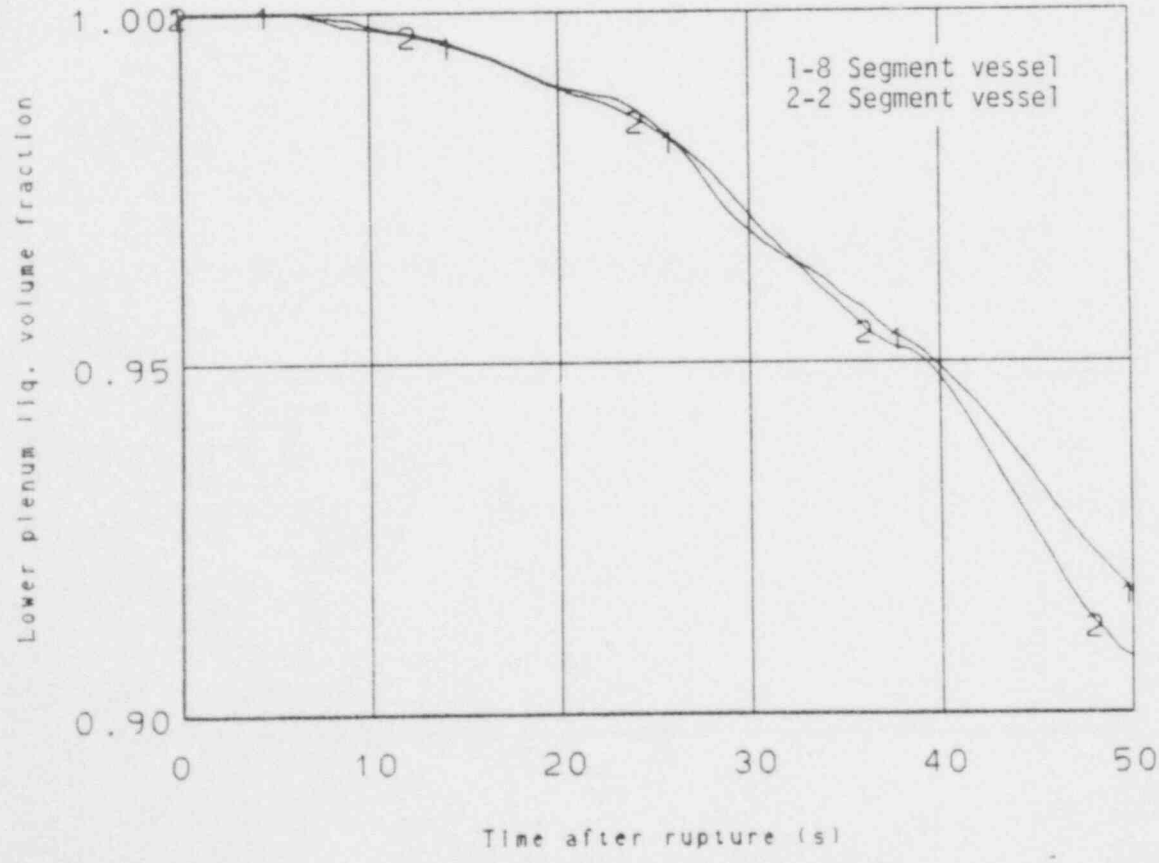

Figure 45. Lower plenum liquid volume fraction comparison for 2 and 8 segment vessel models.

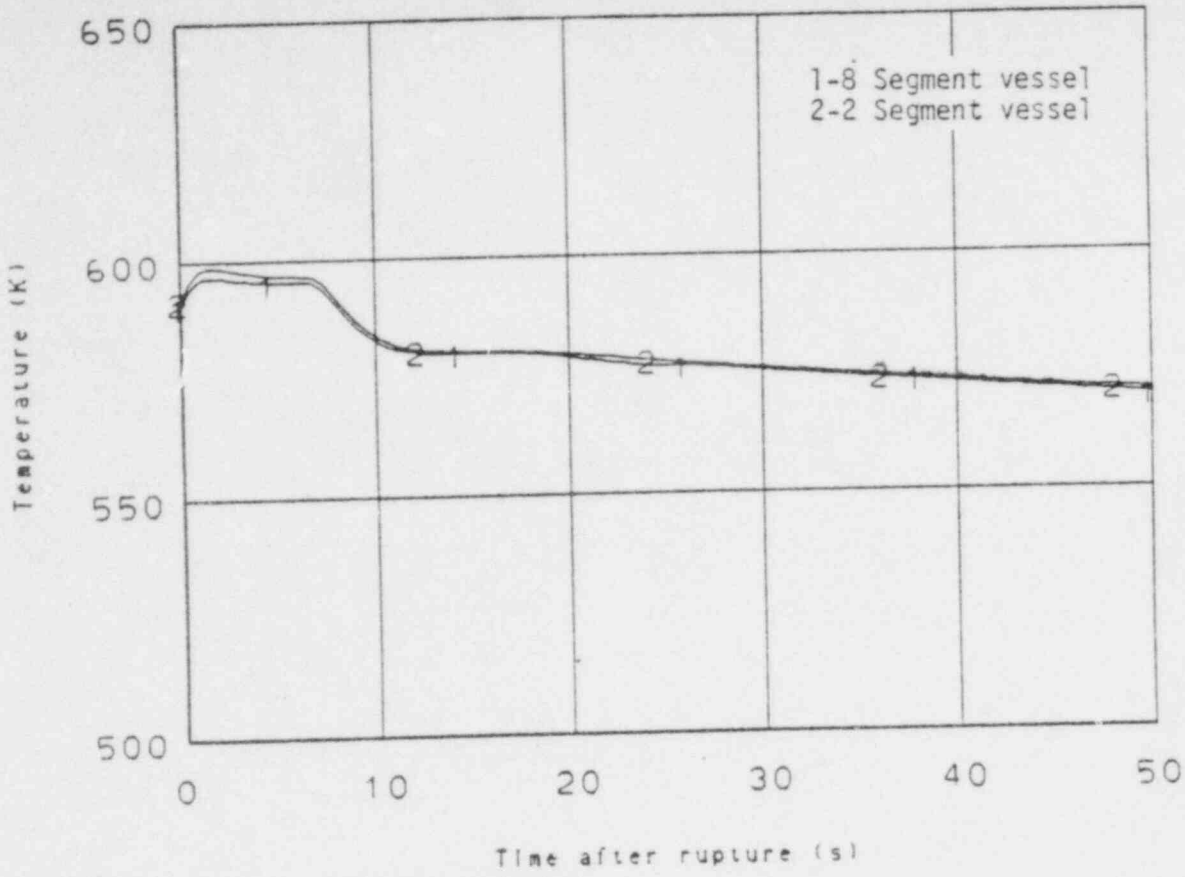

Figure 46. Rod cladding temperature comparison for 2 and 8 segment vessel models.

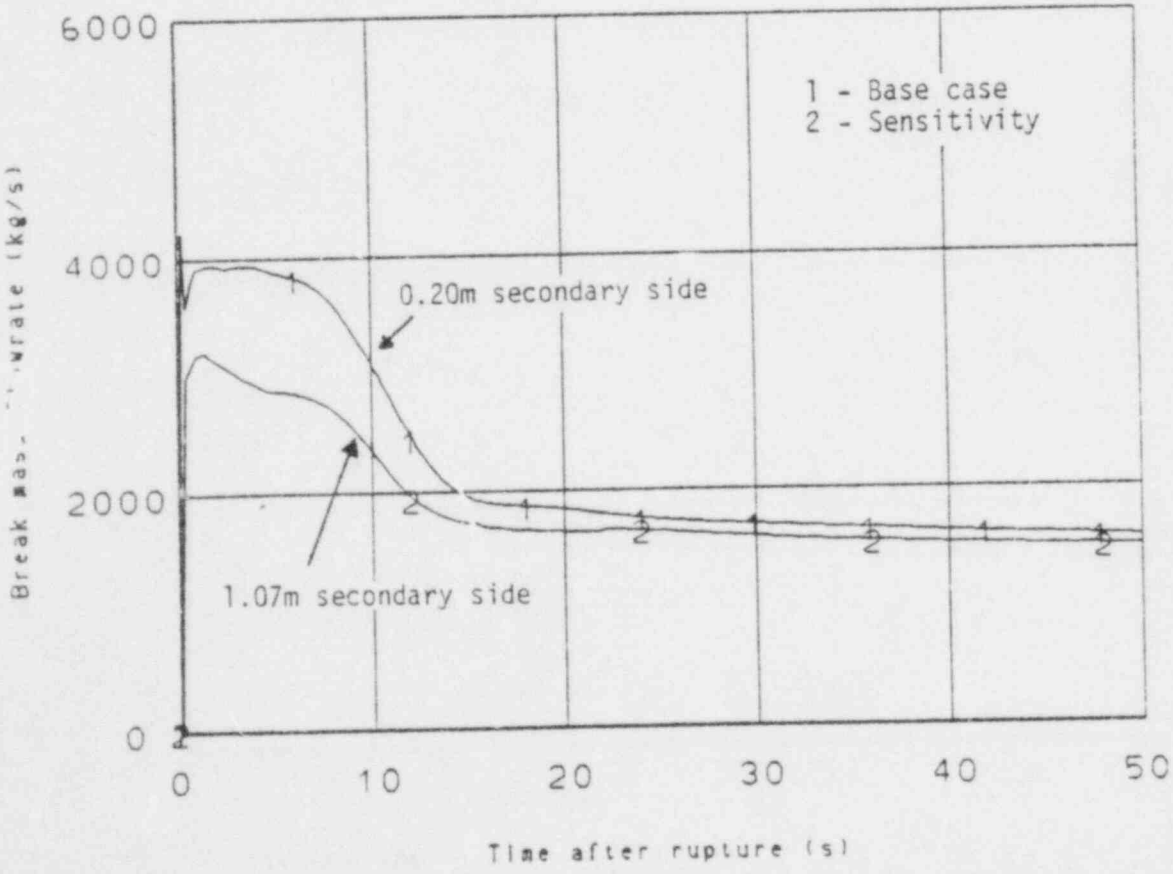

Figure 47. Break mass flow comparison for tee secondary modeling.

flow reduced depressurization of the system shown in Figure 48. The effects of noding tend to disappear after approximately 15 s of transient. At this time the break flow was mostly steam and differs by 200 kg/s. The pressures at this time also agree well. The noding did not significantly change the end results of the intermediate break calculation due to the size of the break and the length of subcooled break flow. A small break calculation may be affected more by the noding. It would be recommended that the secondary side be short for the initial subcooled break flow and then be renoded to avoid the Courant limiting of the time step.

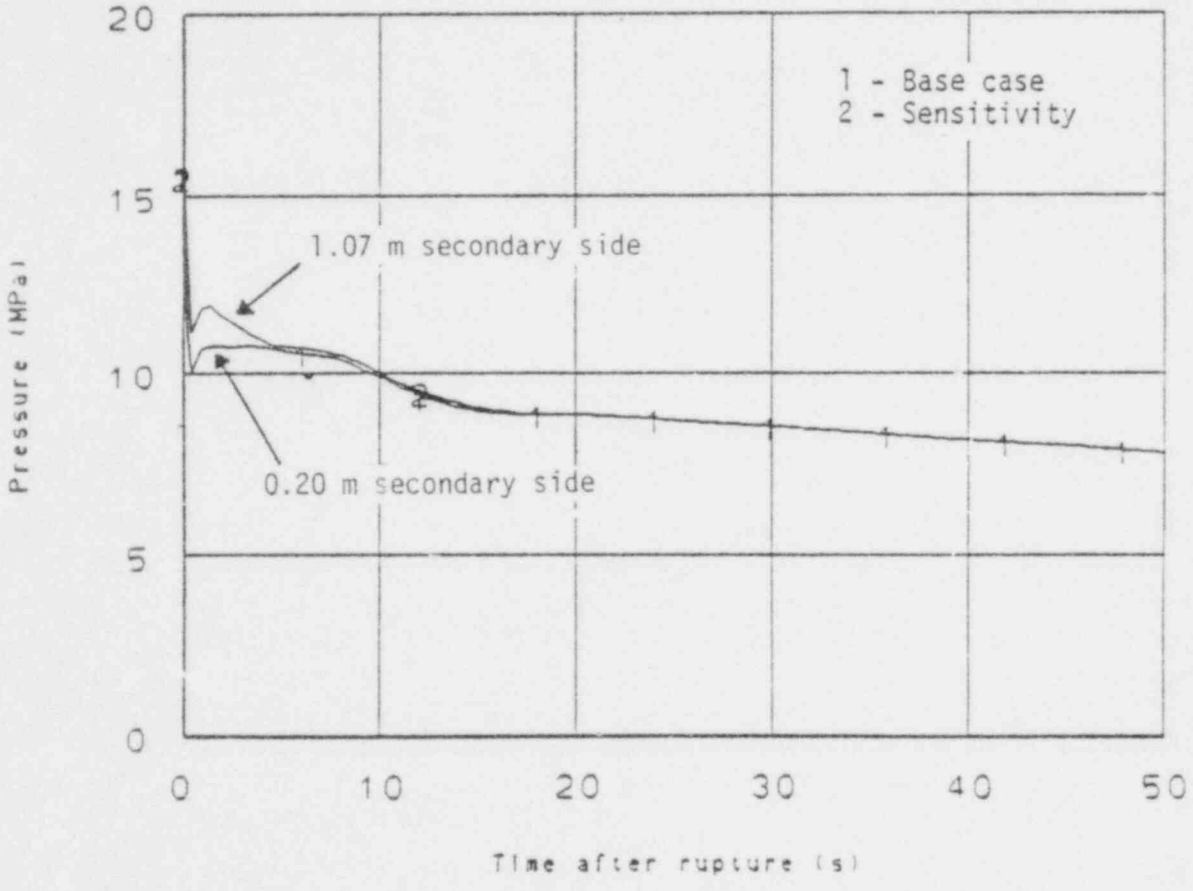

Figure 48. System pressure comparison for tee secondary modeling.

5. RECOMMENDATIONS AND CONCLUSIONS

1. TRAC-P1A was able to calculate the large (200%) cold leg break satisfactorily.

TRAC-P1A calculated results for the large (200%) cold leg break were adequate. The calculated system responses compared qualitatively with previous predictions such as the BE/EM study.[3] Comparisons with LOFT L2 series data also showed similar responses. TRAC-P1A could be used for other large breaks with reasonable confidence.

2. Calculational results of the intermediate break were reasonable.

Calculated thermal-hydraulic responses of the intermediate break calculations appeared adequate. Comparisons with Semiscale S-07-10[11] results showed many similarities. System pressure and heater rod temperatures behaved similarily in both indicating that TRAC-P1A may be useful for intermediate breaks as well as large breaks.

3. The small break calculation illustrates a need for model improvements.

The calculated overall system depressurization appeared reasonable. The calculated steam generator secondary response and the void distribution in the core appeared to be unreasonable. The overall response of the steam generator during small break calculations needs additional analysis.

4. Behavior at vessel connections needs further investigation.

Vessel connection behavior exhibited a peculiarity during the refill period of the transient. The calculated counterflow against the pressure gradient during refill needs further investigation. Various modeling techniques may, however, overcome the problem.

5. *Further investigation of steam generator modeling is suggested.*

A relatively large temperature stratification on the secondary side of the steam generator was calculated for a small break using the TRAC steam generator component. The steam generator secondary was modeled with a negative fill representing the steam flow out the safety relief valve and a fill representing the feedwater flow into the secondary. A modeling study should be performed to investigate steam generator modeling that will reduce the relatively large temperature stratification.

6. REFERENCES

1. J. R. Larson, Calculations of a Large Cold Leg Break with Steam Generator Ruptures in a PWR using the TRAC-P1A Computer Program, EG&G Idaho, Inc., EGG-CAAP-5189, June 1980.

2. M. A. Bolander, TRAC-P1A Calculations for a 200% Hot Leg Break and a 200% Hot Leg Break Simultaneous with a Rupture of 16 Steam Generator Tubes in a Pressurized Water Reactor, EG&G Idaho, Inc., EGG-CAAP-5191, June 1980.

3. G. W. Johnsen et al., A Comparison of "Best Estimate" and "Evaluation Model" LOCA Calculations; The BE/EM study, EG&G Idaho, Inc., Report PG-R-76-009, December 1976.

4. TRAC-P1A, An Advanced Best-Estimate Computer Program for PWR LOCA Analysis, LA-7777-MS, May 1979.

5. Zion Station Final Safety Analysis Report, Docket No. 50-295 (with amendments).

6. J. Sicilian, TRAC Newsletter, Number 1, Los Alamos Scientific Laboratory, July 1979.

7. J. C. Vigil et al., TRAC-P1A Developmental Assessment, LA-8056-MS, October 1979.

8. P. G. Prassinos et al., Experimental Data Report for LOFT Power Ascension Experiment L2-3, NUREG/CR-0792, July 1979.

9. H. S. Crapo et al., Experiment Data Report for Semiscale Mod-1 Test S-04-4, TREE-NUREG-1003, October 1976.

10. U. S. Rohatgi et al., Constitutive Relations in TRAC-P1A, August 1979, p. 6.

11. K. E. Sackett, Experimental Data Report for Semiscale Mod-3 Small Break Test S-07-10, NUREG/CR-1456, May 1980.

10. S. E. Dingman et al., Quick Look Report for Semiscale Mod-3 Small Break Tests S-SB-P1, S-SB-P2, and S-SB-P7, EG&G Idaho, Inc., EGG-SEMI-5137, April 1980.

APPENDIX A

NODALIZATION OF ZION I FOR TRAC

1. VESSEL

The axial and radial noding of the vessel is shown in Figure A-1. The nodalization consisted of 12 axial levels with each level subdivided into 3 radial and 8 azimuthal zones for a total of 288 mesh cells. The noding was revised several times as improved values for volumes, areas and masses were calculated. The noding was somewhat different than that used in the BE/EM or USPWR1 models. Both BE/EM and the USPWR1 modeled the upper and lower portions of the cladding as active fuel in the core. The Zion I model included only the active fuel length of 144 inches. Table A-1 provides a comparison of the vessel fluid volumes, heat slab areas, and heat slab masses for the Zion I model used in these calculations with other PWR models developed for the BE/EM study[1] and by LASL (USPWR1).[2] The PWR model is believed to accurately represent the Zion I plant.

The downcomer region was modeled by the outer ring between levels 3 and 10. The downcomer lumps two actual flow paths on each side of the thermal shield. The barrel-baffle region which provides an additional flow path parallel to the downcomer was not included in the model. Its volume, surface area and mass were evaluated and included in the outer core ring. The flow path was not included.

The lower plenum was noded in three levels. The portion below the downcomer was divided into 2 levels to permit backflow from the core to the downcomer without removing residual liquid from the bottom of the vessel. Level 3 of the lower plenum lies at the bottom of the active core and includes structures such as the core support plate and core mixing plate.

The core consisted of 5 axial levels and 2 radial rings. The top of vessel level 8 corresponded to the top of the active fuel. This noding provided a means for a representative axial and radial power distribution in the core.

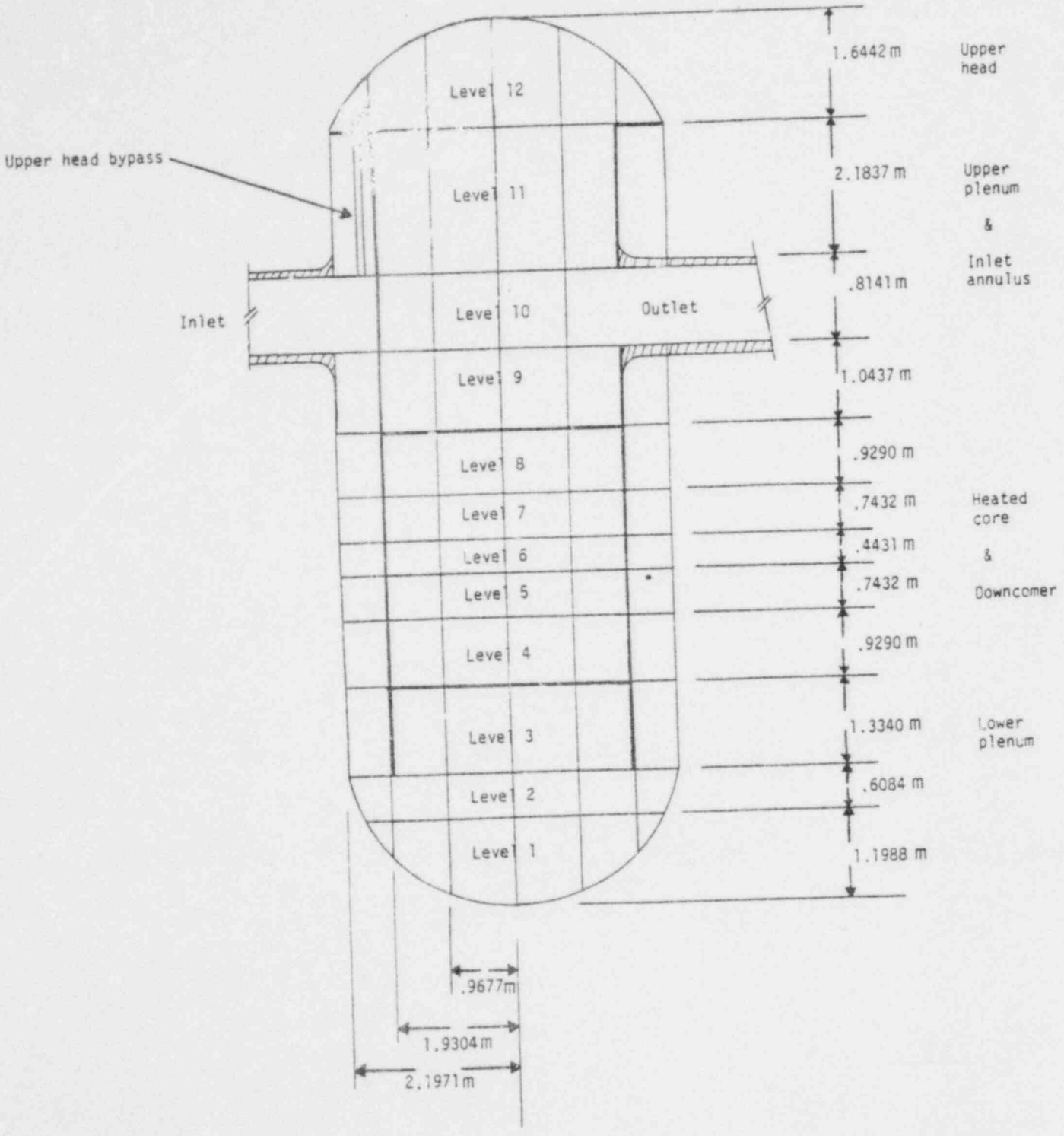

Figure A-1. Zion I vessel noding for TRAC.

TABLE A-1. VOLUMES, HEAT SLAB AREAS AND HEAT SLAB MASSES FOR PWR MODELS

	Lower Plenum Heat Slab Area (m^2)	Lower Plenum Heat Slab Mass (kg)	Lower Plenum Liquid Volume (m^3)	Downcomer Liquid Volume, Core Section (m^3)	Core Liquid Volume (m^3)	Downcomer Heat Slab Area, Core Section (m^2)
Zion I	180.32	2916O.0	28.57	9.68	18.32	195.79
USPWR1	165.40	2503 .0	28.38	9.40	16.83	21 .17
BE/EM	149.13	N/A	30.10	10.12	20.23	210.76

	Core Heat Slab Area[a] (m^2)	Core Heat Slab Mass (kg)	Upper Plenum Volume (m^3)	Upper Plenum Heat Slab Area (m^3)	Inlet Annulus Volume (m^3)	Upper Head Volume (m^3)	Loop Flow Volume (m^3)
Zion I	717.73	10306.0	40.31	329.62	9.31	13.67	42.69
USPWR1	45.56	6544.64	37.64	409.72	9.82	12.64	41.92
BE/EM	4849.0	N/A	40.10	354.79	8.85	13.85	42.70

a. BE/EM model includes fuel rods in heat slab area.

The fuel rod was divided into 9 cells for the fuel, one cell for the pellet-cladding gap and one cell for the cladding. A radial power distribution was input to the fuel pellets and is described in Table A-2.

The upper plenum was noded by three levels: level 9 below the inlet and outlet nozzles, level 10 which was sized to span the outlet nozzle flow area, and level 11 above the nozzles and below the upper head. Level 12 represented the upper head region of the vessel.

2. PRESSURIZER AND ACCUMULATORS

Figure A-2 shows the cell nodalization used for the pressurizer. The accumulators were nodalized in a similar manner. This type of model was recommended at the TRAC Workshop[3] held at LASL in February, 1980.

Basically, the bottom of the pressurizer and accumulators was modeled by a very short node. The connecting cell of the joining tee was also noded the same length as the adjoining pressurizer or accumulator cell but with a flow area equal to that of the pressurizer or accumulator. The appropriate initial liquid volume was obtained by including the connecting tee cell volume as part of the desired pressurizer or accumulator component volume. The fully implicit hydrodynamics option differencing technique was used on the secondary side of the tee to avoid Courant limiting of the time step size and to provide a better representation of the pressure drop calculated at the junction of the components. If there was too high a pressure drop then a smaller mass flow rate would be calculated at the junction using the semi-implicit hydrodynamics option if the tee cell was small in diameter compared to the pressurizer cell. Table A-3 provides a comparison of the pressurizer and accumulator volumes for the Zion I model with the BE/EM[1] and USPWR1 models.[2]

TABLE A-2. RELATIVE FUEL ROD RADIAL POWER DISTRIBUTION

Node	Factor
1 centerline	0.967
2	0.969
3	0.972
4	0.977
5	0.984
6	0.992
7	1.003
8	1.016
9	1.037

TABLE A-3. COMPARISON OF PRESSURIZER AND ACCUMULATOR LIQUID VOLUMES FOR SEVERAL PWR MODELS

Model	Pressurizer Volume (m^3)	Accumulator Volume (m^3)
Zion I	30.39	26.88[b]
USPWR1	30.32	28.96
BE/EM	30.58	28.85

b. Current operating value from Westinghouse.

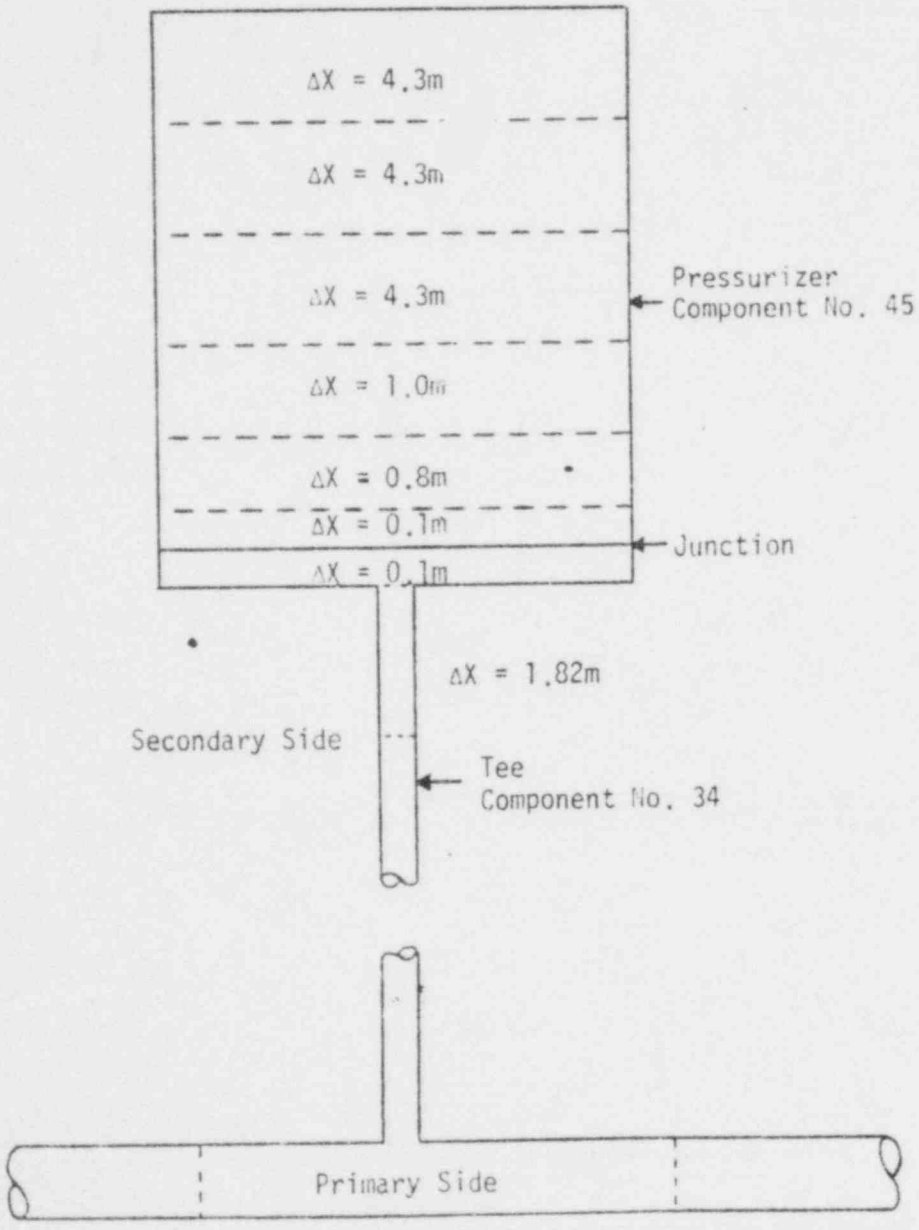

Figure A-2. TRAC noding of the pressurizer and tee.

3. BREAKS

The break piping was nodalized following the guidelines presented in the TRAC-P1A Developmental Assessment Report.[4] The nodalization is shown in Table A-4 and A-5 for the hot leg side break tee 49 and for the cold leg break side pipe 6, respectively. The 14 cells upstream of the break have the same spacing. The break was located just outside the biological shield as was done for the BE/EM study.[1] The length available for the hot leg break piping was determined by the location of the ECC fill component.

A short test run was made with a coarser spacing but little change was noted. Thus it was felt that the selected nodalization was adequate.

4. ECC INJECTION

The fill components for each loop lumped together the charging and safety injection systems. The mass flow rates were specified to be equal for each loop and were a function of the local pressure. The mass flow rate as a function of pressure was taken from the BE/EM study[1] for the intact loop and converted to velocity for input to the TRAC computer code. The mass flow rate is shown in Figure A-3.

5. BREAK NODING FOR SMALL AND INTERMEDIATE CALCULATIONS

The break location was the same distance from the vessel as the 200% break. The nodalization of the tee secondary side connected to the break is shown in Table A-6.

TABLE A-4. TEE 49 BREAK NODALIZATION

Cell No.	Length (m)
1 Junction cell	0.25
2	0.25
3	0.15
4	0.15
5	0.10
6	0.10
7	0.06
8	0.06
9	0.04
10	0.04
11	0.03
12	0.03
13	0.025
14 Break junction	0.025

Total length equals 1.31 m.

TABLE A-5. PIPE 6 BREAK NODALIZATION

Cell No.	Lengtn (m)
1 Break junction	0.025
2	0.025
3	0.03
4	0.03
5	0.04
6	0.04
7	0.06
8	0.06
9	0.10
10	0.10
11	0.15
12	0.15
13	0.25
14	0.25
15	0.34
16	0.45
17	0.667
18	0.667
19	0.667
20	0.667
21	0.667
22	0.667
23 Vessel junction	0.667

Total lengtn equals 6.569 m.

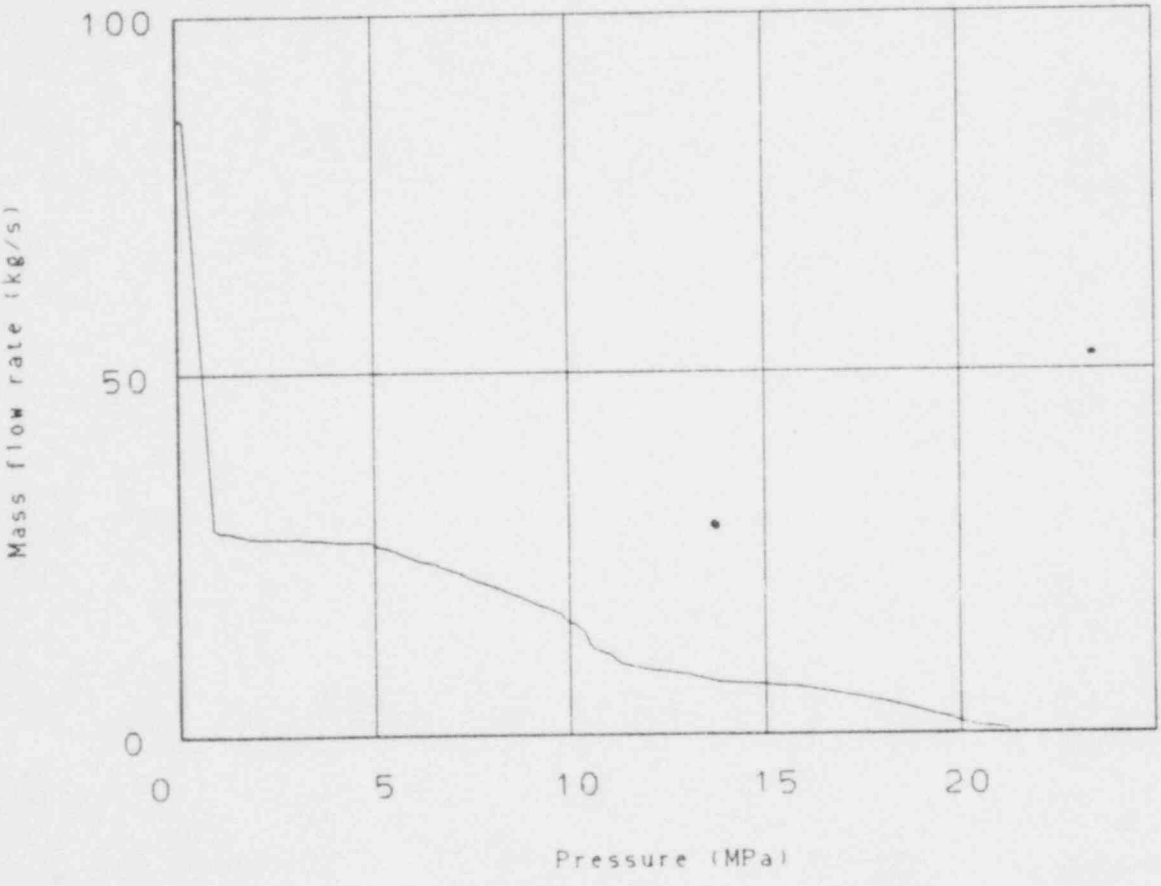

Figure A-3. ECC injection mass flow rate.

TABLE A-6. INTERMEDIATE AND SMALL BREAK TEE NODALIZATION

Primary Cell No.	Length (m)
1 Secondary Junction Cell	0.786
2	0.524
3	0.102
4	0.524
5	0.524
6	7.00
Secondary Cell No.	**Length (m)**
7	0.1010
8	0.0580
9	0.254
10	0.0127
11	0.0064
12 Break Junction	0.0032

REFERENCES

1. G. W. Johnsen et al., A Comparison of "Best Estimate" and "Evaluation Model" LOCA Calculations; The BE/EM study, EG&G Idaho, Inc., Report PG-R-76-009, December 1976.

2. TRAC-P1A, An Advanced Best-Estimate Computer Program for PWR LOCA Analysis, LA-7777-MS, May 1979.

3. J. K. Meier, "Problem Modeling," TRAC Workshop, Los Alamos, New Mexico, February 6, 1980.

4. J. C. Vigil et al., TRAC-P1A Developmental Assessment, LA-8056-MS, October 1979.

APPENDIX B

INITIAL AND BOUNDARY CONDITIONS FOR ZION I COLD LEG BREAKS

1. CORE POWER DISTRIBUTION

The relative axial power distribution for the 5 core levels is tabulated in Table B-1. The distribution is very similar to the BE/EM study.[1] Slight differences occur because the BE/EM study[1] included vessel structure and volume above and below the active core in the top and bottom core volumes.

The relative core radial distribution is shown in Table B-2. The distribution was obtained from the fuel performance report[2] by averaging the peaking factors given for each fuel assembly within the inner and outer rings of the model corresponding to the core. The axial and radial distributions resulted in an average rod midplane steady state power generation of 31.73 kW/m (9.67 kW/ft). The decay heat generation was based on the ANS specification and was taken from the BE/EM study.[1]

2. PUMPS

The primary loop circulating pumps were left on throughout the transient calculation.

3. STEAM GENERATOR FEEDWATER AND STEAM FLOW

Steam flow from the secondary side of the steam generators was shut off between 0.0 s and 1.5 s by linearly closing the valve upstream of the break. The feedwater was terminated and auxiliary feed was begun as shown in Figure B-1.

4. SCRAM

Scram occurred at 0.53 s, the same time used in the BE/EM study.[1]

TABLE B-1. RELATIVE CORE AXIAL POWER DISTRIBUTION

Core Level	Factor
1 bottom	0.8142
2	1.189
3	1.20
4	1.1706
5 top	0.7018

TABLE B-2. RELATIVE CORE RADIAL POWER DISTRIBUTION

Ring	Factor
1 inner	1.0898
2 outer	0.83373

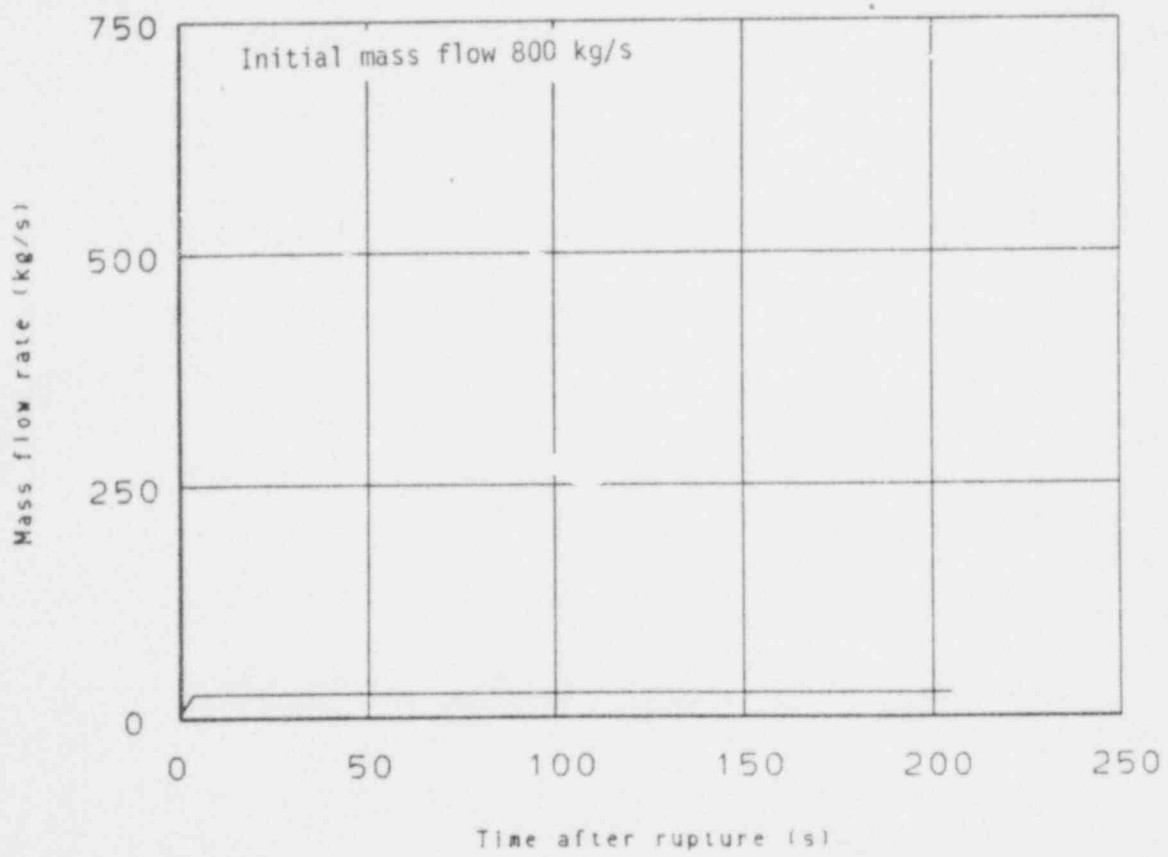

Figure B-1. Steam generator feedwater and auxiliary feedwater mass flow.

5. CONTAINMENT PRESSURE

The containment pressure is shown as a function of time in Figure B-2. It is identical to that used in the BE/EM stud..[1]

6. ACCUMULATORS

The initial conditions for the accumulators are compared to the BE/EM study[1] and are listed in Table B-3.

7. PRESSURIZER

The initial conditions for the pressurizer are compared to those of the BE/EM study[1] and are listed in Table B-4.

8. SMALL AND INTERMEDIATE BOUNDARY CONDITIONS

The boundary conditions for the small and intermediate breaks were the same as the large break with the exception of those listed below.

1. Scram occurs on low pressurizer pressure at 12.7 MPa, with a 3.4 s delay.

2. The steam generator feedwater was terminated with the scram signal and auxiliary feedwater was initiated 50 s later. Steam flow was stopped at the time of the scram. Safety valves were modeled, as a TEE component and FILL component to relieve overpressure in the secondary at 7.62 MPa.

3. Containment pressure was constant at 0.10 MPa.

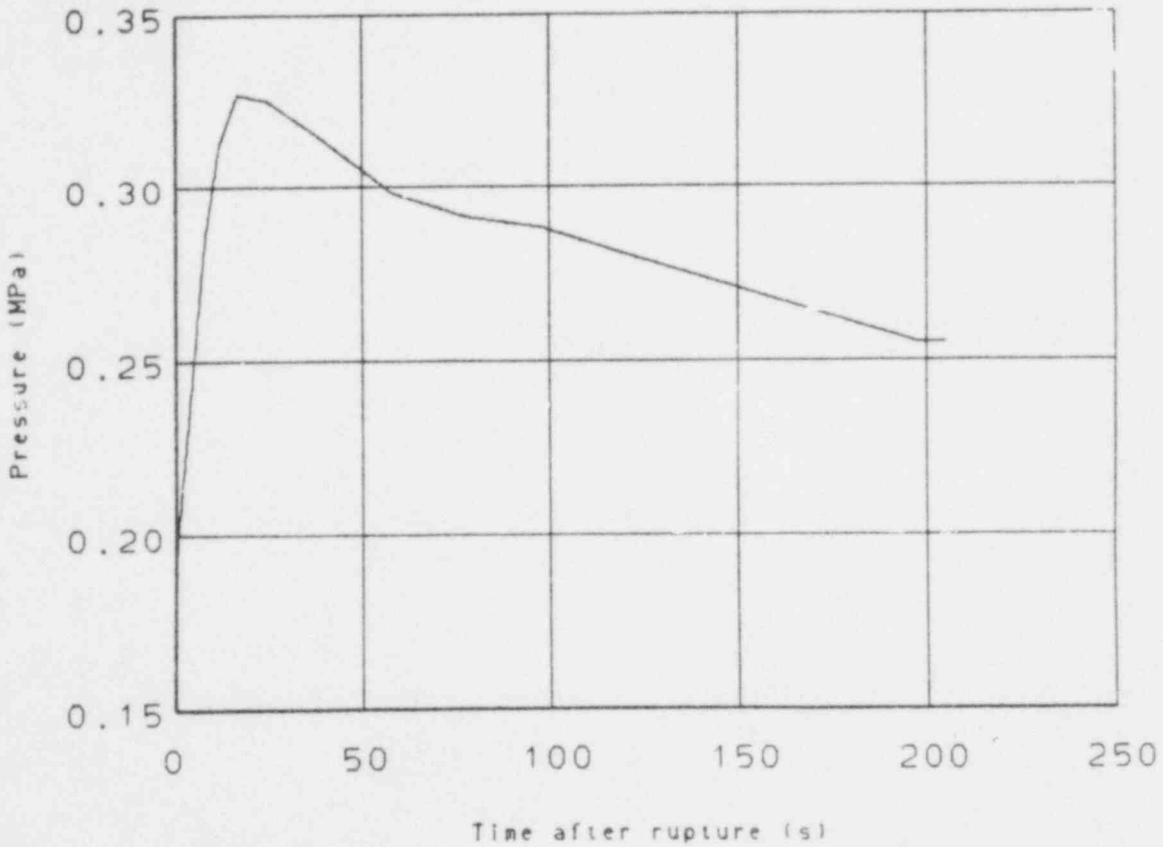

Figure B-2. Containment pressure.

TABLE B-3. INITIAL CONDITIONS FOR ZION I ACCUMULATORS COMPARED TO THE BE/EM STUDY

	Zion I	BE/EM
Pressure (MPa)	4.43	4.43
Temperature (K)	325.0	325.0
Trip Pressure (MPa)	4.08	4.08

TABLE B-4. INITIAL CONDITIONS FOR ZION I PRESSURIZER COMPARED TO THE BE/EM STUDY

	Zion I	BE/EM
Pressure (MPa)	15.43	15.43
Temperature (K)	616	617

REFERENCES

1. G. W. Johnsen et al., A Comparison of "Best Estimate" and "Evaluation Model" LOCA Calculations; The BE/EM Study, EG&G Idaho, Inc., Report PG-R-76-009, December 1976.

2. H. H. Crain et al., Interim Report Zion Unit 1 Cycle 1 Fuel Performance, Westinghouse Electric Corporation, WCAP-8837, December 1976.

APPENDIX C

CODE INPUT FOR COLD LEG BREAKS